PHOTOCHEMICAL SYNTHESIS OF MONO AND BIMETALLIC NANOPARTICLES AND THEIR USE IN CATALYSIS

Andrea Pardoe

A thesis submitted to the

Faculty of Graduate and Postdoctoral Studies

in partial fulfillment of the requirements for the degree of

Master of Science

Specialization in Chemistry

uOttawa

in the Ottawa-Carleton Chemistry Institute

Department of Chemistry, University of Ottawa

Candidate	Supervisor
Andrea Pardoe	Professor J.C. Scaiano

ABSTRACT

Nanomaterials have become a popular topic of research over the years because of their many important applications. It can be a challenge to stabilize the particles at a nanometer size, while having control over their surface features.

Copper nanoparticles were synthesized photochemically using a photogenerated radical allowing spatial and temporal control over their formation. The synthesis was affected by the stabilizers used, which changed the size, dispersity, rate of formation, and oxidation rate. Copper nanoparticles suffer from their fast oxidation in air, so copper-silver bimetallic nanoparticles were synthesized in attempts to overcome the oxidation of copper nanoparticles. Bimetallic nanoparticles were synthesized, but preventing the oxidation of the copper nanoparticles proved difficult.

One important application of nanoparticles that was explored here is in catalyzing organic reactions. Because of the fast oxidation of copper nanoparticles, silver nanoparticles were synthesized photochemically on different supports including TiO_2 and hydrotalcite (HTC). Their catalytic efficiency was tested using alcohol oxidations. Different silver nanoparticle shapes (decahedra and plates) were compared with the spheres to see the different catalytic efficiencies.

ABBREVIATIONS & TERMINOLOGY

4-MBA	4-methoxybenzyl alcohol
4-MBAldehyde	4-methoxybenzaldehyde
Å	Angstrom (10^{-10} m)
Ag@support	Silver nanoparticles attached to support
APTES	Aminopropyltriethylsiloxane
CTAB	Cetyltriethylammonium bromide
CTAC	Cetyltriethylammonium chloride
EtOH	Ethanol
GCMS	Gas chromatography-mass spectrometry
HPLC	High-performance liquid chromatography
HTC	Hydrotalcite
I-2959	Irgacure 2959 (2-Hydroxy-1-[4-(2-hydroxyethoxy)phenyl]-2-methyl-1-propanone)
I-907	Irgacure 907 (2-methyl-1-[4-(methylthio)phenyl]-2-(morpholinyl) phenyl]-1-butanone)
k	Rate constant
LED	Light emitting diode
MeCN	Acetonitrile
M	Molar (mol/L)
mM	Millimolar (10^{-3} M)
m	Metre, basic S.I. unit for length
mL	Millilitre (10^{-3} L)

μm	Micrometre (10^{-6} m)
nm	Nanometre (10^{-9} m)
NP	Nanoparticle(s)
AgNP	Silver nanoparticles
CuNP	Copper nanoparticles
Cu/AgNP	Copper-silver bimetallic nanoparticles
AuNP	Gold nanoparticles
s	Second, basic S.I. unit for time
SEM	Scanning electron microscopy
SiO_2	Silica
SPB	Surface plasmon band
TBABr	Tetrabutylammonium bromide
TBenzylABr	Tetrabenzylammonium bromide
TEABr	Tetraethylammonium bromide
TEM	Transmission electron microscopy
THABr	Tetraheptylammonium bromide
TiO_2	Titanium dioxide, either P90 (90% anatase, 10% rutile) or P25 (80% anatase, 20% rutile)
TiO_2(APTES)	Titanium dioxide functionalized with APTES
TMABr	Tetramethylammonium bromide
TMACl	Tetramethylammonium chloride
TOABr	Tetraoctylammonium bromide
TPABr	Tetrapropylammonium bromide
UVA	Ultraviolet radiation (315-400 nm, centred at ~350 nm)
UVB	Ultraviolet radiation (280-315 nm, centred at ~300 nm)

ACKNOWLEDGEMENTS

I am lucky to have so many people to acknowledge for their help and support throughout this degree. This is a bitter-sweet end to a great 2.5 years! I will miss the friends, the amazing work environment, and daily laughs I had while a member of Scaiano group. I moved to Ottawa knowing almost nobody and now call this my home thanks to all the amazing people I have met through working in the Scaiano group.

Tito: you have been a wealth of knowledge and ideas, a mentor, and someone who I am honoured to have met, looked up to, and worked for. I learned so much from you and am lucky to have had the opportunity to work in your group and learn from you. I can't imagine a better supervisor. I am also lucky to have gotten to know such a generous and kind man who regularly welcomed us into his home for BBQs, dinners, and ski trips. Thank you, Tito, for all your support, guidance, and patience throughout this process.

Dr. Michelle Chrétien: the opportunity you provided me with to work at Xerox to learn about industry and learn from you was an experience that has impacted me in many ways. I enjoyed working at Xerox, meeting the people working there, and the opportunity to meet and work with such a driven and fun person! Your knowledge and mentorship were fundamental in my learning process and I am happy to have had this experience that many don't get in their graduate work.

My colleagues and friends in the Scaiano group: you have all provided me with guidance, suggestions, support, and an uncountable number of good laughs and fun times over the past two years. You made my time at work the most enjoyable and gave me reason to smile even when the experiments weren't working. I will

remember this experience fondly forever. Special thanks go to Dr. Natalia Pacioni and Dr. Geniece Hallett-Tapley. Thank you both for your guidance, support, and always making time to help me throughout this research. I can't imagine what I would have done without your patience and understanding. Kevin, you have helped me an uncountable number of times. Thanks for being my desk-mate and laughing with me, but most of all, thanks for being such a great friend and always being there for me. Paul, you have always been there to explain things and laugh with. I don't know what I would have done without your support and commiseration in thesis-writing. Thanks for putting up with me in 428!

I couldn't have gotten through this process without the help, support, and love from my family. Mum, Dad, and Colin: you have provided me with unconditional love, support, and believed in me when I didn't believe in myself. Geoff: you are my rock and I could not have done this without you. You have supported and loved me through good days and bad, always been a listening ear, and talked me out of many stressful times. Thanks for being there, always picking me up, and sticking by my side. You always know how to put a smile on my face! This thesis is for you, Mum, Dad, Colin, and Geoff. Without you, none of this would have been possible.

TABLE OF CONTENTS:

CHAPTER 1 -

INTRODUCTION

TABLE OF CONTENTS:

TABLE OF FIGURES:

1.1 Introduction

This first part of this thesis will cover the photochemical synthesis of copper nanoparticles and copper-silver bimetallic nanoparticles allowing spatial and temporal control over the synthesis. It will investigate copper nanoparticle stabilization with different ammonium halides, their oxidation, and attempts to prevent copper from oxidizing by making bimetallic copper-silver nanoparticles. The second part of this research will look at the photochemical synthesis of supported silver nanoparticles for their use in alcohol oxidations. It will compare the catalytic efficiency of different supported silver nanoparticle shapes.

1.2 Nanoparticles

Metallic nanoparticle research, once called “finely dispersed metals” by Faraday, began in the late 1970s.[1] Nanomaterials are clusters of a few to many millions of atoms or molecules on the scale of 10^{-9} m whereas an atom measures ~1 Å (10^{-10} m).[2] Properties of nanometer sized materials are different than their bulk counterparts and their study has become increasingly investigated over the past 20 years.[3] As the size of a material decreases, its properties also change (*i.e.* electron confinement in quantum dots), resulting in a material whose properties are different from both their bulk counterparts and individual atoms.[3] As the size decreases, the surface area to volume ratio increases, giving it unique properties not exhibited by the bulk material. Metal nanoparticles have

been found to be useful in catalytic applications, nanoelectronics, biological imaging and drug delivery, information storing, Raman scattering, sensors, and information storage, among others.[3-4]

Metallic nanoparticles exhibit a Surface Plasmon absorption Band (SPB), which is present at a particle size of at least 15 atoms.[1] For metals including Au, Ag, and Cu, the absorption maximum occurs in the visible frequency range giving rise to colourful colloidal solutions. Nanometer sized particles are transparent and light scattering is negligible.[1] Changing the size or shape of a nanoparticle results in a change in the observed colour.[3] The colour of the NP solution is a result of the Surface Plasmon resonant absorption and depends on the shape and size of the nanoparticle and the dielectric constant surrounding the particle.[3] The SPB is a result of a collective excitation and oscillation of free electrons in the nanoparticles in the conduction band under the electric field of incoming light, which results in a dipole excitation across the sphere causing the electrons to oscillate (see Figure 1.1).[1,3] Once the particle size decreases below the electron mean free path, the SPB is observed.[5] These properties coming from nano-sized particles are unique and not seen with bulk metal or atoms.[5]

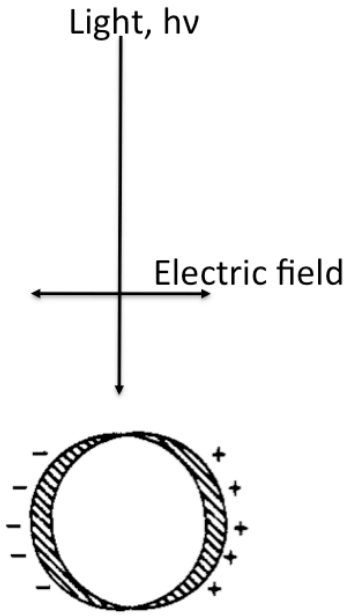

Figure 1.1 Polarization of a spherical nanoparticle by the electric field vector of incoming light.[1]

Silver nanoparticles exhibit a SPB around 400 nm. The SPB and the interband transitions occur at separate wavelengths.[1] Whereas gold and copper nanoparticles also exhibit SPB in the visible region of the spectrum (520 and 570 nm respectively), their resonances are superimposed by interband transitions.[1] The free electrons in the metal can travel through the particle and when the wavelength of light is longer than the nanoparticle size, it generates standing resonance and the wavelength of light in resonance with the Surface Plasmon oscillation causes the free-electrons to oscillate (see Figure 1.2).[3] The electron density is polarized to one surface when light passes and oscillates in resonance with the light's frequency causing a standing oscillation.[3]

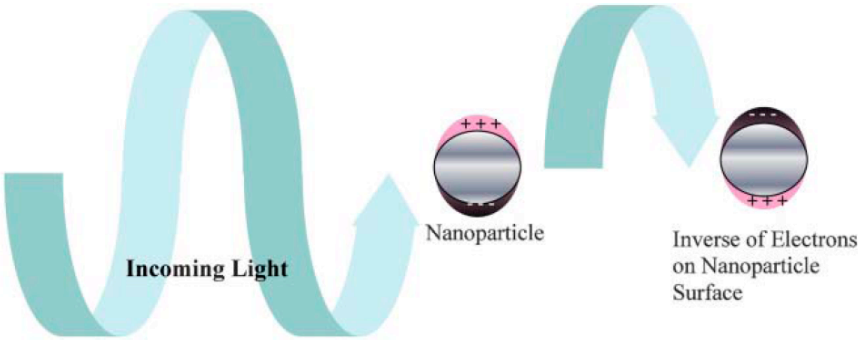

Figure 1.2 Surface Plasmon Resonance resulting from interactions of the electrons in the conduction band with light[3]

The SPB position does not depend on the size of the NP; between 3 and 20 nm there is not a strong dependence on particle size and absorption spectrum.[1] Using a capping agent on the nanoparticle changes the surface and may cause a shift in the SPB since it can change the dielectric constant of the medium with respect to the metal NP.[3]

1.3 Synthesis methods for colloidal nanoparticles

There are two general approaches to obtain metallic nanoparticles: (1) A top down approach where material is removed from bulk material until nanosized particles are left or (2) a bottom up approach where a metal salt is reduced and assembled together to make nanosized particles (see Figure 1.3).[3] Typical top down approaches use photolithography or electron beam lithography, but are a challenge because of the need to remove so much material.[3] Photolithography is also limited by the diffraction limit where electron beam is not, however the instrumentation for electron beam is expensive.[3] Bottom up approaches have a challenge to achieve good monodispersity and the ability to stop reduction and arrest growth of the NP as well as the need for other stabilizing agents.[3]

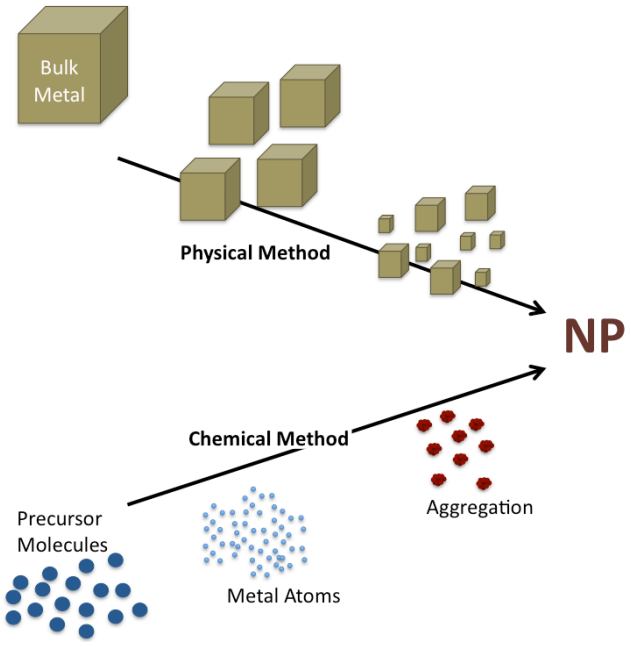

Figure 1.3 Figure illustrating top-down *vs.* bottom-up approaches to making nanoparticles[6]

Most commonly used bottom-up methods for making metallic nanoparticles are chemical methods of reducing a metal salt using a surfactant or capping agent to control the size, shape, and polydispersity of the NP.[3] Common methods are citrate reduction or sodium borohydride reduction requiring high temperatures and/or harsh conditions.[3] Irradiation methods for making colloidal NP have several advantages over chemical reductions. Photochemical methods are reproducible and occur at room temperature in a closed vessel avoiding the introduction of impurities.[1] Furthermore, there is complete temporal and spatial control over the reaction and the reduction is initiated homogeneously since mixing does not control the reduction rate.[1] In the Scaiano group, we use photochemical initiators to produce ketyl (in the case of I-2959)[7-9] or α-amino alkyl (in the case of I-907)[8] radicals, which go on to reduce metal salts in solution through an electron donation (see Figure 1.4 and Figure 1.5). Irgacure undergoes a Norrish type I photocleavage resulting in a ketyl radical in the case of I-2959 and an α-amino alkyl radical in the case of I-907 and a benzoyl radical. The benzoyl radical is not a participant in the reduction since its reduction potential is not comparable to the other radicals (0.2-0.7 V *vs* NHE).[10] The ketyl radical generated from photolysis of I-2959 has a reduction potential of -0.578 V *vs.* NHE (or -0.82 V *vs.* SCE).[11] The α-amino radical generated from the photocleavage of I-907 has a reduction potential of -1.47 V (*vs.* NHE) and is a stronger reductant than the ketyl radical from I-2959.[10]

In a multivalent metal (*i.e.* $Cu(OAc)_2$, holding a charge of 2+, two subsequent electron donations can occur to reduce Cu^{2+} to Cu^0 or a one electron reduction to Cu^+ followed by disproportionation where two M^+ can combine to make M^0 and M^{+2}, see Figure 1.4.

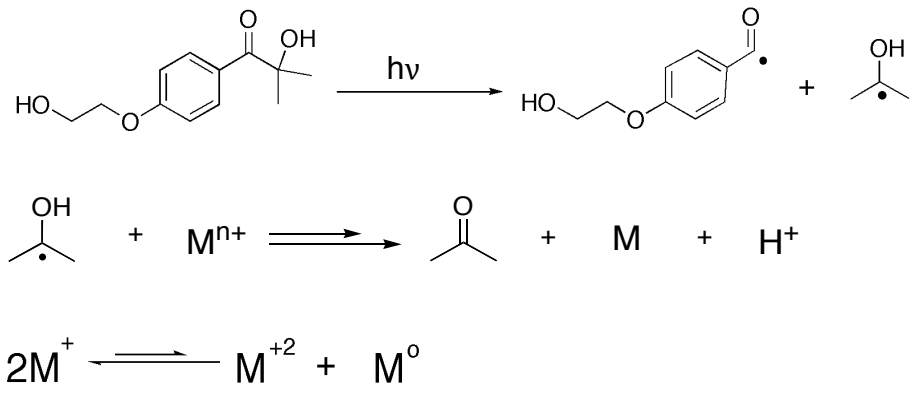

Figure 1.4 Irgacure 2959 photocleavage under UVA photolysis followed by metal (M) reduction. B: Disproportionation after one electron reduction to M^{2+}

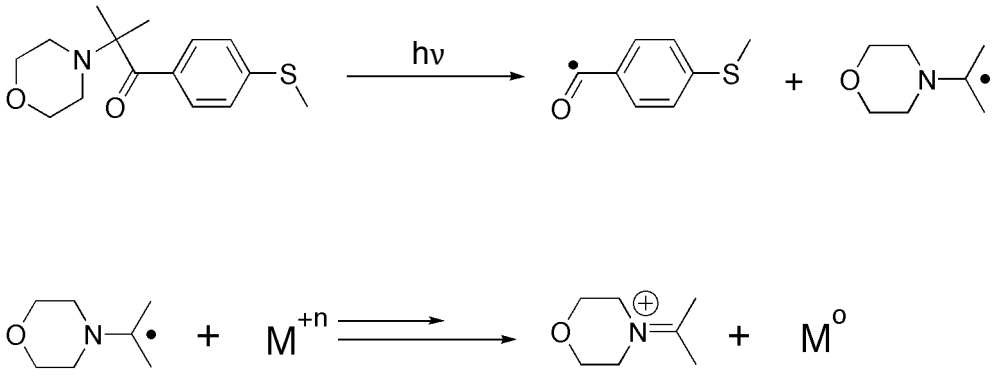

Figure 1.5 Irgacure 907 photocleavage under UV photolysis followed by metal (M) reduction

A Norrish Type I reaction creates a radical pair upon irradiation of a carbonyl compound.[12] This involves the α-cleavage of C-C bond of the C=O portion in ketones resulting in a carbonyl radical and an alkyl radical (see Figure 1.6).[12]

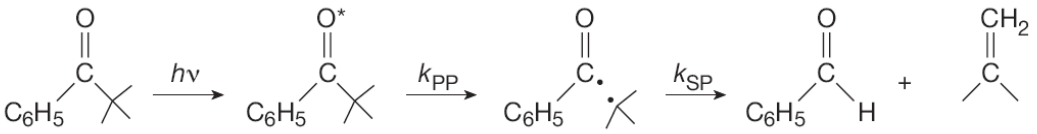

Figure 1.6 Norrish Type I reaction.[12]

When Irgacure (I-907 or I-2959 are the two used in these studies) is irradiated, it absorbs light, produces a singlet, which undergoes intersystem crossing with a high efficiency to form the triplet, which has a longer lifetime of 11 ns.[13] The transient biradical undergoes Norrish type I photocleavage (see Figure 1.6) efficiently to form a benzoyl and keyl radical (see Figure 1.4). The resultant ketyl radical can transfer an electron to reduce a metal species (see Figure 1.4). A hydrogen donating solvent improves this process as it will stabilize benzoyl radical after photocleavage of I-2959 through hydrogen bonding or hydrogen abstraction. For a more detailed diagram of the processes that can occur in the excited state, see Figure 1.7.

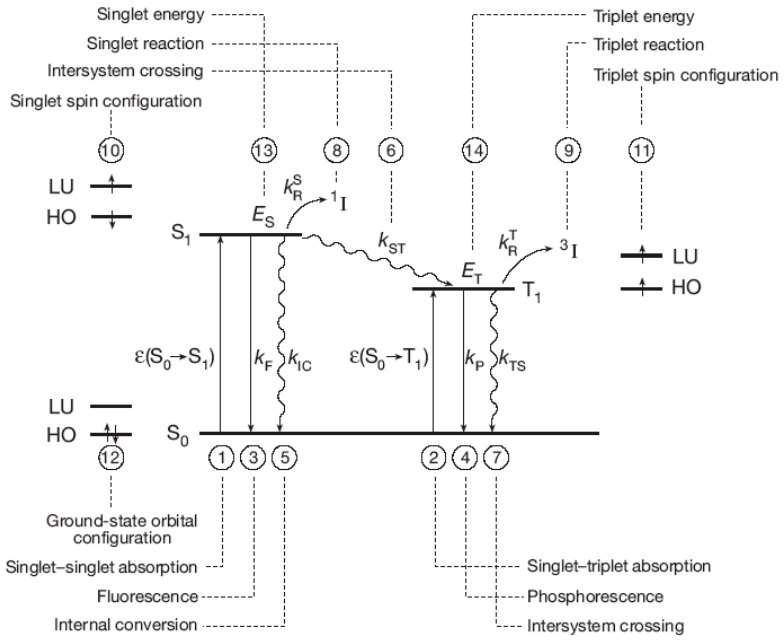

Figure 1.7 Jablonski Diagram showing possible transitions upon excitation by light and the possible transitions back to the ground state, including fluorescence (3), internal conversion (5), or intersystem crossing to form the triplet (6).[12]

1.4 Bimetallic nanoparticles

Bimetallic nanoparticles are nano-sized metallic particles composed of two different metals taking on different conformations depending on the strength of binding to surface ligands, strengths of the bonds between the metal atoms, surface energies of the bulk elements, relative atomic sizes of the metals, and the conditions used.[2] There are four main types of bimetallic nanoparticles (see Figure 1.8): core-shell (a), subcluster segregated (b), mixed (alloy) (c), or three shell (core-shell-shell) (d).[2]

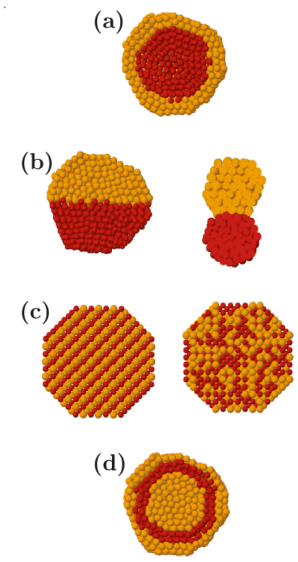

Figure 1.8 Different types of bimetallic structure: (a) core-shell, (b) subcluster segregated, (c) mixed (alloy), (d) three shell[2]

Bimetallic NP taking on the composition of an alloy will exhibit one SPB in between the SPB of the two metals used (providing they exhibit a SPB in the UV-Vis region of the electromagnetic spectrum) (see Figure 1.9).[14,15]

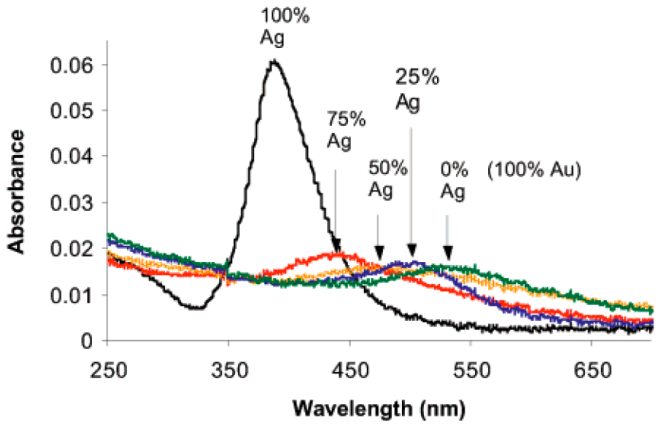

Figure 1.9 Absorbance spectra of NP made with ratios of 100 % up to 0 % Ag content in Ag/Au alloy NP[14]

There is some discrepancy about the absorbance spectra of core-shell type structures, however, some papers[15,16] report core-shell (Au-Ag) nanoparticles showing two SPB; one for AuNP and the other for the AgNP shell (see Figure 1.10). The SPB of the two metals and their respective intensities depend on the thickness of the shell.[15] If the shell becomes thick enough, it may be possible that only one SPB is exhibited since the contribution from the core is ignored by the thickness of the outer metal shell.

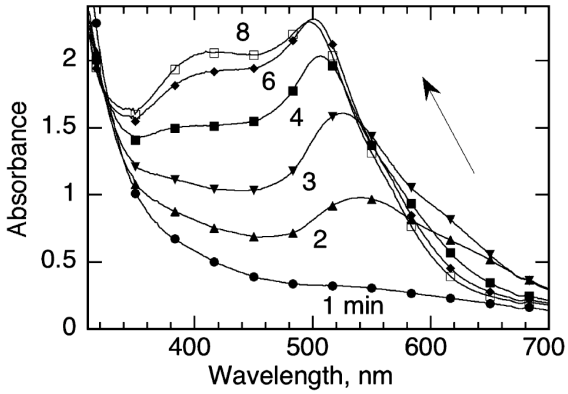

Figure 1.10 Figure showing absorption spectra of core-shell NP (Ag-core Au-shell NP) showing two distinct SPB.[16]

1.5 Nanoparticle Shapes

The shape of nanoparticles can be tuned to make different morphologies, exposing different facets resulting in useful shapes for different applications including SERS and catalysis.[9,17,18] Some methods for changing the shape of spherical AgNP use thermal methods using strong reducing agents and yield a polydisperse particle size.[9,19,20] Photochemical methods have been used to shape nanoparticles more monodispersely and with spatial and temporal control.[9,21] Using a wavelength of light that excites the plasmon resonance of the different shaped particles can change spheres into other morphologies as has been shown.[9,21] Using LED irradiation of a solution of AgNP seeds (~3 nm) stabilized with citrate, results in a shift of the absorbance from 395 nm to the plasmon resonance of the resulting shape (see Figure 1.11).[9]

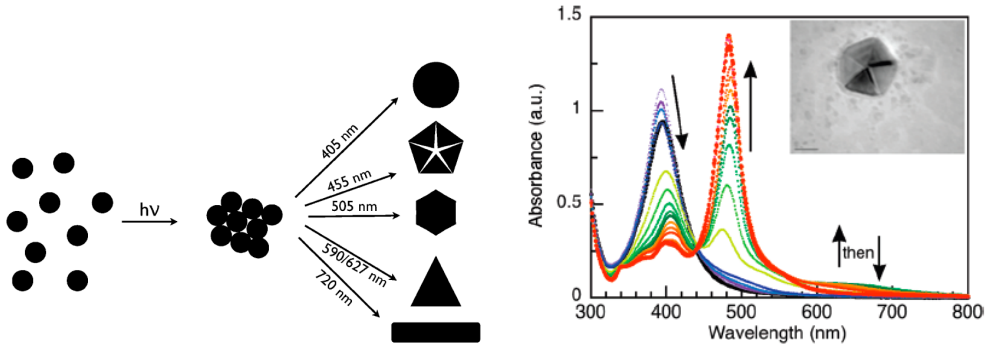

Figure 1.11 Coalescence mechanism of changing spherical AgNP into different shapes based on the wavelength of LED irradiation. UV/Vis absorbance changes over time from spheres absorbing at 395 nm to decahedra absorbing at 480 nm.[9]

1.6 Supported nanoparticles

One of the first goals of nanoparticle research was their use as catalysts through the storage of excess electrons on the particles in solution.[1] Nanoparticles have important properties that make them better catalysts than bulk material; their large surface area to volume ratio giving a large percentage of their atoms to surface sites making them available for catalysis and allow efficient use of expensive metals.[4,6] A constant challenge, however, in the field of nanoscience is reproducibility and attaining a monodisperse sample of nanoparticles.[4] Commonly catalyzed reactions include oxidation, carbon-carbon coupling, hydrosilylation, and hydrogenation among others.[6,22] Nanoparticles are used in both homogeneous and heterogeneous catalytic applications.[18,23,24] Homogeneous catalysis using colloidal nanoparticles suffers from the inability in most cases to effectively separate the NP from the reaction after completion and for this reason are not reusable. In order to effectively use the nanoparticles for heterogeneous catalytic applications, a support is helpful to be able to retrieve the particles after use and separate them from solution for reuse. This could be using magnetic properties, a larger solid for filtration or centrifugation, or extraction methods. Using solid supports; TiO_2, hydrotalcite, SiO_2, MgO, alumina, zeolites, clays, or polymers allow easy separation of the catalyst from the reaction for reuse and are integrated through ion exchange, ligand grafting, metal coordination, microencapsulation, and electrostatic interactions.[25] TiO_2 has been shown to be an important support because the catalytic properties of metals can

be modified by metal-support interactions.[26] Titanium dioxide is a popular support for supported nanoparticle catalysis for this reason. There are two catalytically active types: P25 titania, which consists of 80% anatase and 20% rutile[22] and P90, which is 90% anatase and 10% rutile. The nanoparticles have shown to preferentially locate on the rutile phase.[22] Nanoparticles on metal-oxide supports have been shown to be more catalytically active than either of the two materials on their own.[27]

Most methods of synthesis of NP on support involve a chemical reduction using $NaBH_4$, citrate, or H_2 reduction of the metal salt, attaching it to the support through reduction in the presence of the support and any necessary ligand or in solid state after calcination,[4,24,26,28] or formation of the NP followed by deposition on the support using heat, electrostatic interactions or ligand interactions.[29-31] The main methods for preparing supported metal nanoparticles on metal oxide supports are adsorption and deposition-precipitation.[22] Adsorption of the metal salt on the surface depends on the charge of the metal salt complex and the isoelectric point of the metal oxide support; if there is an attraction, they can adsorb through coulombic interactions.[22] Adsorption can also be the adsorption of preformed nanoparticles on the support.[22] Deposition-precipitation involves changing the pH to force the metal salt to precipitate and adsorb onto the solid support.[22] This method works well with supports having a zero potential charge greater than five since it will be negatively charged at a neutral pH, attracting the metal salt, this includes magnesia, titania, alumina, zirconia, and ceria.[22]

Previous work used a photochemical approach of making these supported nanoparticles but only by photochemically making the nanoparticles followed by liquid deposition on the support.[29] Their attempts to make them ensemble were reported as kinetically inefficient, requiring too many hours to obtain the catalyst because of radiation absorbed or scattered by the support.[29]

Using metal nanoparticles as catalysts provides a greener, reusable, recoverable, and toxic waste free method for many chemical transformations that are important to synthetic and industrial chemistry.[23,24,32]

1.6 References:

(1) Henglein, A. *J. Phys. Chem.* **1993**, *97*, 5457-5471.

(2) Ferrando, R.; Jellinek, J.; Johnston, R. L. *Chem. Rev.* **2006**, *108*, 846-904.

(3) Eustis, S.; El-Sayed, M. A. *Chem. Soc. Rev.* **2006**, *35*, 209-217.

(4) Mori, K.; Kumami, A.; Tomonari, M.; Yamashita, H. *J. Phys. Chem. C Lett.* **2009**, *113*, 16850-16854.

(5) El-Sayed, M. A. *Acc. Chem. Res.* **2001**, *34*, 251-264.

(6) Roucoux, A.; Schulz, J.; Patin, H. *Chem. Rev.* **2002**, *102*, 3757-3778.

(7) McGilvray, K. L.; Decan, M. R.; Wang, D.; Scaiano, J. C. *J. Am. Chem. Soc.* **2006**, *128*, 15980-15981.

(8) Pacioni, N. L.; Pardoe, A.; McGilvray, K. L.; Chretien, M. N.; Scaiano, J. C. *Photochem. Photobiol. Sci.* **2010**, *9*, 766-774.

(9) Stamplecoskie, K. G.; Scaiano, J. C. *J. Am. Chem. Soc.* **2010**, *132*, 1825-7.

(10) Fu, Y.; Liu, L.; Yu, H. Z.; Wang, Y. M.; Guo, Q. X. *J. Am. Chem. Soc.* **2005**, *127*, 7227-7234.

(11) Rao, P. S.; Haydon, E. *J. Am. Chem. Soc.* **1974**, *96*, 1287-1294.

(12) Turro, N. J.; Ramamurthy, V.; Scaiano, J. C. *Modern molecular photochemistry of organic molecules*; University Science Books, 2010.

(13) Marin, M. L.; McGilvray, K. L.; Scaiano, J. C. *J. Am. Chem. Soc.* **2008**, *130*, 16572-16584.

(14) Mallin, M. P.; Murphy, C. J. *Nano Lett.* **2002**, *2*, 1235-1237.

(15) Link, S.; Wang, Z. L.; El-Sayed, M. A. *J. Phys. Chem. B* **1999**, *103*, 3529-3533.

(16) Gonzalez, C. M.; Liu, Y.; Scaiano, J. C. *J. Phys. Chem. C* **2009**, *113*, 11861-11867.

(17) Lu, L.; Kobayashi, A.; Tawa, K.; Ozaki, Y. *Chem. Mater.* **2006**, *18*, 4894-4901.

(18) Xu, R.; Wang, D.; Zhang, J.; Li, Y. *Chem. Asian J.* **2006**, *1*, 888-893.

(19) Samanta, S.; Pyne, S.; Sarkar, P.; Sahoo, G. P.; Bar, H.; Bhui, D. K.; Misra, A. *J. Molec. Liq.* **2010**, *153*, 170-173.

(20) Shen, X. S.; Wang, G. Z.; Hong, X.; Xie, X.; Zhu, W.; Li, D. P. *J. Am. Chem. Soc.* **2009**, *131*, 10812-10813.

(21) Burda, C.; Chen, X.; Narayanan, R.; El-Sayed, M. A. *Chem. Rev.* **2005**, *105*, 1025-1102.

(22) Corma, A.; Garcia, H. *Chem. Soc. Rev.* **2008**, *37*, 2096-2126.

(23) Mitsudome, T.; Arita, S.; Mori, H.; Mizugaki, T.; Jitsukawa, K.; Kaneda, K. *Angew. Chem. Int. Ed.* **2008**, *47*, 7938-7940.

(24) Mitsudome, T.; Mikami, Y.; Mori, H.; Arita, S.; Mizugaki, T.; Jitsukawa, K.; Kaneda, K. *Chem. Comm.* **2009**, 3258-3260.

(25) Trindade, A. F.; Gois, P. M. P.; Afonso, C. A. M. *Chem. Rev.* **2009**, *109*, 418-514.

(26) Grunert, W.; Bruckner, A.; Hofmeister, H.; Claus, P. *J. Phys. Chem. B* **2004**, *108*, 5709-5717.

(27) Hung, W. H.; Aykol, M.; Valley, D.; Hou, W.; Cronin, S. B. *Nano Lett.* **2010**, *10*, 1314-1318.

(28) Chimentao, R. J.; Kirm, I.; Medina, F.; Rodriguez, X.; Cesteros, Y.; Salagre, P.; Sueiras, J. E.; Fierro, J. L. G. *App. Surf. Sci.* **2005**, *252*, 793-800.

(29) Scire, S.; Crisafulli, C.; Giuffrida, S.; Mazza, C.; Riccobene, P. M.; Pistone, A.; Ventimiglia, G.; Bongiorno, C.; Spinella, C. *App. Cat. A: Gen.* **2009**, *367*, 138-145.

(30) Kiyonaga, T.; Jin, Q.; Kobayashi, H.; Tada, H. *Chem. Phys. Chem.* **2009**, *10*, 2935-2938.

(31) Zhou, X.; Xu, W.; Liu, G.; Panda, D.; Chen, P. *J. Am. Chem. Soc.* **2009**, *132*, 138-146.

(32) Ni, J.; Yu, W. J.; He, L.; Sun, H.; Cao, Y.; H.Y., H.; Fan, K. N. *Green Chem.* **2009**, *11*, 756-759.

CHAPTER 2-
PHOTOCHEMICAL SYNTHESIS OF COPPER NANOPARTICLES, BIMETALLIC COPPER-SILVER NANOPARTICLES, AND THEIR OXIDATION

TABLE OF CONTENTS:

TABLE OF FIGURES:

2.1 Introduction

2.1.1 Copper Nanoparticles

Copper nanoparticles (CuNP) are useful for many applications; however pose difficulties because of their instability to oxygen; they will oxidize spontaneously if unprotected.[1] They also have problems with stability in solution and suffer from precipitation if they are not sufficiently stabilized.[2] Copper is an inexpensive metal making bulk production of CuNP feasible for industrial applications. They are of interest because of their application in catalysis, optical applications, conducting properties, electronic applications, and their low cost compared to their gold or silver counterparts.[3-6] Copper nanoparticles are of interest for making microelectronic devices, inkjet printing inks, radio frequency identification tags, and disposable electronics because of their low cost and conductive properties.[4,5] Copper is also attractive for its use in cancer cell killing and germicide properties.[2] Copper is cheaper than silver and is very conductive, only 6% less than silver, making it a feasible replacement for silver nanoparticles in inkjet printing applications.[1] The fast oxidation and low reduction potential of Copper ($E°[Cu^{o}/Cu^{2+}]$ +(0.34 V)) makes their synthesis and stabilization a challenge.[3] Many syntheses use harsh reducing agents such as hydrazine, sodium borohydride, and hydrogen in excess, taking hours for completion.[3] Other syntheses use laser ablation, electrode discharge, sonochemical, radiolytic, or microwave reduction, some of which can be difficult to perform.[7]

2.1.2 Copper-Silver bimetallic NP

For CuNP to be useful in applications, the oxidation must be prevented. Methods used to protect CuNP from oxidation include employing a protective shell of ligands, polymers, or silica; however this is not advantageous since it now has a non-metallic outer layer.[1] Using a thin shell of a non-oxidizable metal around the core of CuNP will overcome both of these obstacles: oxidation of the CuNP is prevented and the NP maintains its metallic properties.[1] This has been done by making CuNP followed by addition of a silver salt where some of the CuNP is sacrificed to reduce the Ag^{+} to Ag^{o} (transmetalation method, see Figure 2.1).[1] Core-shell Cu-Ag NP have also been made through an electrochemical reduction of Cu^{+2} on AgNP formed on graphite.[8]

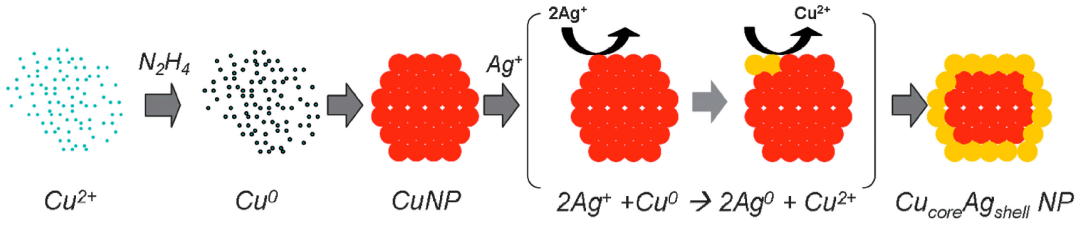

Figure 2.1 Diagram of transmetalation method to make Cu/Ag core-shell NP.[1]

Bimetallic NP can be combined or joined in a variety of ways including (i) an alloy, (ii) bimetallic segregated (two NP of different metals are joined at the edges or each makes half of the NP (see Figure 2.1)), or (iii) a mixture of the two NP metals separate in solution (see Introduction for further explanation).[9]

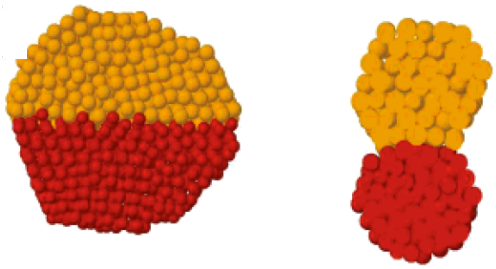

Figure 2.2 Cartoon image of bimetallic segregated NP[9]

The results presented herein are copper nanoparticles synthesized using a photochemical approach avoiding literature preparations using chemical reductions with harsh reducing conditions.[3] The more environmentally benign conditions used in this approach use a photochemical initiator (either Irgacure 2959 or Irgacure 907 in water or acetonitrile respectively.) Upon irradiation with UVA (in the case of I-2959) or UVA or UVB (in the case of I-907) radicals capable of reducing metals salts are produced. The photochemical reduction pathway is in Scheme 2.1. Irgacure 2959 undergoes a Norrish Type I photocleavage producing a ketyl radical where I-907 generates an α-amino alkyl radical, a stronger one-electron reductant.

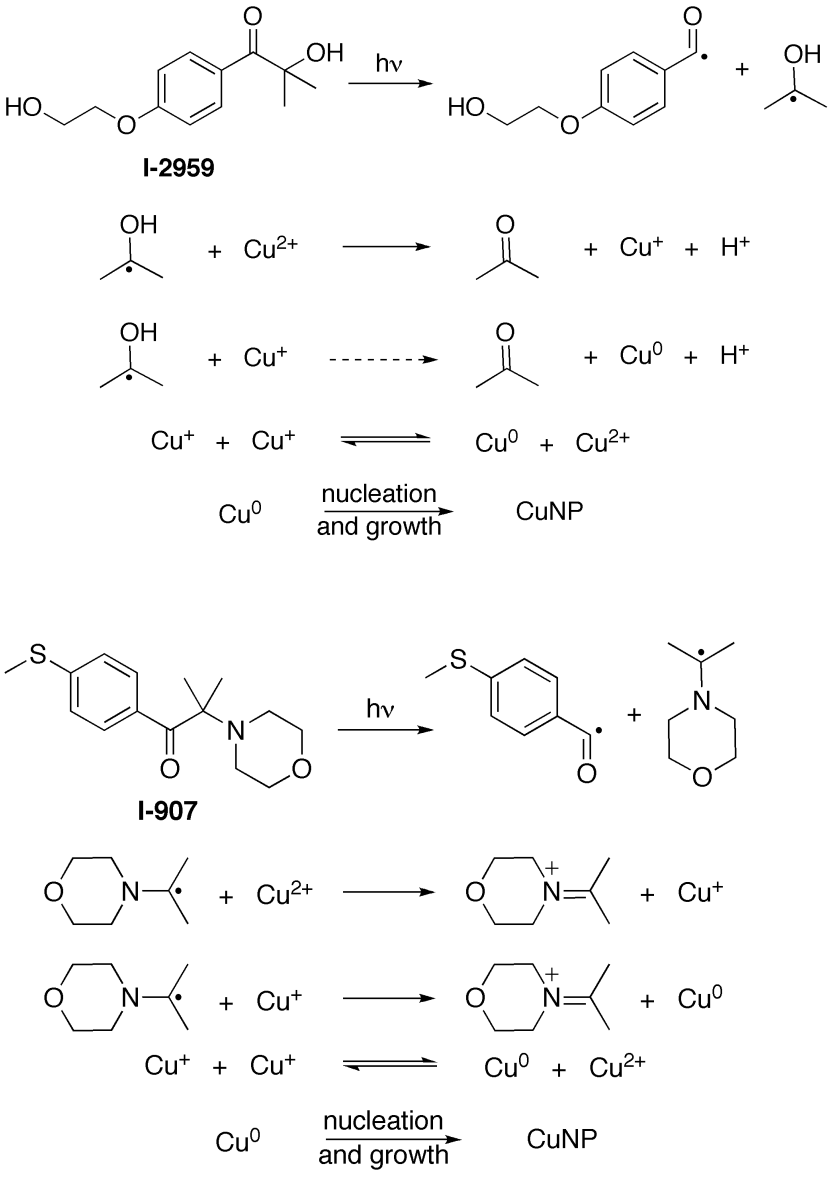

Scheme 2.1 Proposed photochemical reduction pathway of I-2959 and I-907 in water and MeCN respectively.

The benzoyl radical also produced in the photochemical cleavage of the photochemical initiators does not partake in the reduction because its reduction potential is too low (E°[R-(CO)/˙CO(R)] is approximately +(0.2-0.7)V *vs.* NHE)[10] compared to the ketyl radical and α-amino alkyl radical produced from I-2959

($E°[CH_3{\cdot}COHCH_3]$ is -0.578 V *vs.* NHE (-0.82 V *vs.* SCE))[11] and I-907 ($E°[(CH_3)_2{\cdot}CN(CH_3)_2]$ is -1.47 V *vs.* NHE)[10] respectively.

The goals of this research are to photochemically synthesize CuNP allowing spatial and temporal control over the NP synthesis, which is not possible with chemical reductions used previously. It also aims to determine the role of halides as stabilizers for CuNP to ultimately attempt to prevent their oxidation. Copper/Silver bimetallic NP were explored using a photochemical approach in further attempts to protect the CuNP from oxidation.

2.2 Materials and Methods

For the preparation of CuNP in water, $CuSO_4$, $Cu(NO_3)_2$ $3H_2O$, and $CuCl_2 \cdot 2H_2O$ were the copper salt precursors and because of solubility only $Cu(OAc)_2$ was used in acetonitrile. The CuNP synthesis done in water was primarily done by Dr. Natalia Pacioni. All copper precursors were purchased from Sigma Aldrich and used as received. The stabilizers that were used include cetyltrimethylammonium bromide (CTAB), cetyltrimethylammonium chloride (CTAC), NaCl, tetramethylammonium bromide (TMABr), tetramethylammonium chloride (TMACl), tetramethylammonium bromide (TMABr), tetraethylammonium bromide (TEABr), tetrabutylammonium bromide (TBABr), tetrapropylammonium bromide (TPABr), tetraheptylammonium bromide (THABr), tetraoctylammonium bromide (TOABr) were purchased from Sigma Aldrich and used as received. Irgacure 2959 (2-Hydroxy-1-[4-(2-hydroxyethoxy)phenyl]-2-methyl-1-propanone) and Irgacure 907 (2-methyl-1-[4-(methylthio)phenyl]-2-(morpholinyl) phenyl]-1-butanone) were a generous gift from Ciba Specialty Chemicals. Doubly distilled deionized water was used from a Milli-Q system (18 MΩ resistance) and spectroscopic grade acetonitrile was purchased from Fisher Scientific.

The concentrations used in the preparation of the nanoparticles were 0.66 mM of copper salt precursor, stoichiometric amount of Irgacure, and 0.66 mM of stabilizer (unless otherwise stated.) All samples were Ar-purged for 30 minutes prior to irradiation. Samples were irradiated in a fused silica cuvette

(10 x 10 mm) sealed with a septum and placed in a Luzchem LZC-4V photoreactor equipped with up to 14 lamps and a carousel to rotate the samples during photolysis. UVA lamps (centred at ~350 nm) were used for the NP prepared in water with I-2959 (λ_{max} ~ 270 nm) and UVB (centred at ~300 nm with a peak at 313 nm) irradiation was used for those prepared in MeCN with I-907 (λ_{max} ~ 300 nm). In both syntheses (water and acetontrile) the results were found to be quite reproducible with freshly prepared solutions and sufficient Ar-purging.

The characterization of the NP was done using UV-Vis spectroscopy (Varian Cary UV-50, Cary UV-100, Cary UV-500, or SpectraMax M5 spectrometer in cuvette mode), field emission scanning electron microscopy (SEM, JEOL JSM-7500F), and Transmission Electron Microscopy (TEM, JEOL JEM-2100F). The UV-Vis spectroscopy was done in the cuvette used to make the NP scanning between 200 and 900 nm. For the microscopy, approximately 50 µL of solution was dropped onto a copper grid (400 mesh) or a silicon wafer and evaporated under vacuum dessicator in attempts to avoid oxidation while drying. Images were analyzed using ImageJ Software.

2.3 Results and Discussion

2.3.1 Synthesis in Water

2.3.1.1 Synthesis

Copper nanoparticles were photochemically synthesized in water using different soluble Cu (II) salts to find the ideal conditions for CuNP stabilization.[6] The synthesis in water was done using Irgacure 2959 as the reducing agent using UVA light.

Copper (II) chloride, copper nitrate, and copper sulphate were tested as all are soluble in water. After deaerating with Ar and irradiating, the clear solution of $CuSO_4$ turned a reddish-brown colour with a Surface Plasmon Band (SPB) at 575 nm seen from UV-Vis spectroscopy measurements indicative of CuNP.[3,7,12] The CuNP solution from $CuCl_2$ had a pink colour with a SPB red-shifted compared to those made with $CuSO_4$ to 580 nm. The $Cu(NO_3)_2$ solutions had a low yield of NP indicated by the pale colour generated and the weak absorbance. See Figure 2.3 for absorbances of CuNP from each salt. The SPB of CuNP is known to appear in the 560-580 nm region.[1,7,12] Copper nanoparticles with an oxide layer around them from the literature, show an additional absorbance at wavelengths greater than 800 nm.[12,13]

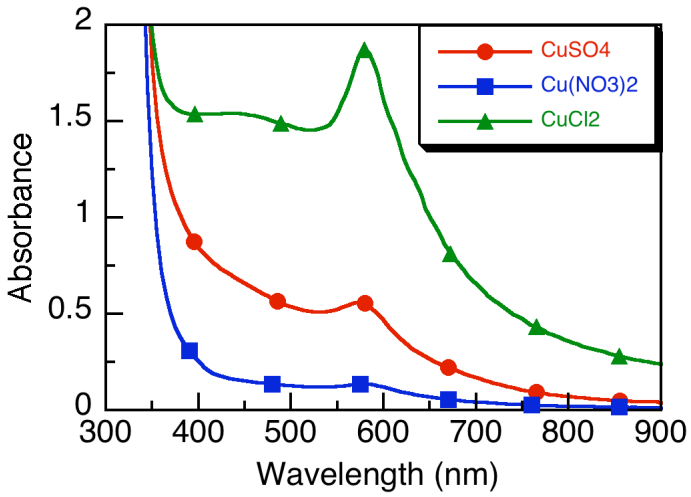

Figure 2.3 Absorbance of CuNP yielded from 0.66 mM $CuSO_4$, $Cu(NO_3)_2$, and $CuCl_2$, with stoichoimetric amount of I-2959 after 30 min of UVA irradiation.

SEM and TEM images show monodisperse spherical NP obtained from $CuSO_4$ with an average diameter of 8.2 nm. Nanoparticles obtained from $CuCl_2$ were more polydisperse with an average diameter of 18 nm. This precursor also yielded particles larger than 100 nm with a broader SPB and a rise in absorbance intensity, which could also be caused by the increased scattering at longer wavelengths.

When investigating the kinetics of CuNP formation, it was noted that the rate of formation is fastest with $CuCl_2$ compared to $CuSO_4$ and $Cu(NO_3)_2$ (see Figure 2.4). This was attributed to the chloride counter anion, likely responsible for stabilizing and catalyzing the NP growth. It is known that Cl^- adsorbs to the surface of copper.[14] The growth of CuNP in the presence of Cl^- begins immediately, where a delay is noted in the CuNP formation when no Cl^- is present. The delay without Cl^- present indicates that the ketyl radical does not

reduce Cu(I) until the Cu(II) is depleted, whereas with the Cl^- present disproportionation occurs quickly, forming CuNP. Disproportionation is the main mechanism proposed with the chloride anion because of these experimental observations (see Figure 2.5). This is also seen in SEM results where nanoparticles made with chloride are more polydisperse because of their fast formation.

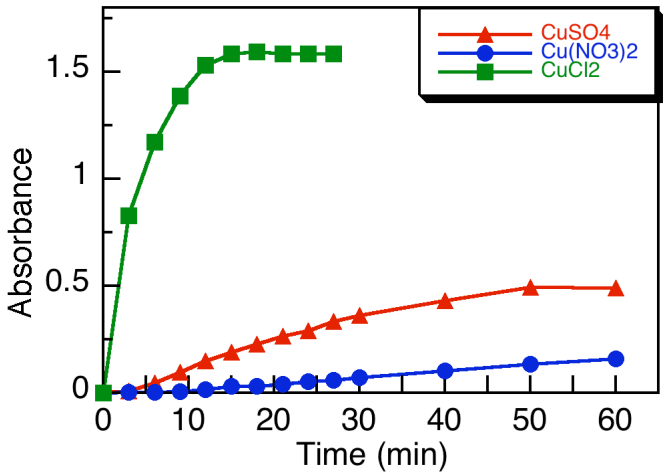

Figure 2.4 Growth of CuNP over time monitoring the absorbance maximum of the SPB of 0.66 mM $CuCl_2$, $CuSO_4$, and $Cu(NO_3)_2$.

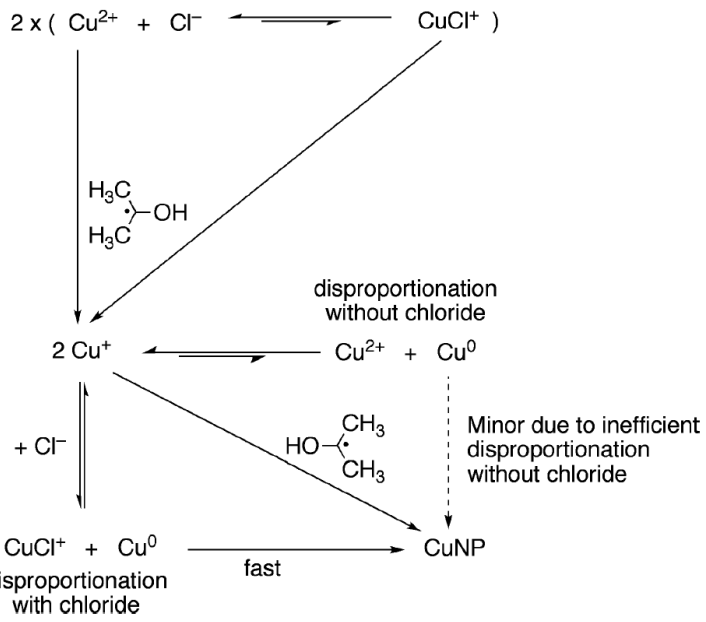

Figure 2.5 Proposed mechanism of CuNP synthesis in water in the presence of chloride.[6]

2.3.1.2 Stabilizers

The effect of different halides as stabilizers was studied as well as the concentration on the formation of CuNP from $CuSO_4$. By using NaCl as the source of the Cl^- ion, it was found that it was not concentration dependent, implying the catalytic role of the chloride ion (see Figure 2.6). With no NaCl, very few NP formed based on the observed low absorbance at the SPB of 0.08, and with a small amount of NaCl (0.08 mM) the absorbance increases 6-fold to 0.5 (Figure 2.6). The absorbance of the CuNP increases to 0.54 when the concentration of NaCl is nearly quadrupled to 0.3 mM indicating the catalytic role of the chloride anion.

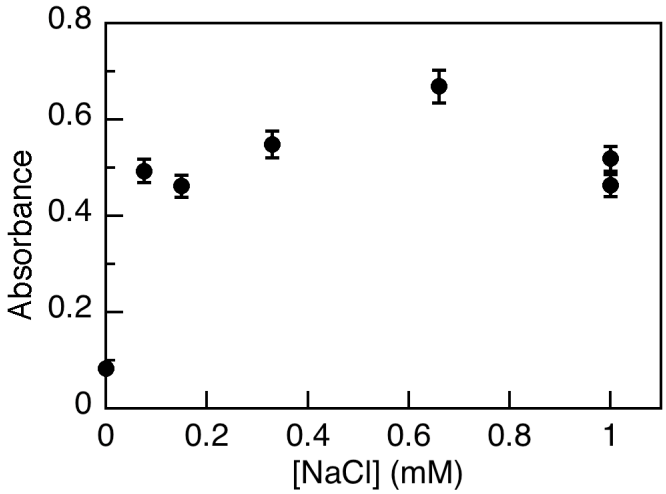

Figure 2.6 Absorbance of CuNP at the maximum SPB while changing the concentration of NaCl using 0.33 mM $CuSO_4$ solutions and UVA irradiation.

2.3.2 Synthesis in Organic Solvents

2.3.2.1 Synthesis

Synthesis of CuNP is of interest in organic solvents for increasing the applicability and the usefulness of organic solvents in industrial applications because of organic solvents' low boiling points and easy removal. Other studies have synthesized CuNP in acetonitrile-water solvent mixtures and found that the acetonitrile captures the CuNP and prevents oxidation.[2] It has been reported that acetonitrile stabilizes Cu^{+} ions, making their reduction to Cu^{o} more difficult than in water ($E°(Cu^{+}/Cu^{o})$= -0.29 V *vs.* SHE).[15,16] For this reason, I-2959 was not effective as a reductant and disproportionation was not the proposed mechanism as in the case of water.

Copper nanoparticles in this study were synthesized in acetonitrile using Copper (II) acetate, I-907 as the reducing agent and CTAC as a stabilizing agent. The photoproducts from Irgacure 907 are stronger reducing agents and I-907 absorbs more strongly in the UVB region (λ_{max}=300 nm), thereby producing more reducing radicals in a shorter amount of time. Both irradiation types (UVA and UVB) work for both photoinitiators (I-907 and I-2959), but because of availability of bulbs, stability of NP when reduced at a faster/slower rate, and effectiveness, UVA was used for I-2959 and UVB was used for I-907.

Using $Cu(OAc)_2$ in acetonitrile, no nanoparticles form without the use of CTAC (see Figure 2.7). Without CTAC, the absorbance remaining around 670 nm and 375 nm is that of the $Cu(OAc)_2$ and the absorbance less than 350 nm is that of the Irgacure. There is no CuNP SPB absorbance around 575 nm for the sample without CTAC.

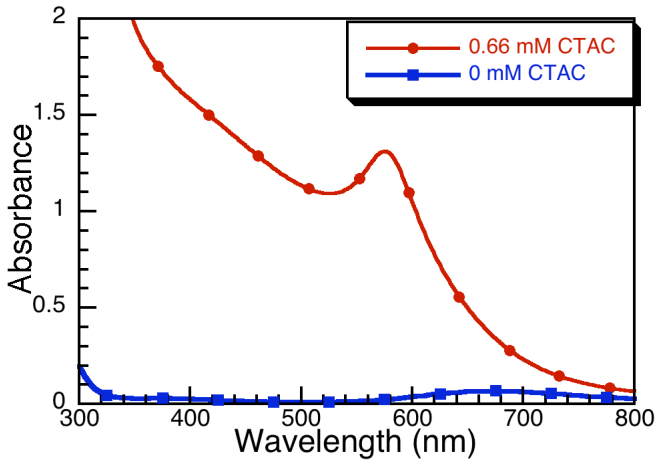

Figure 2.7 Absorbances of solutions containing 0.33 mM $Cu(OAc)_2$, 0.66 mM I-907, and 0 mM or 0.66 mM CTAC after 15 mintues of UVA irradiation (9 lamps) and 30 minutes of Ar-degassing.

The synthesis of CuNP in acetonitrile with CTAC as a stabilizer under UVA irradiation after degassing the solution with argon was monitored over time to see the appearance and growth of the SPB. Initially, the absorbance of the copper acetate is seen at 670 nm, around 8 minutes the growth of the SPB appears at 575 nm and the solution changes from blue to a pinkish colour. The SPB stops growing after 60 minutes of irradiation (see Figure 2.8).

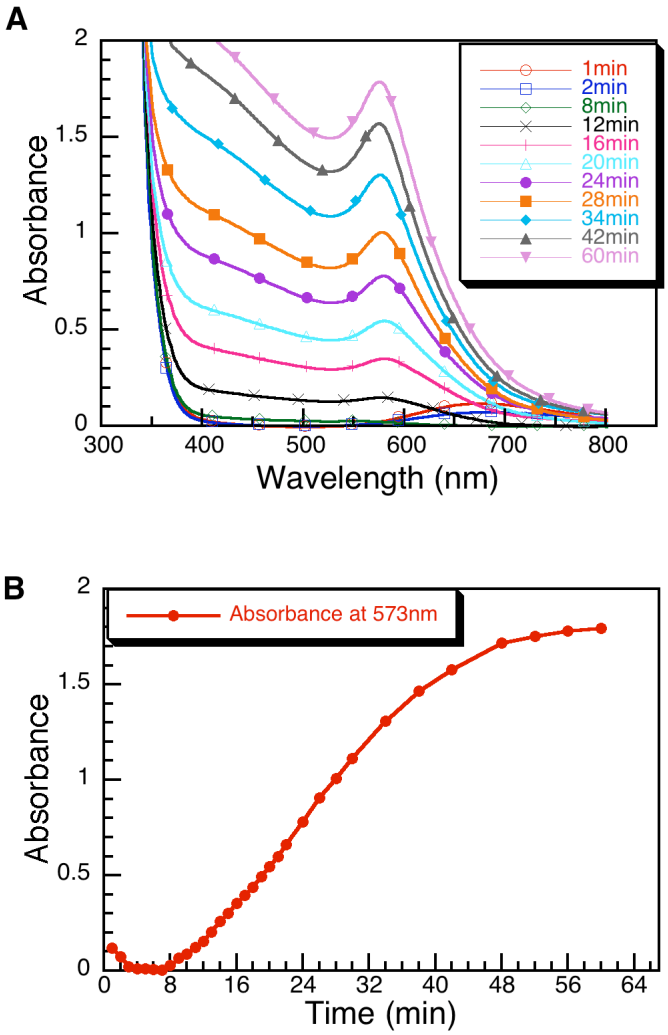

Figure 2.8 A: Monitoring the growth of the SPB of CuNP over time from 0 to 60 minutes of UVA irradiation using UV-Vis spectroscopy. Solution contains 0.66 mM $Cu(OAc)_2$, 1.32 mM I-907, 0.66 mM CTAC. B: Absorbance at the SPB maximum (573 nm) of the CuNP with time of irradiation.

There is an induction period between 0 minutes and 8 minutes when the SPB first appears. We propose this period as the reduction of all Cu^{+2} to Cu^{+} followed by the further reduction to Cu^{o} by the radical. There is also a nucleation period where the particles are too small to have a SPB, and once they aggregate and reach the critical size (around 15 atoms[17]) begin absorbing around 575 nm. After 4 minutes, the peak for $Cu(OAc)_2$ disappears, indicating the reduction of

Cu^{2+} and thus disappearance of its absorbance at 670 nm. After 12 minutes the peak for CuNP appears at 575 nm. It has been established that once CuNP begin to form, they catalyze the reduction of more Cu^{+}.[18]

Since I-907 absorbs in the UVB region of the electromagnetic spectrum, the difference in growth time and the resulting NP were investigated. A comparison of 8 UVA lamp and 4 UVB lamp irradiation of a solution of 0.66 mM $Cu(OAc)_2$, 0.66 mM CTAC, and 1.98 mM I-907 is shown in Figure 2.9. The NP formation is twice as fast with UVB irradiation forming in 30 minutes with half the lamps compared to UVA irradiation, which takes 60 minutes. Using 8 UVB lamps compared to 4 UVB lamps does not make a significant difference in the rate of formation of the NP (see Figure 2.9A).

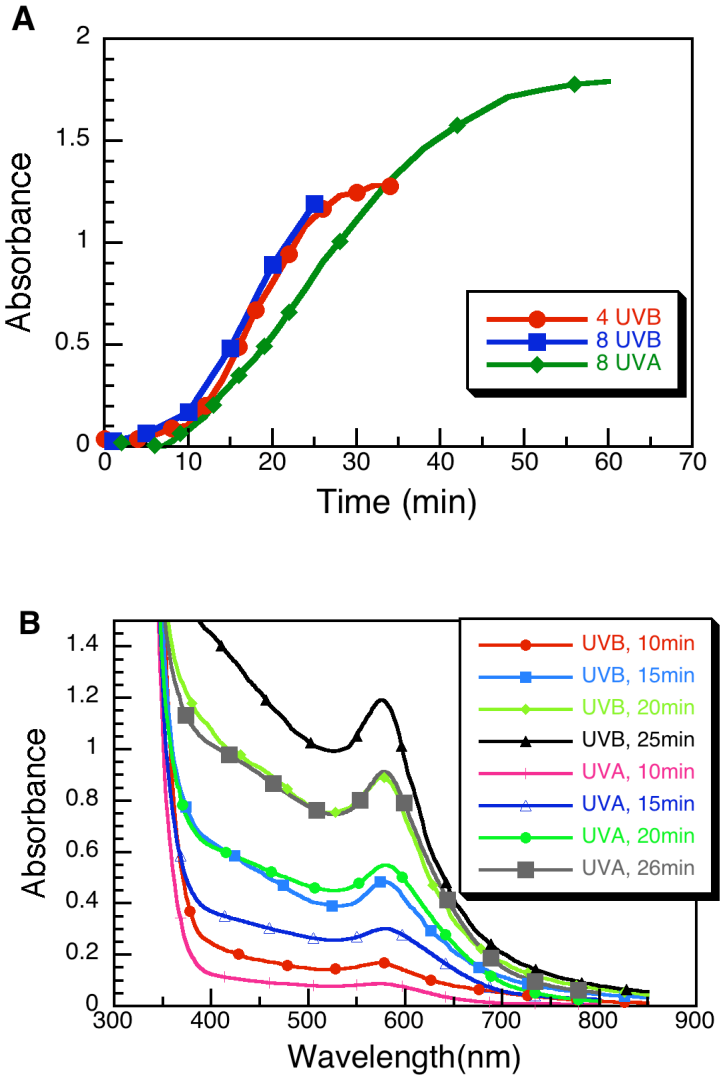

Figure 2.9 (A) Absorbance of CuNP at the SPB maximum *vs.* time for solutions of 0.66 mM $Cu(OAc)_2$, 1.98 mM I-907, and 0.66 mM CTAC with 8 UVA, 4 UVB, or 8 UVB. (B) Absorbance after specified irradiation times with UVA (8 lamps) or UVB (4 lamps).

The effect of concentration of CTAC was looked at to find the optimal concentration for a good yield of NP. Using a sample of 0.66 mM $Cu(OAc)_2$, 1.32 mM I-907, and changing the concentration of CTAC the absorbance and SPB maximum were monitored with UV-Vis spectroscopy. As the concentration of CTAC increased from 0.15 mM to 0.33 mM to 0.66 mM, the absorbance of the

SPB increased along with a simultaneous blue-shift (see Figure 2.10). As the concentration was increased further, from 0.66 mM to 0.99 mM, the absorbance decreased significantly. The CTAC concentration of 0.66 mM resulted in the narrowest and most blue-shifted absorbance at 575 nm (see Figure 2.10). SEM imaging in Figure 2.11 showed nanoparticles made with 0.66 mM CTAC have a mean diameter of 19 nm (± 7 nm). With 0.15 mM CTAC the mean size is 14.5 nm (± 8 nm). This increased absorbance could be because as more stabilizer is added (up to 0.66 mM), more particles are stabilized allowing more to form. There is more stabilizer present to associate with the particles as they form preventing growth of each particle, resulting in more particles of a smaller size. When you reach a certain point (0.99 mM) the concentration of the stabilizer is too high and it prevents more nucleation by getting in the way of reducing Cu^{+2} and Cu^{+} resulting in a low yield and slower formation of NP as can be seen in Figure 2.10B. Energy-dispersive X-ray spectroscopy (EDS) was done and confirmed the presence of elemental Cu, Figure 2.12. We proposed that the delay of SPB appearance between 0 and 10 minutes (Figure 2.10C) suggested that reduction from $Cu^{+} \rightarrow Cu^{o}$ may be solely a radical reduction in acetonitrile rather than disproportionation, and it is slowed by the presence of bulky stabilizers.

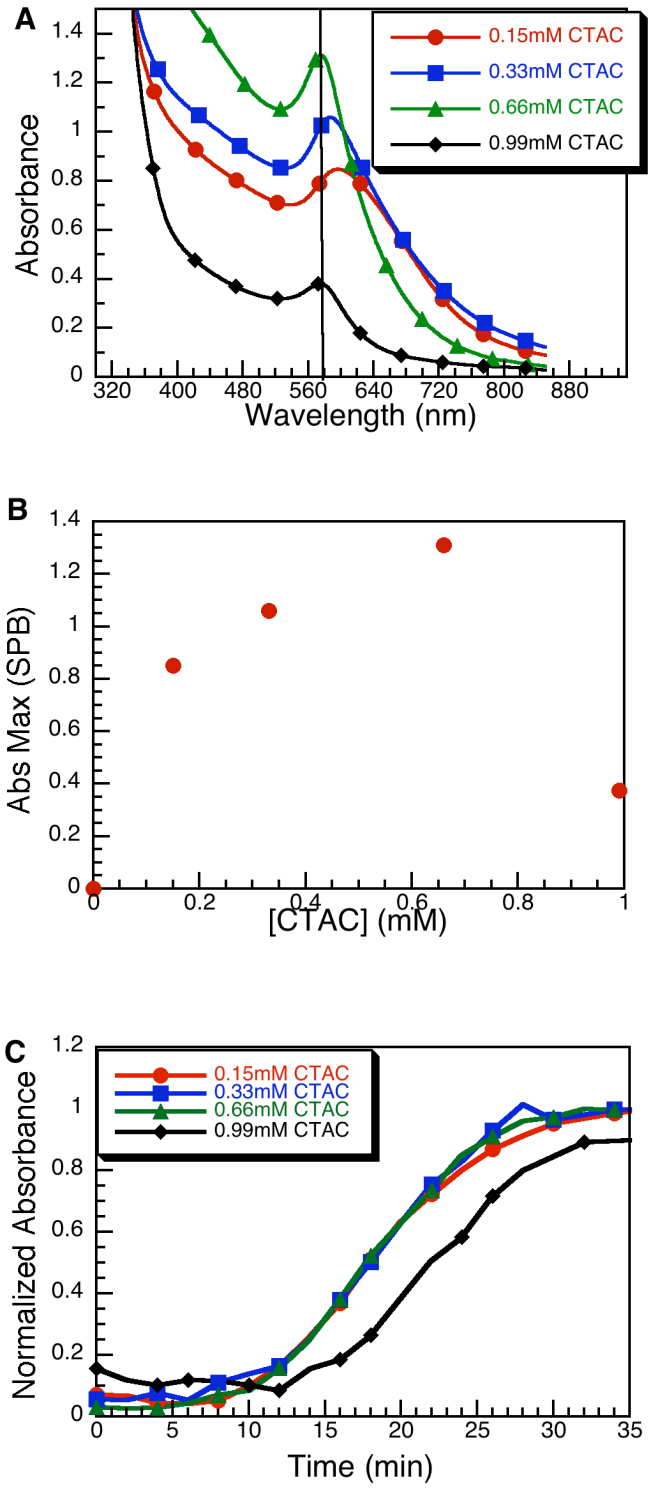

Figure 2.10 Solution of 0.66 mM $Cu(OAc)_2$ with 1.32 mM I-907, irradiated with 8 UVA lamps for 55 minutes. CTAC concentration varied from 0.15 to 0.99 mM. (B) Maximum absorbance at SPB of CuNP *versus* each concentration of CTAC (C) Normalized absorbance *vs.* time.

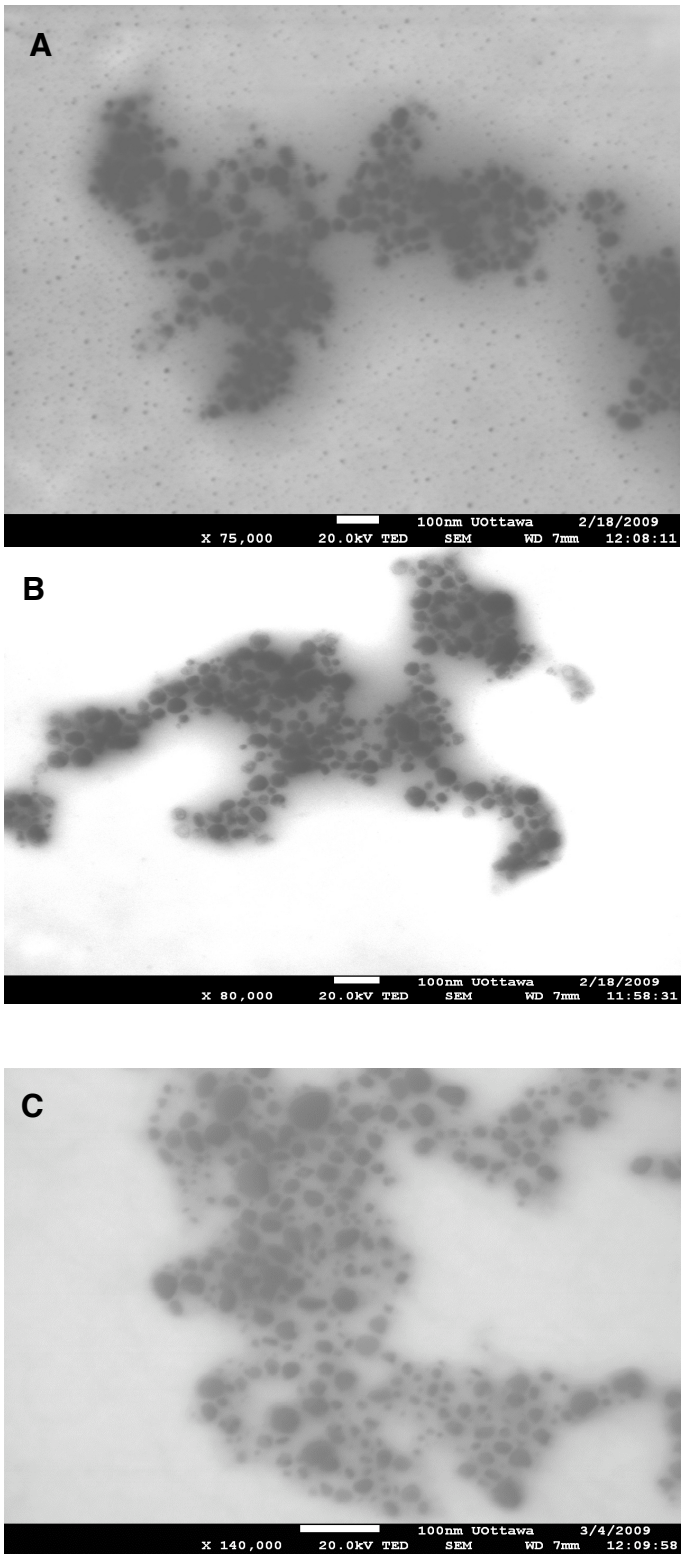

Figure 2.11 SEM images of CuNP with differing concentrations of CTAC. All three samples contained 0.66 mM $Cu(OAc)_2$, 1.32 mM I-907. A & B: 0.66 mM CTAC; C: 0.15 mM CTAC. Size bars in all images are 100 nm.

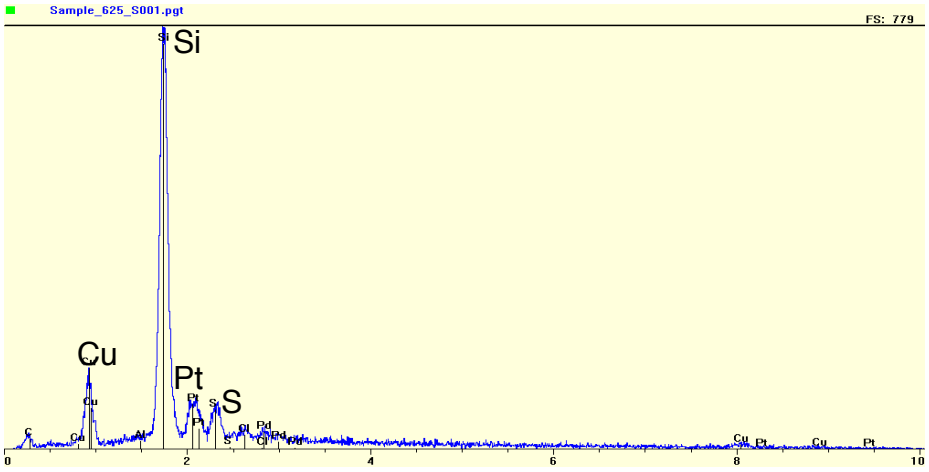

Figure 2.12 EDS spectrum of CuNP made with 0.66 mM CTAC and 1.98 mM of I-907. NP drop cast onto a silicon wafer.

2.3.2.2 Reducing Agent

The photochemical reducing agent commonly used in our lab is I-2959, but I-907 is also able to reduce metal salts to form nanoparticles. The strongly reducing α-aminoalkyl radical produced is able to reduce $Cu(OAc)_2$ to Cu^o in acetonitrile (see Scheme 2.1) where I-2959 is not effective in the reduction. The concentration of I-907 plays a role in the position of the final SPB and the final absorbance. With more Irgacure, the SPB is more blue-shifted, which may indicate smaller nanoparticles formed[19,20] (see Figure 2.13). Also, a higher yield of nanoparticles is achieved with a higher concentration of Irgacure. With a 2:1 ratio of I-907:Cu^{+2} (stoichiometric amount), the SPB appears at 580 nm and a lower absorbance than with a 3:1 or 4:1 ratio (see Figure 2.13A). With a 3:1 ratio of I-907:Cu^{+2}, the SPB maximum position was shifted to ~572 nm with a doubled

final absorbance (from 0.7 with a 2:1 ratio to 1.36) as seen in Figure 2.13A. This is likely because more reducing radicals are produced with the same dose of light at one time allowing more nucleation centres to form. This results in more NP of a smaller size. It could also be explained by the increased amount of amine stabilizers coming from the I-907 photoproducts, which could be aiding in the CuNP stabilization as the concentration of I-907 increases. Interestingly, the concentration of the reducing agent does not affect the rate of nanoparticle formation (see Figure 2.13B). This could be because in all cases Cu^{+2} is being reduced to Cu^{+}, but they still need to be subsequently reduced to Cu^{o} by the α-amino alkyl radical and there is a lag as the nucleation centres form and become large enough to support a SPB.[17] The lowest concentration of I-907 (1.32 mM) had the shortest nucleation time since there are likely less nucleation centres formed because of the lower number of reducing radicals produced. Because there are less nucleation centres, there are less centres for addition and further Cu^{+} reduction will occur more likely on these centres forming larger NP that support a SPB faster (see Figure 2.13B).

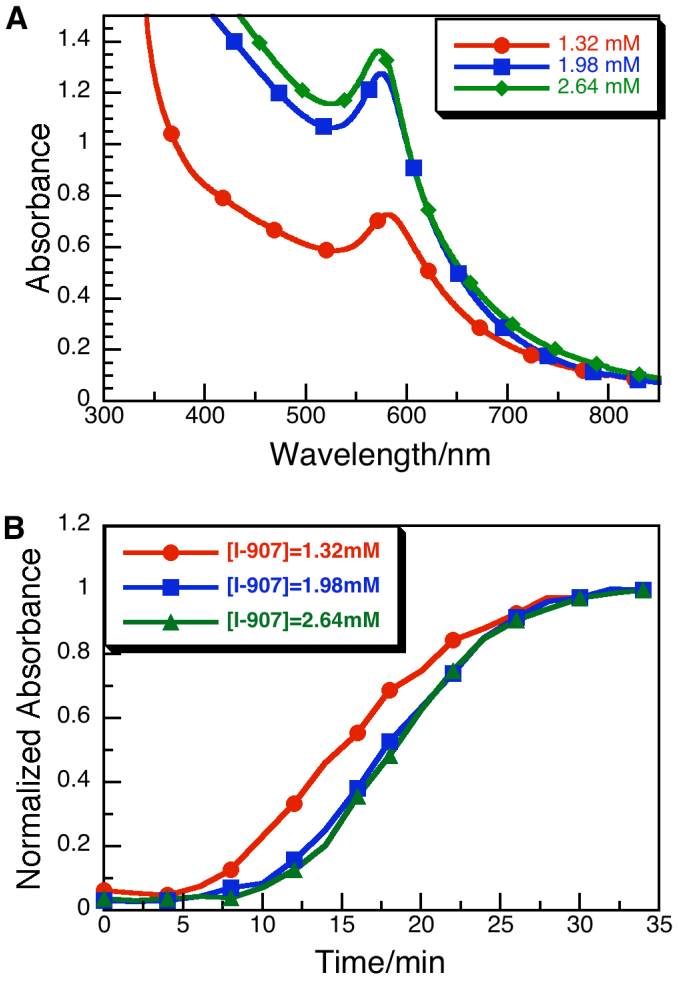

Figure 2.13 Solution of 0.66 mM $Cu(OAc)_2$, 0.66 mM CTAC, and 1.32 mM, 1.98 mM, or 2.64 mM I-907 (A) after 35min irradiation 4 UVB lamps. (B) Normalized Absorbance of the SPB maximum of each I-907 concentration with time. Plot is normalized to the maximum absorption of each I-907 concentration in A.

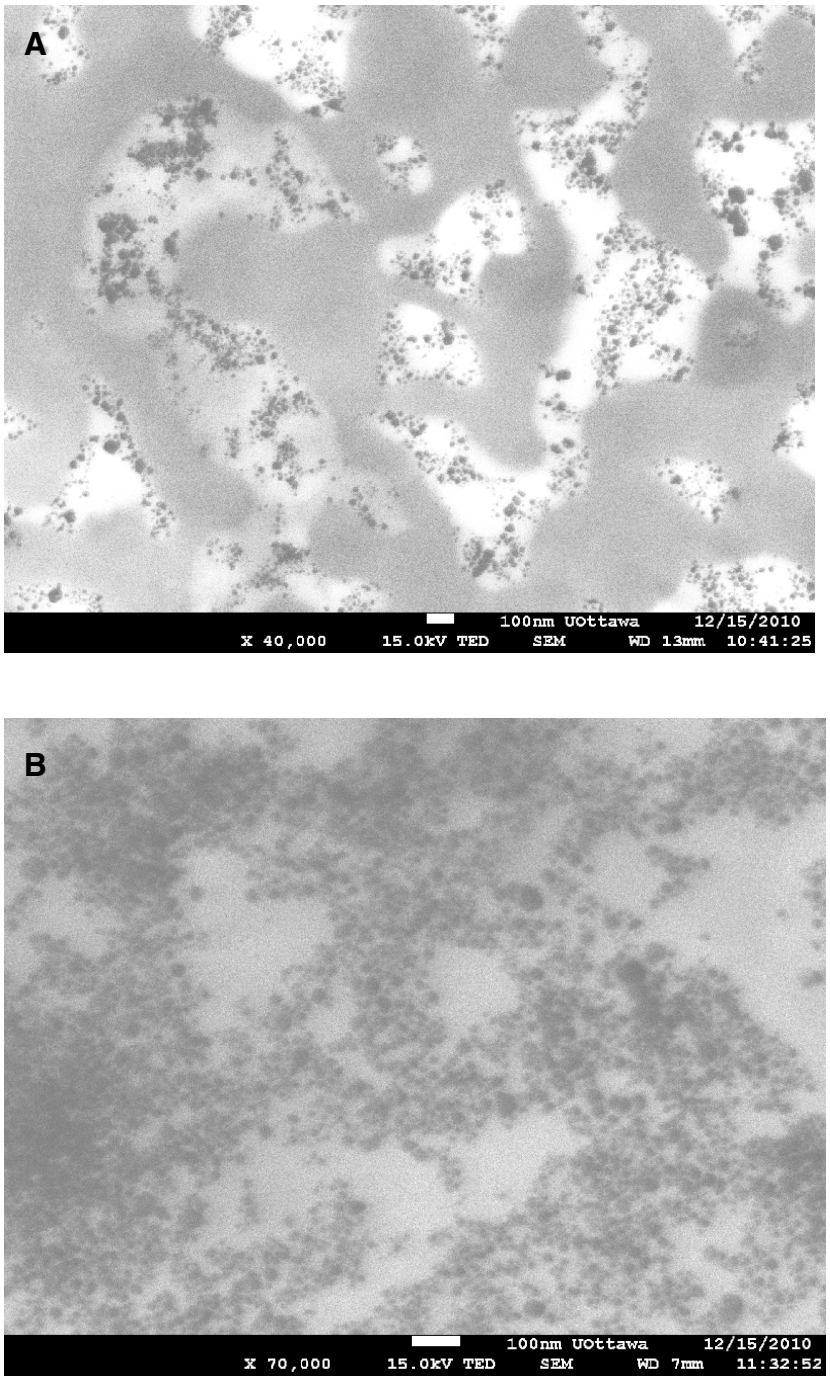

Figure 2.14 SEM images of CuNP formed with 0.66 mM $Cu(OAc)_2$, 0.66 mM CTAC and 1.32 mM I-907 (A) or 1.98 mM I-907 (B). Average particle size for A is 17 nm (± 10 nm) and for B is 10 nm (± 3 nm). Scale bars indicate 100 nm.

2.3.2.3 Stabilizers

Different stabilizers were tested to try to find optimal conditions for the growth of CuNP as well as prevent their oxidation. As seen in the case of water, the chloride ion is an effective stabilizer for CuNP in MeCN as well. In attempts to better stabilize the NP to the atmosphere, other stabilizers were studied, including TOPO (trioctylphosphine oxide), cyclohexylamine, thiophene, and PVP (Molecular weight: 55K and 10K). These were also used in attempts to grow a shell around the CuNP of another metal (Au or Ag.) Cyclohexylamine, thiophene, and PVP yielded some NP but the colour was more grey and the SPB was red-shifted to around 585 nm or 590 nm in the case of TOPO, likely indicating larger particles.[19,20] It is even more red-shifted with the 10K PVP to 604 nm compared to 587 nm with the 55K PVP. These stabilizers were not further explored because they were shown to be ineffective at stabilizing smaller CuNP and often lead to precipitation of the NP in solution.

Our attention turned to stabilizers containing a halide anion to see how the different counter anions and lengths of alkyl chains would affect the NP. The counter ion of the ammonium stabilizer showed large variations on the SPB maximum as well as the rate of NP formation. When comparing CTAC with CTAB under UVB irradiation (4 bulbs), the SPB maximum of CTAB is more blue-shifted (572 nm), narrower, and a higher intensity with the bromide counter anion of CTAB than with the chloride counter anion of CTAC (SPB maximum 575 nm), (Figure 2.15). This indicates smaller,[19,20] more monodisperse NP, as seen via

SEM (Figure 2.16). SEM indicated the average NP size with CTAB was 16 nm (± 11 nm) whereas for CTAC the average NP size was 27 nm (± 18 nm). The reason for the increased monodispersity and smaller NP size with the bromide counteranion is not known, but could be because the chloride ion is smaller and has a stronger electric field, attracting it to the ammonium cation.[21] The ammonium cation of CTAC is closer associated and may hinder its ability to effectively stabilize the NP at a smaller and more monodisperse size compared to CTAB.

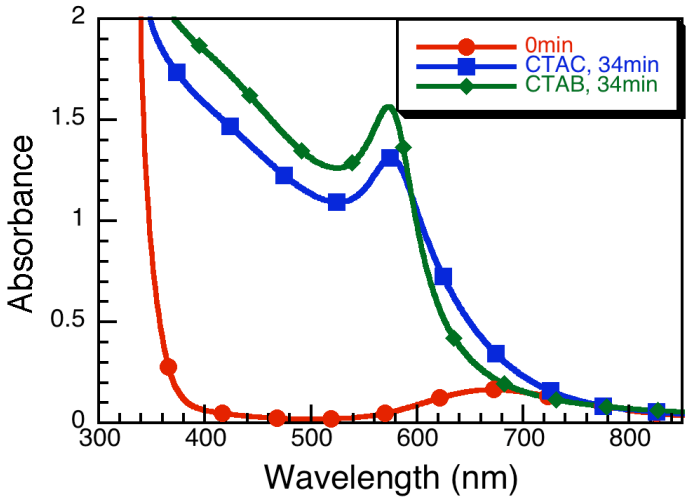

Figure 2.15 Final absorbance spectra of CuNP from solutions of 0.66 mM $Cu(OAc)_2$, 1.32 mM I-907, and 0.66 mM CTAC or CTAB. Red trace denotes samples before irradiation.

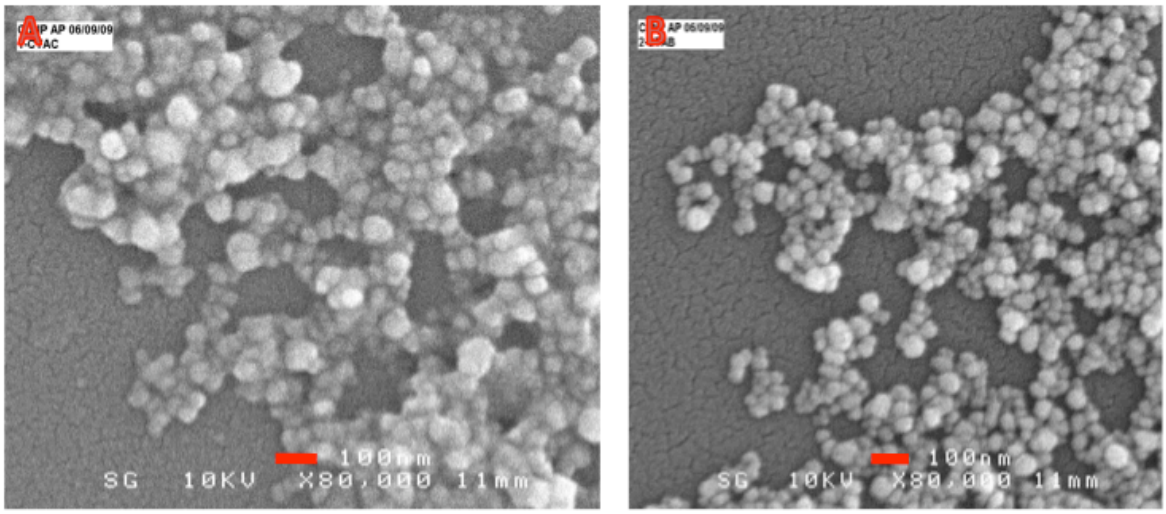

Figure 2.16 SEM image of the NP above. A: CTAC, B: CTAB. Scale bar in each is 100 nm.

The effect the bromide ion had on the position of the SPB provoked further investigation into stabilizing agents with different counter anions and cations. To investigate the counter ammonium cation, different alkylammonium salts with chloride counterions were investigated. When looking at the effects of different alkyl substituents from the ammonium salt using the bromide counter anion, there were noticeable differences depending on the length of the alkyl chain and the structure of the ammonium salt. Stabilizers CTAB, TMABr, TBABr, THABr, and TOABr were examined to see how they affected the NP formation. The most blue-shifted absorbance was that of THABr at 570 nm (see Figure 2.17A). The others were fairly close with CTAB and TOABr at 572 nm, TMABr and TBABr at 571 nm. The SPB positions are likely shifted as a result of the different medium of alkyl chains surrounding the NP, which has been shown for AgNP as the alkyl chain length changes.[22]

CTAB shows the highest absorption after 34 minutes of irradiation but also takes the longest to complete the growth (see Figure 2.17). The rates of formation of all the NP are similar except for CTAB, which takes longer to complete than the other bromide alkylammonium salts (see Figure 2.17B). The induction period for the CTAB is also much longer than with the other stabilizers. For CTAB it is around 8 minutes, whereas the others have induction periods around 3 or 4 minutes (see Figure 2.17B). The formation of the NP may be slower with the CTAB because of its structure of three short chain methyl groups and one longer alkyl group (cetyl), which cause the anion to associate closer preventing it from immediately stabilizing the NP. A previous report[21] showed that the association between the anion and cation in alkylammonium salts in acetonitrile changes depending on the alkyl substituents. They found the shorter the chains, the closer the association to the counter anion.[21] Perhaps the CTAB has a close association with its counter anion because of its short methyl chains keeping the ammonium cation and bromide anion close preventing immediate stabilization of the NP by the Br^-. Another possible explanation could be that as the Cu^{+2} is reduced to Cu^o by subsequent α-amino alkyl radical reduction, the remaining Cu^+ is attracted to the negative media around the Cu^o atom and the CTAB may be better at encapsulating or surrounding it and temporarily preventing the α-amino alkyl radical from further reducing the Cu^+ and slowing the process of nucleation (see Figure 2.18).

Tetrabenzylammonium chloride (TBenzylACl) was also tested as a potential stabilizer. It had a short induction period (see Figure 2.19B) but formed NP with a more red-shifted absorbance and more scattering (see Figure 2.19A).

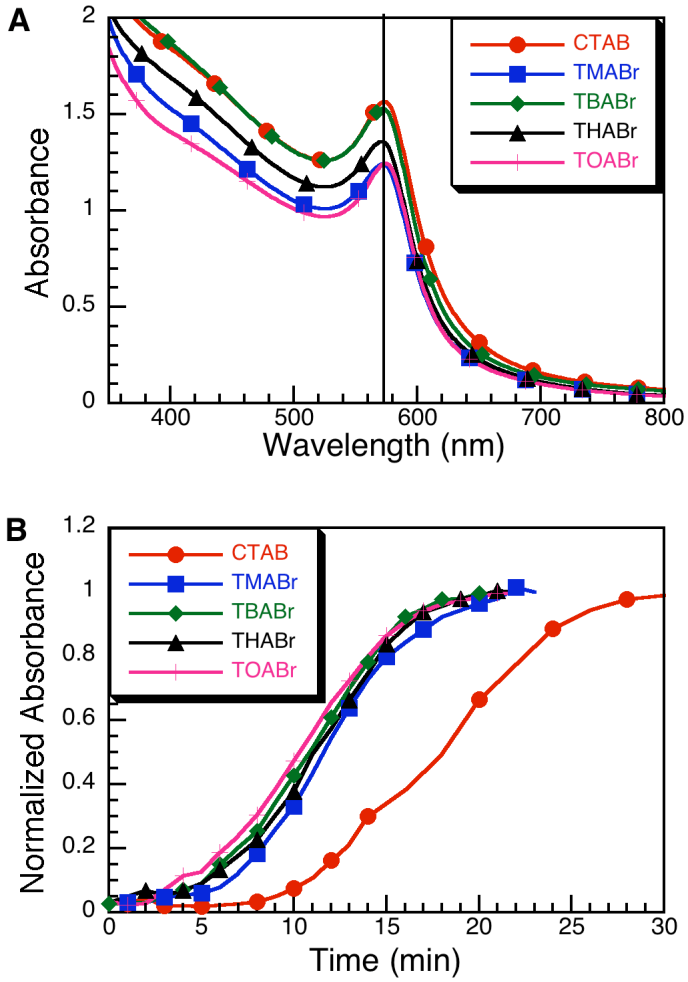

Figure 2.17 A: Final absorption of CuNP after irradiation of degassed MeCN solutions of 0.66 mM $Cu(OAc)_2$, 0.66 mM stabilizer, and 1.98 mM I-907 with 4 UVB bulbs. CTAB: 34 minutes, TMABr, TBABr, THABr, TOABr: 23 minutes. B: Normalized absorption over time of CuNP formation with each alkylammonium bromide salt at the SPB maximum. B is normalized to the maximum absorption achieved in A.

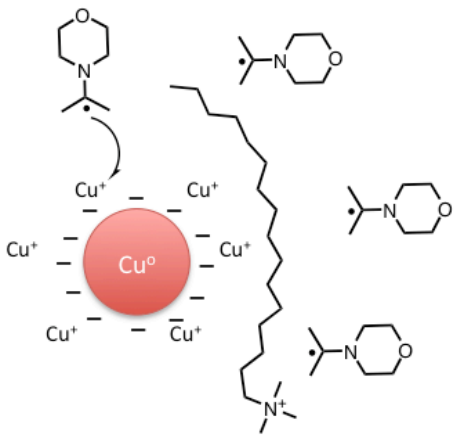

Figure 2.18 Proposed cartoon mechanism for slowed nucleation and growth of CuNP using CTAB. Not to scale.

The difference between the bromide and chloride counter anions triggered testing the iodide counter anion. Figure 2.19 shows that the CuNP formed with TBAI have the most blue-shifted absorbance at 568 nm compared to CTAC and CTAB. The rates of formation in the presence of TBABr and TBAI are similar but TBAI has a much shorter induction period, the particles show a SPB immediately, whereas for TBABr it takes 3 minutes before the SPB appears and 9 minutes for TMACl (see Figure 2.19B).

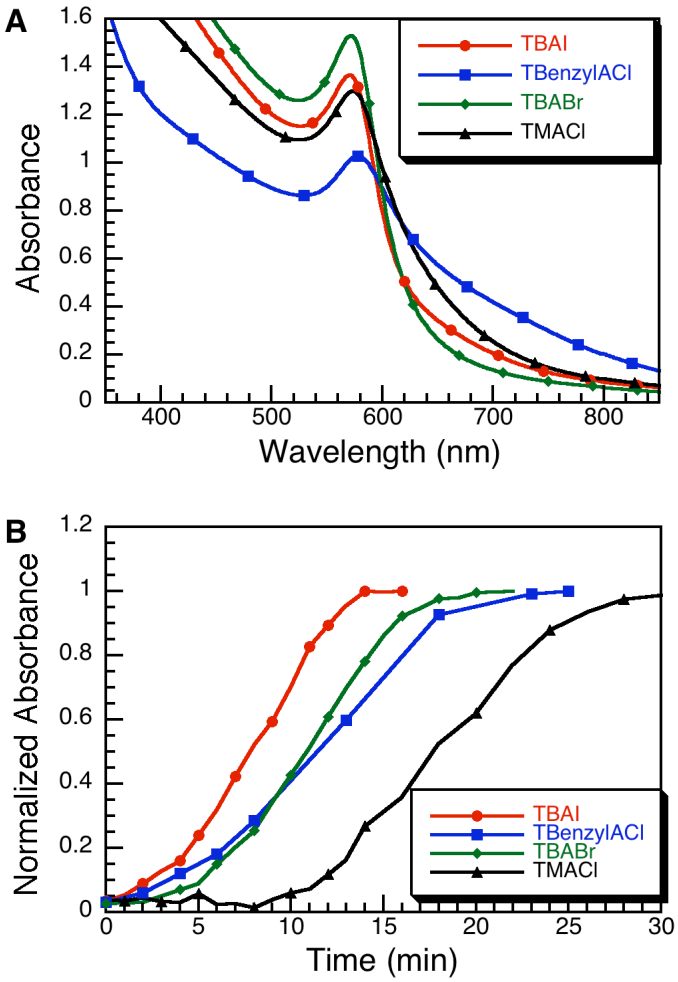

Figure 2.19 A: position of SPB after reduction completed. B: Normalized absorbance at the SPB maximum with respect to time of irradiation. B is normalized to the maximum absorption reached in A.

It seems that the counter anion plays a large role in the initial rate of NP formation. It could be by catalyzing the nucleation and changing the rate at which the reduced Cu^{o} coalesce to form clusters large enough to support a SPB. It could also be the anion's association with the Cu^{+} species and how easily the Cu^{+} can undergo another electron reduction to Cu^{o}. The catalytic effects increase

as you move down the periodic table with $Cl^- < Br^- < I^-$ in terms of the time at which initial NP formation begins. This could reflect the size and electric field around the anion catalyst. As the catalyst anion becomes smaller and its electric field increases, it is more tightly bound to the ammonium cation centre and less associated with the NP. It is also possible that the close ammonium cation blocks further nucleation of Cu^o on the surface. A previous study comparing iodide and bromide in alkylammonium salts found bromide is more closely associated potentially because of a higher electric field around it and its smaller size.[21] This ignores solvation effects of the ions in the acetonitrile. Another explanation could be that the chloride anion binds strongest with the Cu^o as it is nucleating and occupies sites where more Cu^o can add in the nucleation period, slowing the growth of the NP.[23]

The main difference between the growth of CuNP in the presence of the chloride and bromide counter anion with the TMA salt is in the induction period during nucleation (see Figure 2.20). The growth period for both has a similar slope, indicating once nucleation is done and the size of the NP is large enough to support a SPB, the rates for both are the same. The different induction periods indicate that Cu(I) → Cu(0) is counter anion dependent since the absorbance of Cu(II) at 670 nm disappears immediately. The delay of NP formation indicates that Cu(I) → Cu(0) is a radical reduction not disproportionation of Cu(I) + Cu(I) → Cu(0) + Cu(II) (see Chapter 1).

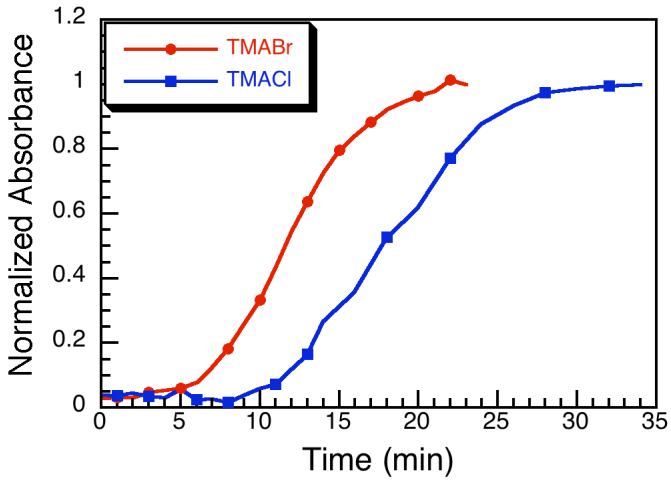

Figure 2.20 Normatlized growth of CuNP stabilized with TMABr and TMACl comparing the maximum absorbance of the SPB of CuNP with time. These are normalized to the maximum absorption reached in each case.

2.3.2.4 Copper Nanoparticle Oxidation

One of the main challenges of working with CuNP is their oxidation, which happens quickly when exposed to air. The effect of the different stabilizers on the oxidation time of CuNP was explored but showed limited reproducibility. The CuNP were made in a quartz cuvette with a neck for degassing. Once the NP were made, the cuvette was opened to the atmosphere and placed in the Cary spectrometer to monitor the SPB maximum every minute.

When first looking at the tetraalkylammonium bromide salts, it was seen that as the length of the alkyl chain increased, the time for oxidation increased (see Figure 2.21). The total oxidation times, which is the time it takes for the SPB of CuNP to disappear completely from the absorbance spectrum, for TMABr, TBABr, THABr, and TOABr are 100, 110, 130, 135 minutes respectively (see Figure 2.21 and Table 2.1) It seemed as the length of the alkyl chain increased, the oxidation time slowed by 45 minutes in the case of TMABr and TOABr. To see if a different arrangement of alkyl chains would have an effect, benzyl triethylammonium chloride (BenzylTEACl) was used to see if the benzyl group would potentially stabilize the CuNP further through π interactions with the aromatic ring. The BenzylTEACl did not lengthen the time for total oxidation compared to TOABr, it was only a slight improvement over TMABr with the oxidation beginning at 40 minutes. The oxidation time increases as the length of the alkyl chain on the ammonium salt increases (time for oxidation

methyl<butyl<heptyl<octyl) (see Figure 2.21). This could be a result of the longer alkyl chain interacting with the nanoparticle, shielding it temporarily from oxygen and protecting it from oxidation. When comparing CTAC and CTAB, the oxidation time is greater for the bromide containing ammonium salt. This could be because the chloride anion is more closely associated with the alkylammonium cation and it is a poor stabilizer of the NP, as seen in their formation compared to bromide or iodide, making the chloride stabilized NP less stable and more open to oxidation. The oxidation time is faster for CuNP in acetonitrile than it is in water, which can be explained by the higher solubility of oxygen in MeCN compared to water (8×10^{-3} mol/L *versus* 1.2×10^{-3} mol/L at 25°C, respectively).[24,25] It is worthwhile to note that during these experiments, the cuvette was opened to the air but was not stirred or agitated throughout the duration of the experiment. For more reproducible results and accurate results, stirring needs to take place. This, however, could not be done because of complications incorporating stirring with the spectroscopy instrument.

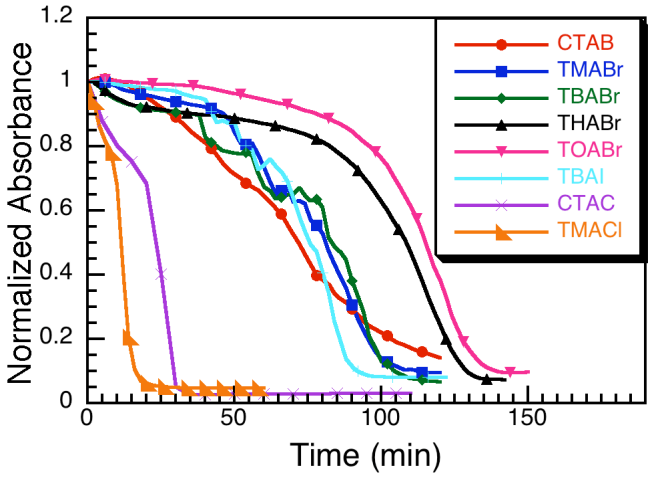

Figure 2.21 Normalized absorbance at the SPB maximum for each sample monitored over time after opening the cuvette to air, unstirred. Respective absorbance spectra can be found in Figure 2.17 and Figure 2.19.

Table 2.1 Table summarizing time for growth of NP, time when oxidation began, and time for complete oxidation of the CuNP with the different stabilizers. Data taken from figures 2.18, 2.20, and 2.22.

Stabilizer	Growth Time of NP (min)	Time when Oxidation begins (min)	Time for Complete Oxidation (min)
CTAB (570 nm)	32	20	120
TMABr (572 nm)	23	55	100
TBABr (570 nm)	20	75	110
THABr (570 nm)	21	95	130
TOABr (572 nm)	22	100	135
TBAI (569 nm)	13	60	85
CTAC (575 nm)	34	25	30
TMACl (573 nm)	30	8	20
BenzylTEACl (578 nm)	25	40	100

It is important to note that when the CuNP oxidize, they return to their original state as Cu^{+2} and do not make CuO NP, which absorb around 800 nm.[12,13] This is evident from the colour reverting back to the original blue as before irradiation and the absorbance spectra seen in Figure 2.22. The reversion back to the original Cu^{2+} rather than CuO has been noted in other reports as well.[26]

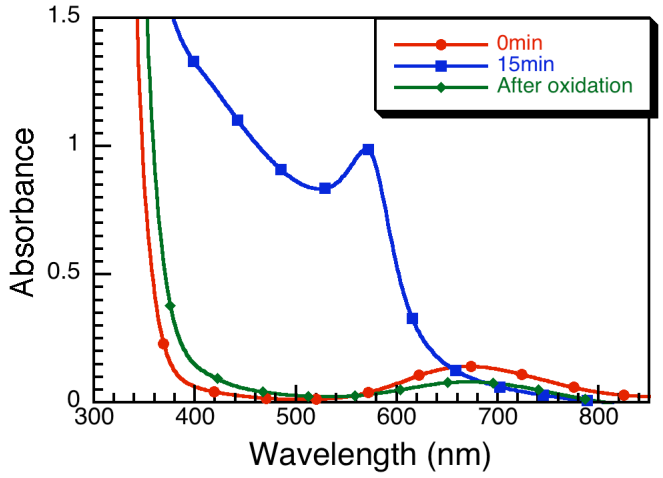

Figure 2.22 Spectra of CuNP solution before irradiation and before and after oxidation. 0.66 mM $Cu(OAc)_2$, 1.98 mM I-907, and 0.66 mM TOABr in deaerated MeCN.

2.3.3 Bimetallic Cu/Ag NP

In attempts to protect the CuNP from oxidation, bimetallic Cu/Ag were made in the hope of capping the CuNP with a small amount of Ag to protect from oxidation making a core-shell (Cu-Ag) type structure (see Figure 2.1 for image). Making bimetallic structures was possible, but characterizing the type (core-shell, alloy, segregated, etc. (see section 2.1.2 and Chapter 1)) was challenging. The reduction potentials of the two metals do not promote the desired core-shell structure. With the reduction potentials of +0.34 V for Cu^{o}/Cu^{2+} and +0.799 V for Ag^{o}/Ag^{+} (*vs.* SHE), silver will be reduced first followed by copper leading to the formation of Ag-core Cu-shell.[1,27]

2.3.3.1 Synthesis

Different syntheses were attempted to obtain a core-shell type structure and control the morphology (all methods are briefly described in Table 2.2). The first was irradiation of both salts at the same time with a solution of 0.66 mM $Cu(OAc)_2$, 0.33 mM $AgNO_3$, 1.65 mM I-907, and 0.66 mM CTAC in MeCN followed by Ar-purging and UVA irradiation (Referred to as method 1 or M1). The ratio of Cu:Ag was varied to optimize the synthesis. In all attempts the $Cu(OAc)_2$ concentration was kept at 0.66 mM and the ratio of Cu:Ag was 1:1, 1:2, or 2:1. Figure 2.23 shows that both SPB appear when the ratio is 2:1 Cu:Ag indicating that both nanoparticles have formed. SEM images of the 2:1 Cu:Ag NP can be seen in Figure 2.24 and have a size of 25 nm ± 10 nm. They are polydisperse

and no discernable difference in the SEM images can be made between the two metals to identify them (see Figure 2.24).

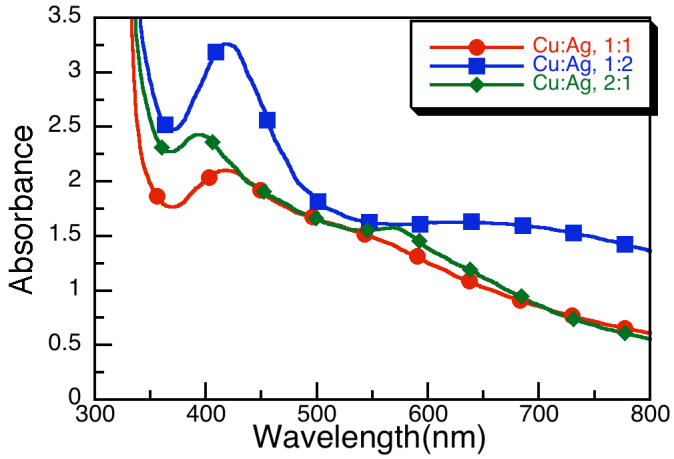

Figure 2.23 Different ratios of Cu:Ag made together with a stoichiometric amount of I-907 and 0.66 mM CTAC in MeCN with 20 minutes of 8 UVA lamp irradiation after degassing with Ar. $Cu(OAc)_2$ concentration was kept constant at 0.66 mM.

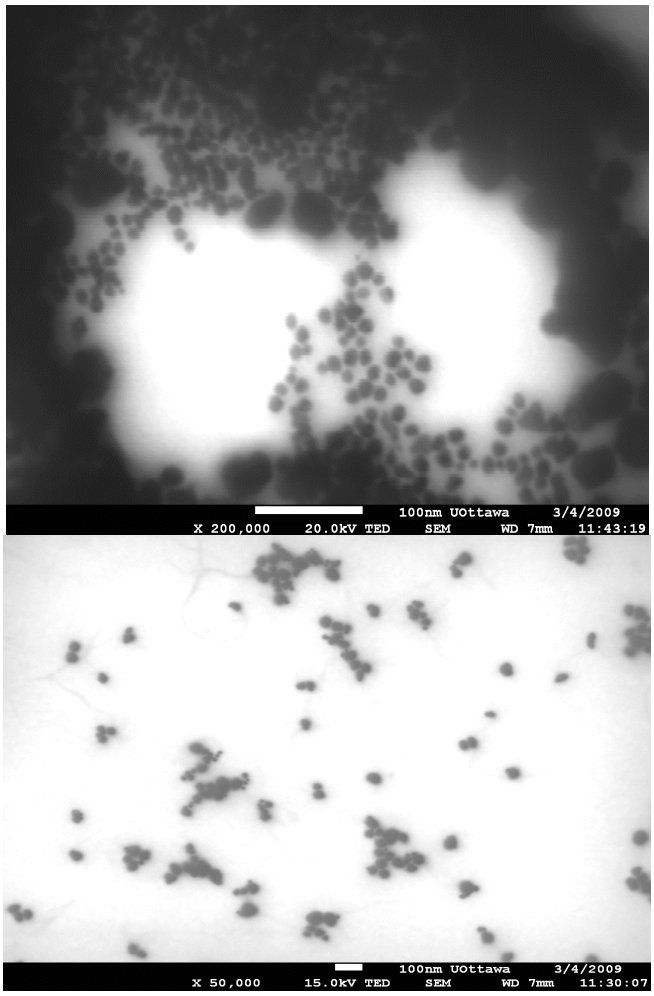

Figure 2.24 SEM images of (M1) Cu/Ag bimetallic NP (0.66 mM $Cu(OAc)_2$, 0.33 mM $AgNO_3$, 0.33 mM CTAC, 1.65 mM I-907). No difference can be seen between the CuNP and AgNP in these images.

The concentration of CTAC was also varied to achieve optimum conditions. With 2:1 Cu:Ag solutions, the CTAC concentration was varied between 0 mM and 0.66 mM. With no CTAC, no NP of any type formed but scattering across the entire spectrum was noted (see Figure 2.25). With 0.15 mM CTAC, no absorption for CuNP appeared, only a broad absorption with a maximum around 670 nm where the $Cu(OAc)_2$ absorbs (see Figure 2.25). With 0.33 mM of CTAC, a SPB for CuNP appeared around 580 nm, but has low intensity along with absorption at longer wavelengths. At a 0.66 mM CTAC

concentration, the results improved significantly with two SPB for AgNP and CuNP and less scatter at longer wavelengths (see Figure 2.25).

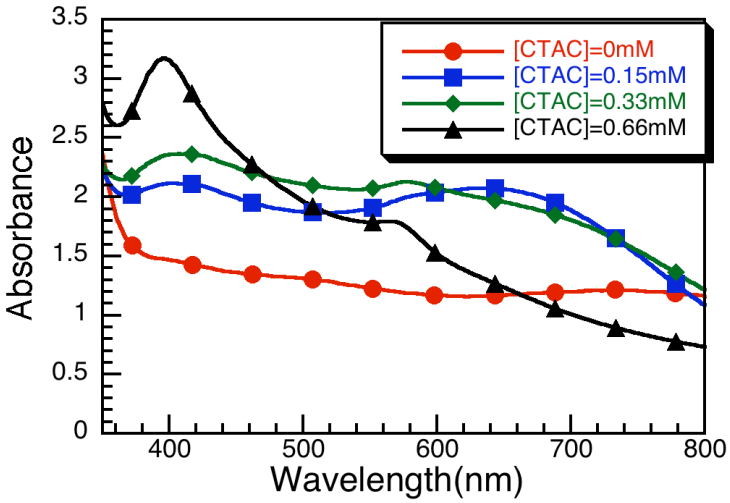

Figure 2.25 Varying the CTAC concentration after degassing solutions of $Cu(OAc)_2$ (0.66 mM), $AgNO_3$ (0.33 mM), and I-907 (1.65 mM) with Ar in MeCN and irradiating with 8 UVA lamps for 20 minutes.

In this method, the $AgNO_3$ reduces first as expected from the reduction potential (0.799 V[27] for Ag^o/Ag^+ compared to 0.34 V[1] for Cu^o/Cu^{+2} *vs.* SHE) followed by the $Cu(OAc)_2$, giving rise to two SPB at 395 nm and 568 nm, respectively (see Figure 2.26). When monitoring the kinetics of formation, the AgNP first showed a SPB at 408 nm and subsequently blue-shifted to 395 nm after about 10 minutes, the same time that the CuNP SBP began appearing (see Figure 2.26). Previous reports of core-shell NP state that blue-shifting occurs for the core of the NP when the outer shell is formed and is related to an increase in the thickness of the shell and the dielectric constant.[28] The CuNP SPB was blue-shifted with respect to where it would normally fall under monometallic conditions

(Figure 2.26), which could be a result of the interaction with AgNP if they are the core because reports of core-shell have noted similar results explained by plasmon hybridization.[28] The outer layer nuclei will have a stronger attraction to the outer electrons of the core than the ligands in solution, resulting in coupling that increases the energy required for oscillation of the electrons.[28] If these Cu/Ag NP are core-shell, the silver is the core and the copper nuclei will be attracted to the electrons in the silver increasing the oscillation energy and blue-shifting its absorbance as seen in Figure 2.26.

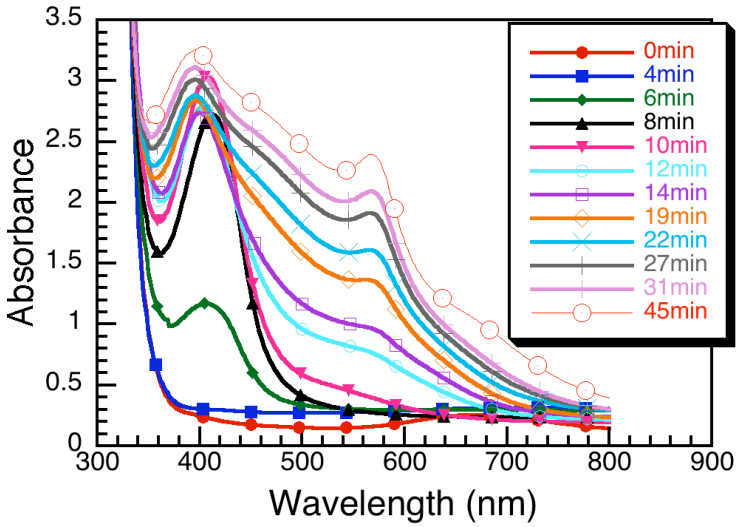

Figure 2.26 Kinetics of (Method 1) Cu/Ag NP growth in degassed MeCN from 0 to 45 minutes. 0.66 mM $Cu(OAc)_2$, 0.33 mM $AgNO_3$, 1.65 mM I-907, and 0.66 mM CTAC with 8 UVA lamps.

2.3.3.2 Rate

The rate of NP growth was investigated under monometallic and bimetallic conditions to see if the presence or absence of another metal or salt influenced the rate of growth the NP.

Silver nanoparticles will not form readily on their own without a stabilizer in solution and do not form with CTAC as the stabilizer, so the rate could not be compared in the same way as CuNP. Using a Cl^- or Br^- containing stabilizers can be a problem since AgCl and AgBr will precipitate in solution.[29] Silver NP will form in a solution containing the copper salt and stabilizer if irradiation is stopped before CuNP begin forming (before SPB is seen) but are not stable to oxidation and oxidize within 8 days (see Figure 2.27). The $Cu(OAc)_2$ must be assisting the formation of the AgNP, but not enough to prevent eventual oxidation. When using chloride or bromide containing stabilizers, the solution of Cu/Ag turned a bit cloudy, but after irradiation, both CuNP and AgNP are formed. If the solution is filtered before irradiation to remove AgCl/Br precipitate, no NP form. AgNP have been made in water using CTAC[28] or CTAB[30] as a stabilizer. The AgCl precipitate was noted but reported to dissolve over the course of the reaction,[28] which was also the case in this study with Cu/Ag NP. Before irradiation, Cu/Ag solutions were a cloudy blue colour and upon irradiation became transparent.

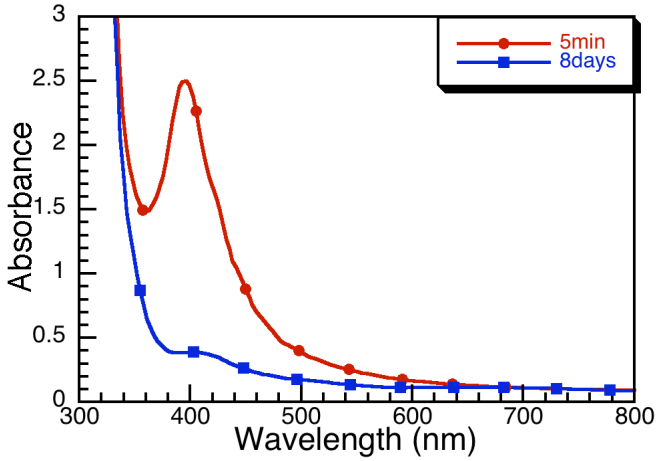

Figure 2.27 Silver nanoparticles made by irradiating a solution of 0.33 mM $AgNO_3$, 0.66 mM $Cu(OAc)_2$, 1.65 mM I-907, and 0.66 mM CTAC in de-aerated MeCN for five minutes with 8 UVA lamps. Left in dark for 8 days, and spectrum taken again.

When monitoring CuNP made alone in solution, their rate of formation is slower than when AgNP are already in solution (in bimetallic conditions, the Ag reduces first) (see Figure 2.28). There is still an induction period of nucleation before a SPB is supported in the bimetallic system but once growth begins the rate of formation of the CuNP is greatly affected by the presence of AgNP (see Figure 2.28). The copper nanoparticles still have the same induction period regardless of the presence of AgNP, but the CuNP made in the presence of preformed AgNP seem to form at a faster rate (see Figure 2.28). It has been reported that CuNP formation is catalyzed by the presence of AgNP in solution.[3] They found that with an atomic ratio of 0.1 Ag:Cu, the reaction time decreased from 2 hours to 10 minutes.[3]

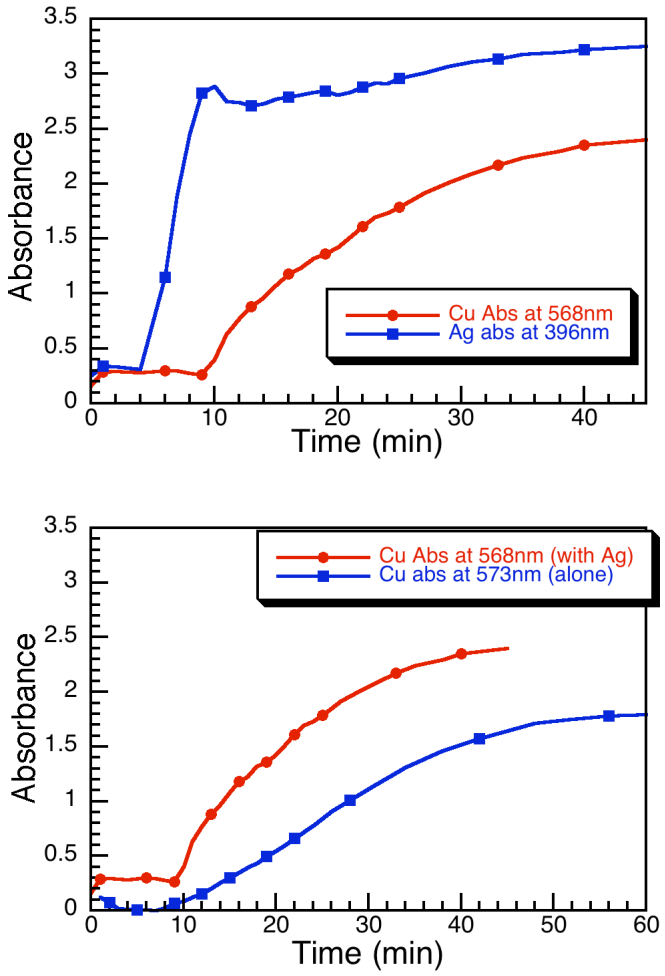

Figure 2.28 Growth of Cu and Ag NP monitoring their respective absorption SPB maxima with time of irradiation with 8 UVA lamps.

2.3.3.3 Different Copper/Silver Nanoparticle Bimetallic Syntheses

Since the oxidation was not prevented using this method of bimetallic synthesis (see section 2.3.3.5) and if the structure was core-shell, it was a silver core, based on UV-Vis kinetics of the NP growth (Figure 2.26). Attempts were made to synthesize CuNP, followed by addition of a silver salt (either $AgNO_3$ or

AgTFA) (referred to as Method 2 and known as transmetallation method) in Ar-purged MeCN in hopes to reduce the silver second and form a shell on the preformed CuNP. To make the CuNP, 0.66 mM $Cu(OAc)_2$, 1.98 mM I-907, 0.66 mM TOABr or CTAC, in MeCN and 0.15 to 0.3 mM Ag^+. A smaller amount of Ag had to be added with respect to the Cu to ensure the reduction of silver did not result in complete oxidation of the CuNP. Because of their oxidation potentials, Ag^+ can be reduced by the CuNP at the expense of the CuNP oxidation. When AgTFA or $AgNO_3$ was added to the cuvette, a peak appears around 420 nm while maintaining a peak around 575 nm assigned to the CuNP (see Figure 2.30 and Figure 2.31). The colour of the cuvette changes to a brown/orange colour (all the colours and descriptions of how bimetallic NP are made can be found in (Table 2.2). The spectrum is similar to that of Cu/AgNP made together in solution (see Figure 2.30 and Figure 2.31). The same result is observed using $AgNO_3$ as the silver salt added after the formation of the CuNP (see Figure 2.30).

Table 2.2 Descriptions of the types of mono and bimetallic NP combinations with Ag and Cu and their resulting colour.

Type of NP	Description	Colour	SPB locations (nm)
CuNP	CuNP made in MeCN	Pink/red	~575 nm
AgNP	AgNP made in MeCN	Yellow	~400 nm
Cu/Ag NP (Method 1/M1)	CuNP and AgNP made at the same time in the same solution	Dark purple	Cu: ~570 nm Ag: ~418 nm
CuNP+Ag^+ (Method 2/M2)	CuNP made in MeCN, degassed Ag^+ added	Brown/orange	Cu: ~575 nm Ag: ~418 nm
CuNP+AgNP (Method 3/M3)	CuNP made in MeCN, AgNP made in a separate solution of MeCN. Two solutions combined.	Pink-yellow	Cu: ~577 nm Ag: ~430 nm

To try to determine the bimetallic structure of these two methods, CuNP and AgNP were made separately and added together (referred to as Method 3). CuNP are made with 0.66 mM $Cu(OAc)_2$, 1.98 mM I-907, and 0.66 mM CTAC in de-aerated MeCN and AgNP are made using 0.2 mM $AgNO_3$, 0.2 mM I-907, and 0.6 wt% PVP (55K) in de-aerated MeCN. AgNP could not be made with CTAC because of the insolubility of the resulting AgCl.[29] The two solutions of NP were added together and the resulting spectrum taken right after addition can be seen in Figure 2.29 and is a combination of the two SPB of CuNP and AgNP. An SEM image of these NP is in the Appendix. The combination of the two NP solutions

does not have significant shifts in the SPB of the NP, which may indicate the two NP are not interacting with each other.[28]

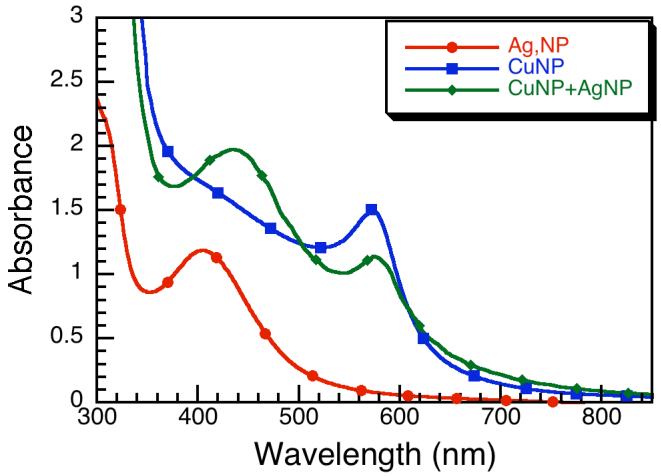

Figure 2.29 CuNP made with 0.66 mM $Cu(OAc)_2$, 1.98 mM I-907, and 0.66 mM CTAC with 20 min UVB irradiation and AgNP made with 0.2 mM AgTFA, 0.2 mM I-907, 0.6wt% PVP then adding the two solutions together to form the green trace (M3).

The spectra of all three syntheses were compared (see Figure 2.30 and Figure 2.31). Based on the spectra, it is difficult to tell whether the NP of Cu and Ag are forming monometallic NP separately in solution (green trace) or if they are a core-shell structure. They are not forming an alloy because the spectra would appear as a single peak in between the two positions of the two SPB.[31,28] Based on spectra, and previous reports of core-shell NP,[28,32] the Cu/Ag (M1) could be forming a core(Ag)-shell(Cu) structure. Because the copper and silver Plasmon bands are blue-shifted compared to the addition of the two NP (M3), it could indicate the presence of core-shell NP.[28] However, when looking at the SEM and TEM images of these NP, the composition of the bimetallic NP were not able to be determined (see Appendix and Figure 2.32). The size of the NP made with Cu/Ag together followed by reduction (M1) have a mean size of 26 ± 12 nm. The

size of CuNP with Ag^{+} added to the solution are 14 ± 7 nm. CuNP alone are 27 ± 13 nm.

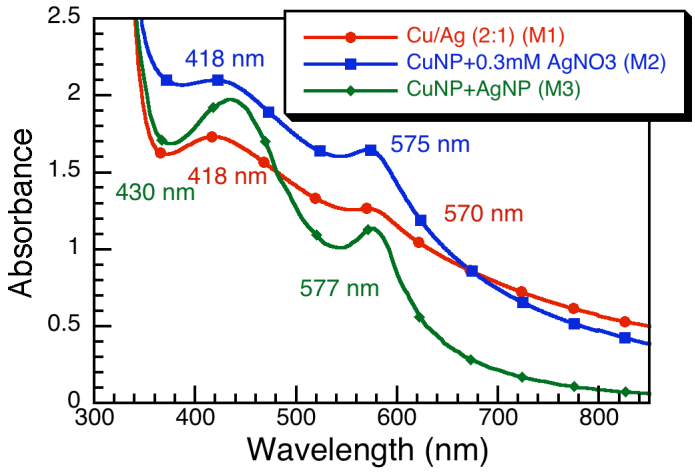

Figure 2.30 Spectra comparing (M1) Cu/Ag NP made together in solution (0.66 mM $Cu(OAc)_2$, 0.3 mM $AgNO_3$, 1.65 mM I-907, 0.33 mM CTAC degassed and irradiated for 20min with 4UVB). (M2) CuNP made (0.66 mM $Cu(OAc)_2$, 1.98 mM I-907, 0.66 mM CTAC with 20 min 4UVB) then adding 0.3 mM $AgNO_3$ and irradiating for reduction. CuNP (0.66 mM $Cu(OAc)_2$, 1.98 mM I-907, 0.66 mM TOABr) and (M3) AgNP (0.2 mM $AgNO_3$, 0.2 mM I-907, 0.6wt% PVP) made separately and added together.

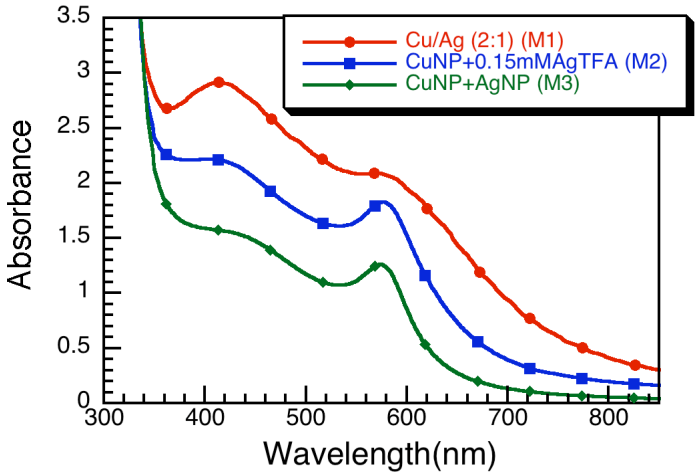

Figure 2.31 Spectra comparing (M1) Cu/Ag NP made together in solution (0.66 mM $Cu(OAc)_2$, 0.3 mM AgTFA, 2.31 mM I-907, 0.66 mM CTAC degassed and irradiated for 20min with 4UVB). (M2) CuNP made (0.66 mM $Cu(OAc)_2$, 1.98 mM I-907, 0.66 mM CTAC with 20 min 4UVB) then adding 0.15 mM AgTFA and irradiating for reduction. (M3) CuNP (0.66 mM $Cu(OAc)_2$, 1.98 mM I-907, 0.66 mM TOABr) and AgNP (0.2 mM AgTFA, 0.2 mM I-907, 0.6wt% PVP) made separately and added together.

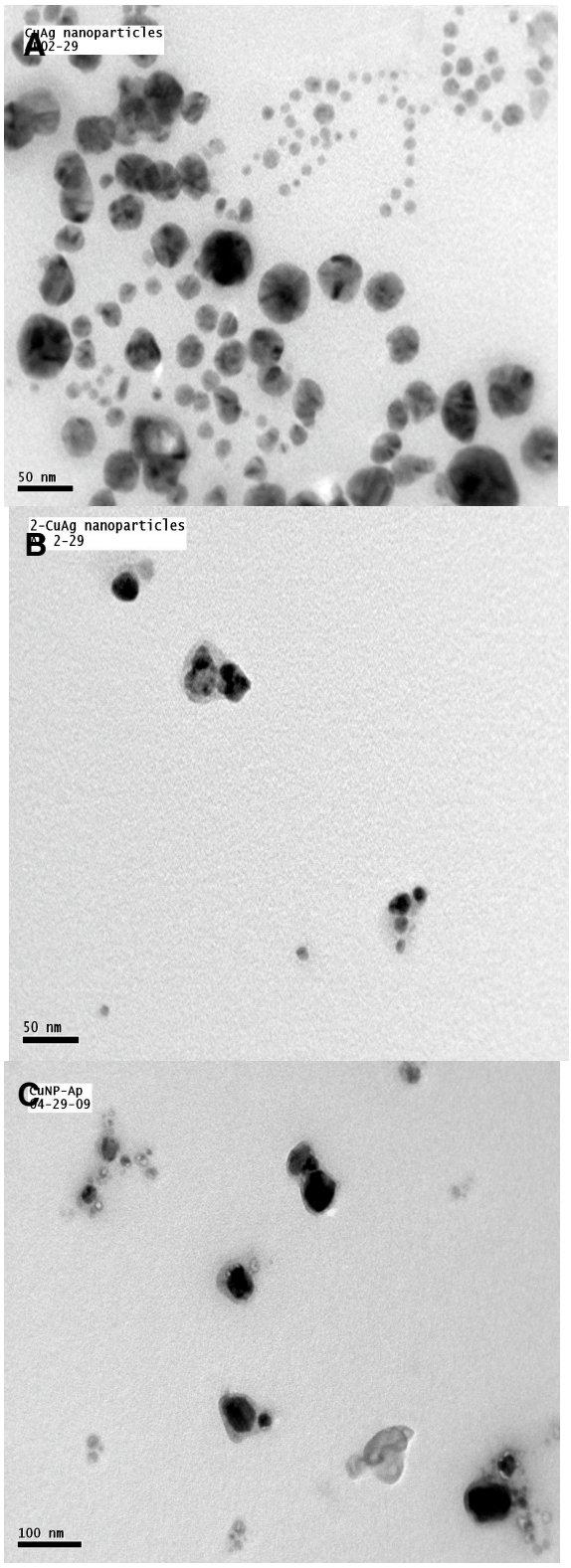

Figure 2.32 TEM images of A: (M1) Cu/Ag NP (0.66 mM:0.33 mM), B: (M2) CuNP + $AgNO_3$ (0.66 mM + 0.3 mM) made together in solution, and C: CuNP alone (0.66 mM). No difference can be seen between CuNP and AgNP in these images making determining the Cu/Ag composition not possible.

2.3.3.4 Copper/Gold Nanoparticle Attempts

The capping of CuNP was also attempted using $HAuCl_4$ instead of using silver. The synthesis using gold was not successful and the NP were not stable. Using 0.66 mM $Cu(OAc)_2$, 0.33 mM $HAuCl_4$, 0.33 mM CTAC and stoichiometric amount of I-907 in de-aerated MeCN, followed by 20 minutes of UVB irradiation. When looking at the spectrum, the formation of what appeared to be alloy Cu/Au NP formed with a peak at 564 nm[28,31] (see Figure 2.33). They were not stable under atmospheric conditions, so this was not followed further.

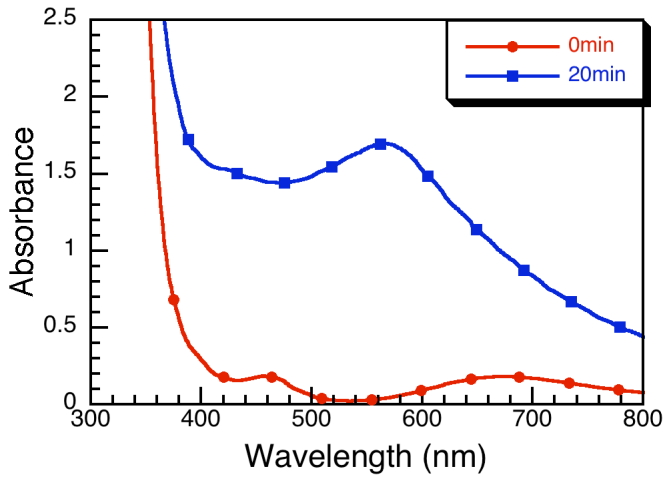

Figure 2.33 Cu/Au NP made together in solution using 0.66 mM $Cu(OAc)_2$, 0.33 mM $HAuCl_4$, 0.33 mM CTAC, and stoichiometric amount of I-907 in de-aerated MeCN under 4 UVB lamp irradiation.

Unsuccessful attempts were made to make CuNP followed by addition of $HAuCl_4$ to make a shell of AuNP around the CuNP. Different stabilizers were used including CTAC, TOABr, thiophene, and dibenzothiophene in attempts to attract the gold to the surface of the CuNP. Unfortunately, the thiol-containing stabilizers would not stabilize the CuNP so these attempts were unsuccessful.

2.3.3.5 Copper/Silver Nanoparticle Oxidation

The oxidation of the Cu/Ag NP (M1) was investigated to see if the rate of CuNP oxidation was altered by the presence of AgNP. If the particles have a core-shell Cu-Ag structure, the oxidation of the CuNP should be prevented. This is unlikely, however, given the reduction potentials of the two metal salts (0.34 V for Cu^{o}/Cu^{+2} and 0.799 V for Ag^{o}/Ag^{+} *vs.* SHE) and the kinetics of formation (see Figure 2.26).[3,27] The oxidation of the bimetallic species synthesized by making Cu/Ag together (Method 1) from $Cu(OAc)_2$ and $AgNO_3$ (see Table 2.2 for description and section 2.3.3.2 for experimental details) showed both NP were being oxidized at the same rate through UV-Vis scanning kinetics after 120 minutes (Figure 2.34). By morning, there was no absorbance left for any NP and all species were completely oxidized.

Next, the oxidation of particles made with method 2 showed both species were reduced at the same rate and after 120 minutes the only absorbance left belonged to $Cu(OAc)_2$ and Irgacure (see Figure 2.35). It is notable that in both cases both species oxidized rather than just the CuNP. Silver nanoparticles can be oxidized as well,[33] but not as readily as CuNP. Silver nanoparticles can be stable on their own under ambient conditions indefinitely depending on the environment and stabilizers. If they are core-Ag shell-Cu, the oxidation of the copper may catalyze and promote the oxidation of the AgNP as well, since AgNP can oxidize.[33] After oxidation, the absorbance is the same as before irradiation; The absorbance of the $Cu(OAc)_2$ salt at 670 nm and any remaining Irgacure

around 330 nm can be seen (see Figure 2.35) showing NP do not oxidize to CuO, which would absorb at 800 nm.[12,13]

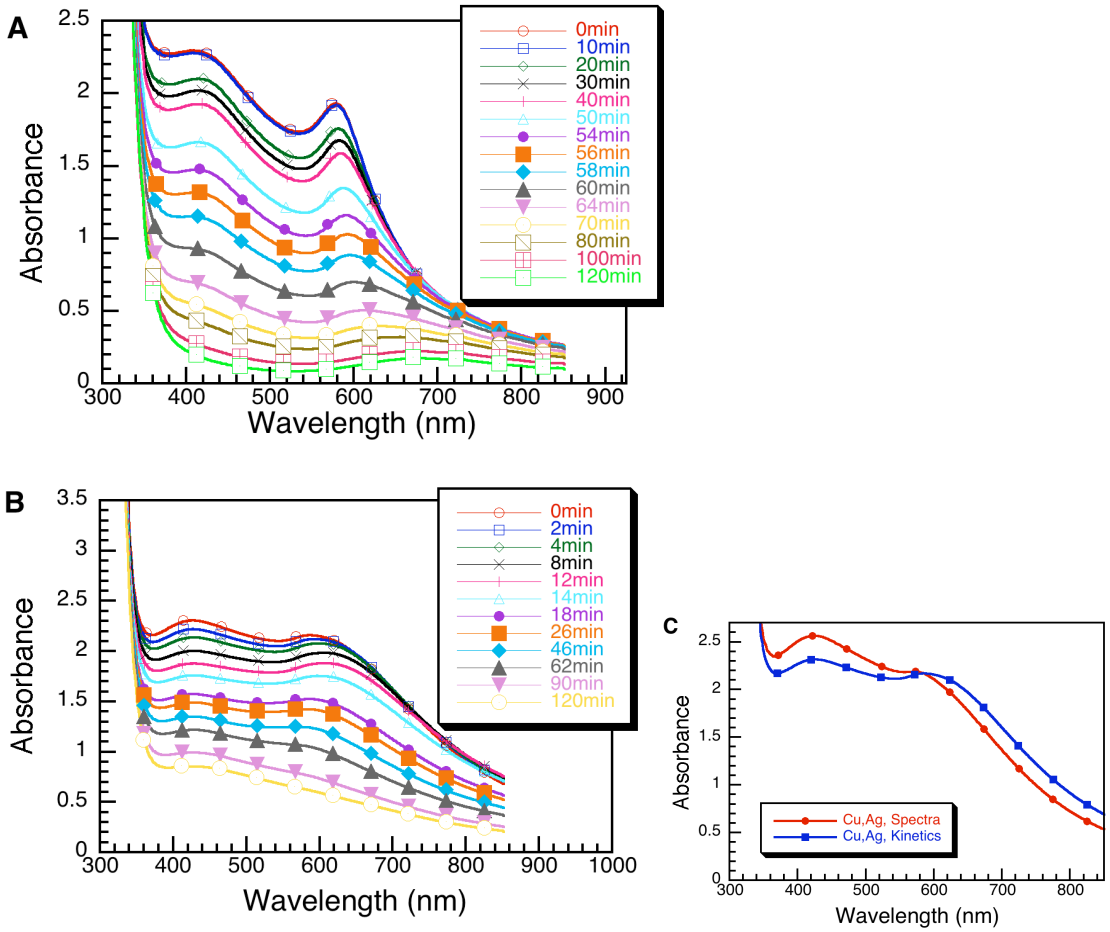

Figure 2.34 A: CuNP+AgTFA (M2) (0.66 mM $Cu(OAc)_2$, 1.98 mM I-907, 0.66 mM TOABr, Ar-purged and irradiated with 4 UVB for 15 min followed by addition of 0.15 mM AgTFA and 20 min irradiation) followed by monitoring absorbance oxidation kinetics from 0 to 120 minutes after opening cuvette. Concentrations are 0.66 mM $Cu(OAc)_2$, 0.33 mM $AgNO_3$, 0.66 mM CTAC, 2.28 mM I-907. B: Cu/Ag NP made together in solution (M1) monitoring absorbance kinetics from 0 to 120 minutes. Concentrations are 0.66 mM Cu(OAc)2, 0.66 mM TOABr, 1.98 mM I-907, and addition of 0.15 mM AgTFA. C: Note that in B the absorbances in kinetics mode measured are not accurate, see C for actual absorbances.

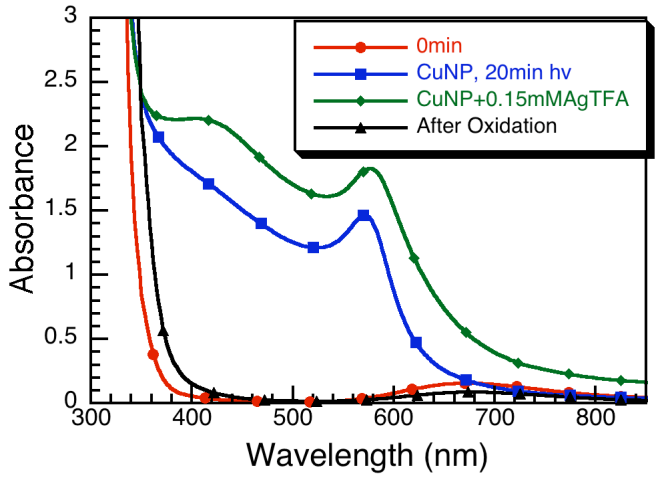

Figure 2.35 CuNP before and after addition of AgTFA. Spectra before irradiation showing absorbance of $Cu(OAc)_2$ before irradiation and after oxidation.

When comparing the oxidation of CuNP alone in solution to those made with silver (either method 1 or method 2), the presence of the AgNP slows the overall time for oxidation (Figure 2.36). This indicates that the presence of AgNP slow the oxidation of the CuNP, but not knowing the composition makes it difficult to predict how. The AgNP oxidation could be happening because as the CuNP begin to oxidize, this destabilizes the AgNP and they oxidize and are no longer stable and return to Ag^+ in solution. This was seen when AgNP were made in the presence of $Cu(OAc)_2$ and were not stable over time (Figure 2.27). In that case, they are stable for over a week, which shows that the CuNP oxidation is quickening their oxidation when they are present in solution.

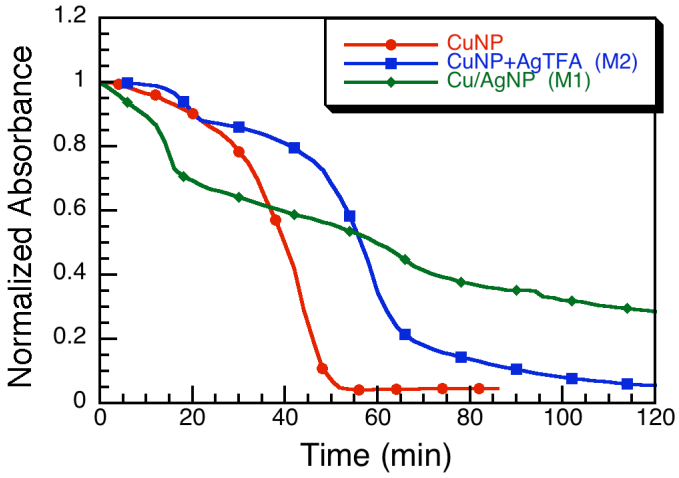

Figure 2.36 Oxidation of Cu and Cu/Ag NP made by either making them together (M1) or making CuNP then adding AgTFA (M2) both with 0.66 mM TOABr. Absorbance monitored at SPB maximum of the CuNP over time. CuNP alone made using 0.66 mM TOABr as a stabilizer.

2.4 Conclusions

CuNP were formed photochemically using a photochemical radical generation followed by a series of electron donations. A summary of the conditions can be seen in Table 2.3. CuNP can be made photochemically in aqueous and organic media from a variety of Cu^{+2} precursors. These nanoparticles are stable in inert environments but oxidize when exposed to air. When making CuNP using this photochemical approach, a halide counter anion is necessary to stabilize the NP.

In acetonitrile, the synthesis of the CuNP was faster in the presence of tetralkylammonium bromide salts compared to the chloride analogues. The chloride counter anion also produced larger nanoparticles compared to the bromide counter anion.

Table 2.3 Summary of conditions required for NP and the different sizes (of those known) and growth time. The lines in bold indicate the best conditions for CuNP synthesis.

Solvent	Radical precursor	Irradiation	Cu^{2+} salt	Stabilizer	NP size (nm)	Time for complete growth (min)
Water	**I-2959**	**UVA**	**$CuSO_4$**	**none**	**8**	**30**
Water	I-2959	UVA	$CuCl_2$	none	18	14
MeCN	I-907	UVB	$Cu(OAc)_2$	CTAC	27	30
MeCN	**I-907**	**UVB**	**$Cu(OAc)_2$**	**CTAB**	**16**	**30**
MeCN	I-907	UVB	$Cu(OAc)_2$	TMACl	--	30
MeCN	I-907	UVB	$Cu(OAc)_2$	TM/B/H/OABr	--	18
MeCN	I-907	UVB	$Cu(OAc)_2$	TBAI	--	12

Bimetallic nanoparticles of Cu/Ag were synthesized but their composition could not be determined by spectroscopy and other techniques were difficult because the particles readily oxidized. Imaging techniques were not definitive in the composition of the NP.

The oxidation of the CuNP and the bimetallic Cu/Ag NP were monitored and in all cases, the particles oxidized readily when exposed to air. In the case of the bimetallic species, both the Cu and Ag oxidized leaving Cu^{+2} and Ag^{+} in solution after oxidation.

In the case of CuNP oxidation, preliminary experiments showed that the stabilizing agent affected the rate of oxidation. The longer the alkyl chain on the alkylammonium salt resulted in a slower oxidation process than with a short alkyl chain.

2.5 References

(1) Grouchko, M.; Kamyshny, A.; Magdassi, S. *J. Mater. Chem.* **2009**, *19*, 3057-3062.

(2) Abdulla-Al-Mamun, M.; Kusumoto, Y.; Muruganandham, M. *Mat. Lett.* **2009**, *63*, 2007-2009.

(3) Grouchko, M.; Kamyshny, A.; Ben-Ami, K.; Magdassi, S. *J. Nanopart. Res.* **2009**, *11*, 713-716.

(4) Lee, Y.; Choi, J.; Lee, K. J.; Stott, N. E.; Kim, D. *Nanotech.* **2008**, *19*, 415604-45611.

(5) Luechinger, N. A.; Athanassiou, E. K.; Stark, W. *Nanotech.* **2008**, *19*, 445201-445207.

(6) Pacioni, N. L.; Pardoe, A.; McGilvray, K. M.; Chretien, M. N.; Scaiano, J. C. *Photochem. & Photobiol. Sci.* **2009**, *9*, 766-774.

(7) Prucek, R.; Kvitek, L.; Panacek, A.; Vancurova, L.; Soukupova, J.; Jancik, D.; Zboril, R. *J. Mater. Chem.* **2009**, *19*, 8463-8469.

(8) Ng, K. H.; Penner, R. M. *J. Electroanal. Chem.* **2002**, *522*, 86-94.

(9) Ferrando, R.; Jellinek, J.; Johnston, R. L. *Chem. Rev.* **2006**, *108*, 846-904.

(10) Fu , Y.; Liu, L.; Yu, H.; Wang, Y.; Guo, Q. *J. Am. Chem. Soc.* **2005**, *127*, 7227-7234.

(11) Rao, P. S.; Hayon, E. *J. Am. Chem. Soc.* **1974**, *96*, 1287-1294.

(12) Pileni, M. P. *New J. Chem.* **1998**, *22*, 693-702.

(13) Yanase, A.; Komiyama, H. *Surf. Sci.* **1991**, *248*, 11-19.

(14) Lang, G. G.; Ujvari, M.; Horanyi, G. *J. Electroanal. Chem.* **2002**, *522*, 179-188.

(15) MacLeod, I. D.; Muir, D. M.; Parker, A. J.; Singh, P. *Aust. J. Chem.* **1977**, *30*, 1423-1437.

(16) Kratochvil, B.; Zatko, D. A.; Markuszewski, R. *Anal. Chem.* **1966**, *38*, 770-772.

(17) Henglein, A. *J. Phys. Chem.* **1993**, *97*, 5457-5471.

(18) Johnston, F. J. *Int. J. Radiat. Appl. Instrum. Part C* **1989**, *33*, 113-118.

(19) Chu, Y.; Crozier, K. B. *Optics Lett.* **2009**, *34*, 244-246.

(20) Lee, K. C.; Lin, S. J.; Lin, C. H.; Tsai, C. S.; Lu, Y. J. *Surf. & Coat. Tech.* **2008**, *202*, 5339-5342.

(21) Harkness, A. C.; Daggett, H. M. *Can. J. Chem.* **1965**, *43*, 1215-1221.

(22) Thomas, K. G.; Zajicek, J.; Kamat, P. V. *Langmuir* **2002**, *18*, 3722-3727.

(23) Stamplecoskie, K. G.; Ju, L.; Farvid, S. S.; Radovanovic, P. V. *Nano Lett.* **2008**, *8*, 2674-2681.

(24) Turro, N. J.; Ramamurthy, V.; Scaiano, J. C. *Modern molecular photochemistry of organic molecules*; University Science Books, 2010.

(25) Battino, R. *Solubility Data Series*; Pergamon Press: Oxford, 1981; Vol. 7.

(26) Giuffrida, S.; Condorelli, G. G.; Costanzo, L. L.; Fragal, I. L.; Ventimiglia, G.; Vecchio, G. *Chem. Mater.* **2004**, *16*, 1260-1266.

(27) Weast, R. C. *Handbook of Chemistry and Physics*; 52nd ed.; Chemical Rubber Publishing Company: Cleveland, 1971.

(28) Gonzalez, C. M.; Liu, Y.; Scaiano, J. C. *J. Phys. Chem. C* **2009**, *113*, 11861-11867.

(29) Yugang, S.; Mayers, B. T.; Xia, Y. *Nano Lett.* **2002**, *2*, 481-485.

(30) Khan, Z.; Al-Tnabaiti, S. A.; El-Mossalamy, E. H.; Obaid, A. Y. *Coll. and Surf. A: Physiochem. Eng. Asp.* **2009**, *352*, 31-37.

(31) Chen, H. M.; Liu, R. S.; Jang, L.-Y.; Lee, J.-F.; Hu, S. F. *Chem. Phys. Lett.* **2006**, *421*, 118-123.

(32) Link, S.; Wang, Z. L.; El-Sayed, M. A. *J. Phys. Chem. B* **1999**, *103*, 3529-3533.

(33) Qi, H.; Alexson, D.; Glembocki, O.; Prokes, S. M. *Nanotech.* **2010**, *21*, 215706-251711.

CHAPTER 3 – PHOTOCHEMICAL SYNTHESIS OF SUPPORTED SILVER NANOPARTICLES, SUPPORTED SILVER NANOPARTICLE SHAPES, AND THEIR CATALYTIC BEHAVIOUR

TABLE OF CONTENTS:

TABLE OF FIGURES:

3.1 Introduction

Using nanoparticles toward the catalysis of organic reactions has become an important application of metallic NP in recent years. Many different reactions are being explored to see how efficient certain nanoparticles are at catalysis.

Copper nanoparticles have important uses as catalysts in chemical reactions.[1,2] Copper is known to be an effective catalyst in hydrogenation and oxidation reactions, as well as Suzuki cross coupling and addition-elimination reactions between methylene and imine compounds.[3,4] Copper (I) is known to catalyze click reactions and recently CuNP have been used to catalyze click reactions between alkynes and azides and are shown to be reusable.[5]

Conversely, silver nanoparticles as catalysts have been less explored than copper and gold.[6] Bulk silver has been used to catalyze partial oxidation reactions, including oxidation of methanol to formaldehyde and ethylene epoxidation.[6] Some work has suggested the surface and subsurface oxygen atoms in a silver catalyst are essential for activity and selectivity of silver-catalyzed reactions.[6] Recent work with HRTEM (High Resolution Transmission Electron Microscopy) and DFT (Density Functional Theory) found that the oxygen atoms are on the edge and steps of the Ag surfaces and increased the catalytic activity of the AgNP catalyst.[6]

Alcohol oxidations are a fundamental reaction in industrial and synthetic chemistry, and thus have attracted attention in the field of nanoparticle

catalysis.[7,8] Previously these oxidations required strong, toxic, and expensive oxidizing agents, including permanganate and dichromate, leading to waste and a non-environmentally friendly reaction.[7,8] Being able to carry out these oxidations in environmentally benign conditions, with a reusable catalyst, and no harsh by-products is appealing.[7-10]

In particular, the use of supported metal NP offers significant advantages to the development of these methods. Supports are important for catalyst recovery and easy separation from the reaction mixture, and often play an important role in the catalytic reaction. Some supports are shown to be active in the catalytic reaction and others are found to be inactive.[11,12,13] Active supports in oxidation reactions include TiO_2, Fe_2O_3, and CeO_2, and inactive include SiO_2, MgO, and Al_2O_3.[11,12,13] Active supports can enhance activity by providing better stabilization for NP in harsh conditions, preventing agglomeration of NP, and providing a source of oxygen atoms.[11,12,13] Titanium dioxide is of interest because it has been shown to have higher catalytic properties through the modified metal-support interactions.[14] TiO_2 has also been shown to be very catalytically efficient at larger NP sizes.[12]

Almost all the previous work found in the literature using supported silver nanoparticles as catalysts involved making the catalyst using a chemical reduction method of Ag^+ (KBH_4, hydrazine, H_2 reduction, or sodium citrate) yielding small NP between 2 and 6 nm.[7,10,15] The only photochemical approach found used Ag(acac) and yielded NP around 8 nm.[16] The NP size has a distinct

effect on the ability of the NP to act as catalysts where smaller NP have been shown to be better catalysts.[17] One study showed a 77% decrease in conversion from *sec*-phenethyl alcohol to acetophenone when using 5.8 nm NP compared to 2.7 nm NP.[7]

Previous work on similar alcohol oxidations, all using *sec*-phenethyl alcohol converting to acetophenone has shown the following results: One paper used a green approach with water, AuNP@TiO_2, and hydrogen peroxide as the oxidant.[8] With 0.4 μmol of Au, the authors were able to achieve 99% conversion to acetophenone.[8] Another example using AuNP as a catalyst supported on hydrotalcite (HTC) using 0.0045 mmol of Au, at 80°C under air, had 99% conversion to acetophenone in 20 min for an alcohol oxidation.[7] In another example using AgNP (3.3 nm diameter) on HTC (45 nmol of Ag) at 130°C under a flow of Ar resulted in 99% conversion in 16 hours.[10] This work also looked at other alcohol oxidations including 4-methoxybenzyl alcohol, which had 98% conversion to 4-methoxybenzaldehyde in 14 hours.[10]

The oxidation of alcohols is a well-studied catalytic reaction using mainly AuNP and thus is a good reaction to test new catalysts synthesized here. The goals of this work include synthesizing AgNP@support in a one-pot synthesis as well as tethering AgNP shapes (seeds, decahedra, and plates) to support. Different alcohol oxidations will be explored in different solvent systems to ultimately determine ideal conditions to test the different AgNP shapes and compare their different catalytic efficiencies.

3.2 Materials and Methods

Silver supported nanoparticles were made using $AgNO_3$ or Ag(acac), trisodium citrate, Irgacure 2959, and support (TiO_2 (P25 and P90), hydrotalcite, SiO_2). The silver precursors, $AgNO_3$ or Ag(acac), and trisodium citrate were purchased from Sigma Aldrich and used as received. Irgacure 2959 (2-Hydroxy-1-[4-(2-hydroxyethoxy)phenyl]-2-methyl-1-propanone) was a generous gift from Ciba Specialty Chemicals and was recrystallized twice from ethyl acetate. The supports: titanium dioxide (TiO_2) (P25: 20% rutile, 80% anatase and P90: 10% rutile, 90% anatase),[18] were a generous gift from Degussa Chemicals, zeolites (NH_4Y, NaY) and hydrotalcite (HTC) were purchased from Sigma Aldrich, and silica (SiO_2) from Fluka Chemicals, all used as received.

Doubly distilled deionized water was used as a solvent from a Milli-Q system (18 MΩ resistance) for silica and titanium dioxide supports. A mixture of doubly distilled deionized water and spectroscopic grade acetonitrile was used for supported silver nanoparticles made with hydrotalcite.

For silver supported nanoparticles synthesized directly on the support, a 1% loading of Ag (by mass with respect to the support) (equivalent to 1.2 mM concentration in 20 mL of water) was used with 10 times the amount of trisodium citrate (equivalent to 12 mM) and a stoichiometric amount of I-2959 (1.2 mM) with respect to the silver. All of these components for this method (slurry method), the

solution of silver salt, Irgacure 2959, and citrate were combined in 20 mL of water and stirred until well mixed (~15 minutes) in an Erlenmeyer flask followed by addition of the support (250 mg) with stirring (~20 minutes). Once mixed, the flask was placed into a Luzchem LZC-4V photoreactor equipped with 14 UVA lamps and the stirring function on. The flask is stirred while being irradiated for 10 minutes (in the case of TiO_2) and 45 min (in the case of hydrotalcite) to yield an orange/brown slurry. Solutions were centrifuged, decanted, and re-centrifuged until no coloured supernatant was present and all the photoproducts were washed off (5-6 times). This synthesis is quite reproducible but the actual loading of Ag on the support was not verified.

Copper nanoparticles on hydrotalcite were prepared similarly using $Cu(OAc)_2$ (1.2 mM) (from Sigma Aldrich and used as received), tetraoctylammonium bromide (TOABr) (1.2 mM) (from Sigma Aldrich and used as received), and I-907 (2.4 mM) (a gift from Ciba Specialty Chemicals) in stoichiometric amount, and HTC in spectroscopic grade acetonitrile. The solution was deaerated for 30 minutes with argon prior to irradiation. Solution was irradiated with 8 UVB lamps revealing a pink solution where all NP were on the support.

The shaped silver nanoparticles were synthesized by first making a seed solution of silver nanoparticles using 0.2 mM $AgNO_3$, 0.2 mM I-2959, and 2 mM trisodium citrate in doubly distilled deionized water.[19] This solution is deaerated using argon gas for 30 minutes in an Erlenmeyer flask followed by irradiation for

1 minute with 14 UVA lamps in a photoreactor. Following this, 4 LED lights of either 455 nm or 590 nm were used to irradiate a solution through a flow cell cuvette. The LED setup was 4 LED lights attached to 4 aluminum plates to transfer the heat into two heat sinks, to make a square where a cuvette could fit and be irradiated from all four sides. This was used to irradiate a solution of 50 mL of seeds by flowing through the cuvette. Either 455 nm LEDs (to make decahedra) or 590 nm LEDs (to make plates) were used for 3 to 7 days until shapes were made and confirmed spectroscopically.[19]

Seeds (irradiated for 5 minutes) and shapes were only able to adhere to TiO_2 (P90) functionalized with aminopropyl triethyl siloxane (APTES). This was done by adding 0.5% by weight of Ag to the TiO_2(APTES) and stirring for five minutes followed by centrifugation, decanting and re-centrifuging (3 times). All NP adhere to the support and the supernatant is clear. Support is dried by rinsing with EtOH and roto-evaporating off the solvent leaving the supported NP. This synthesis is very reproducible and all NP loaded on to the support adhere resulting in good reproducibility from batch to batch.

The TiO_2 is functionalized with APTES by adapting a procedure for functionalizing SiO_2 with APTES.[20] 60 μL of APTES was added to a stirred slurry of 500 mg of TiO_2 (P90) in 99% ethanol, followed by heating to reflux at 70°C for 3 hours.[20] The mixture was then centrifuged and washed with EtOH until no APTES was left in solution (this confirmed that all APTES was on the TiO_2 and not left in solution). The detection of APTES was done with luminescence

measurements. APTES was confirmed to be functionalizing the surface of the TiO_2 through luminescence measurements of a film of the TiO_2 before and after adding a drop of fluorescamine (4-phenyl-spiro [furan-2(3H),1'-phthalan]-3,3'–dione) (from Sigma Aldrich), which only displays fluorescence in the presence of primary amine groups.[21] A solution of the TiO_2 in EtOH was dropped and dried on a quartz disc. After a measurement was taken, a drop of the fluorescamine was dropped on and dried. The same was done with the supernatant, to ensure there was no APTES free in solution and all was attached to the TiO_2. A film of the supernatant was made, followed by putting a drop of fluorescamine to ensure there was no fluorescence, thus no APTES in the supernatant. The measurement was done using a luminescence spectrometer (Perkin Elmer LS 50) scanning between 370 and 800 nm, exciting at 365 nm and observing the fluorescence at 470 nm. Fluorescence was observed only after the fluorescamine was added to the disc.

The characterization of the supports and NP in solution was done through diffuse reflectance and UV-Vis Spectroscopy using a Varian Cary UV-1 or Varian Cary UV-100, SEM (field emission scanning electron microscopy JEOL, JSM-7500F), and TEM (Transmission Electron Microscopy, JEOL JEM-2100F). The diffuse reflectance measurements were done between two quartz discs enclosed with Teflon tape and scanning between 300 and 800 nm. The UV-Vis spectroscopy was done in a 10 x 10 mm quartz precision cuvette scanning between 200 and 900 nm. For the microscopy, approximately 50 µL of solution

was dropped onto a copper grid (400 mesh) and evaporated under vacuum dessicator. Images were analyzed using ImageJ Software. Supported NP were prepared for microscopy, by suspending a small amount (<1 mg) of support in MeCN (~1 mL) and sonicated for 1 minute followed by drop-casting 50 µL onto a copper grid and drying in a vacuum dessicator. Copper nanoparticles on support could only be characterized visually by their colour and by SEM since upon opening to the atmosphere, they readily oxidized. A Diffuse Reflectance spectrum could not be done because the NP oxidized while drying the solid.

Catalysis reactions on the bench were done using 4-methoxybenzyl alcohol (4-MBA) (from Sigma Aldrich, used as received) in HPLC grade toluene, and supported AgNP in a round bottom flask heated in an oil bath at 75°C with stirring for the specified time. The system was kept under a positive oxygen atmosphere. The reactions were aliquoted as specified and repurged after every aliquot with oxygen.

Catalysis reactions done using the SYMYX High Throughput Facility were done at 75°C in a 96 well plate leaving every other well free to avoid solvent or reactant contamination in neighbouring cells. The plate was put under 30 psi of oxygen and stirred while heating using a metal block surrounding the plate for 16 hours.

All catalysis reactions were monitored by Gas Chromatography Mass Spectroscopy (GCMS) (Agilent Technologies 5973 *inert* Mass Selective Detector)

or High-Performance Liquid Chromography (HPLC) (Waters 996 Photodiode Array Detector). The wavelength was monitored where the product absorbs (275 nm for 4-MBA and 240 nm for *sec*-phenethyl alcohol) and integrated to get the percent conversion to the product.

3.3 Results and Discussion

3.3.1 Synthesis

The supported nanoparticles were prepared in a variety of ways. The main approach was to prepare the NP@support directly using a known photochemical approach from our group.[19,22,23] In this method a photochemical reducing agent, Irgacure 2959 undergoes Norrish type I α-cleavage upon exposure to UVA light to form a ketyl radical that can then donate an electron and reduce the metal salt to its zero valent state, followed by nucleation and growth to form nanoparticles (see Scheme 3.1).

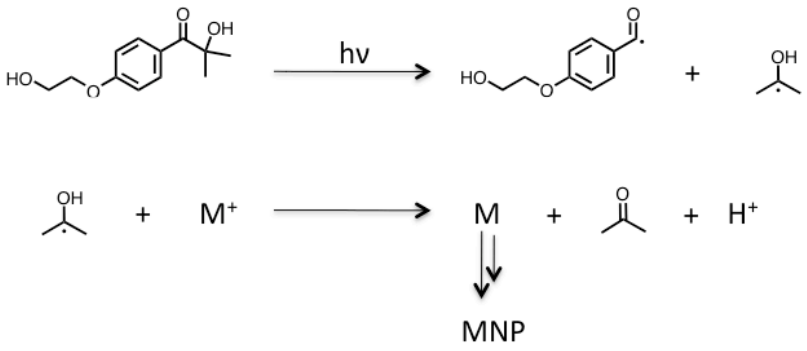

Scheme 3.1 Norrish type I α-cleavage of I-2959 forming a benzoyl and a ketyl radical followed by reduction of a metal salt (M) to its zero valent state.

3.3.1.1 Slurry Method

Preparation of AgNP using the slurry method was carried out using $AgNO_3$ as the metal salt at 0.5 - 4% Ag loading with respect to the support and I-2959 in a stoichiometric amount with respect to the Ag^+. Trisodium citrate was also used

as a stabilizer for the nanoparticles in an excess of 10 times the amount of silver added.[19] The $AgNO_3$ (0.0039 g for 1% loading), citrate (0.059 g), and I-2959 (0.0052 g) were all added to a solution of Milli-Q water (20 mL) or a combination of 50:50 MeCN:H_2O for HTC in an Erlenmeyer flask and stirred for about 15 minutes until all components had been solubilized. Following this, 250 mg of support was added to the flask and stirred for another 20 minutes followed by irradiation with 14 UVA lamps while stirring (see Scheme 3.2).

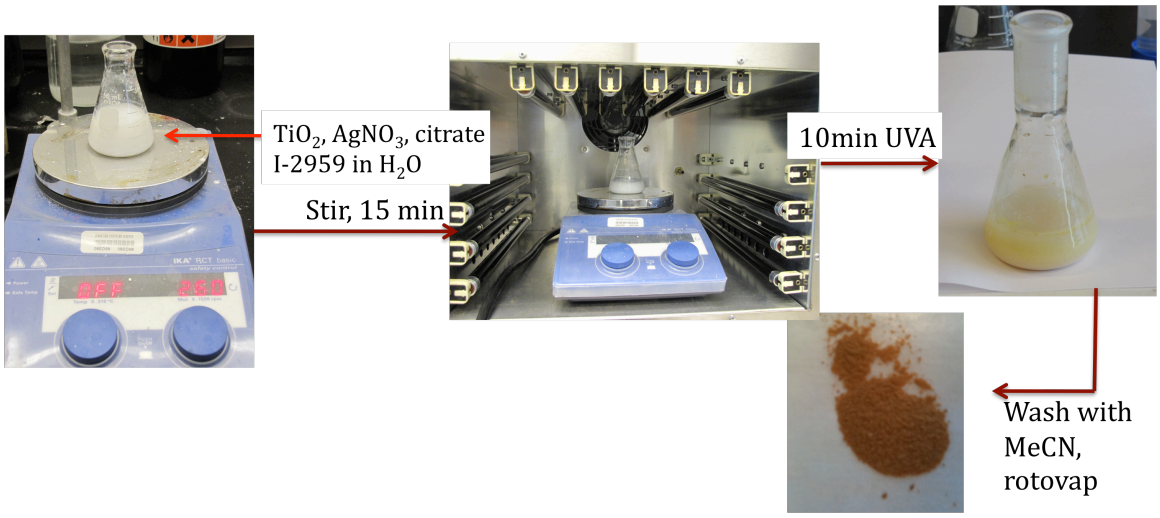

Scheme 3.2 Scheme of AgNP@TiO_2 synthesis used in this approach. Solution shown stirring, irradiating while stirring, and the final slurry of AgNP@TiO_2 before and after drying.

After NP formation, the orange/brown solution was centrifuged at a low speed (1900 rpm); Most of the nanoparticles are on the support and do not remain in the supernatant. The support was washed multiple times to remove any photoproduct or nanoparticles not adhered to the support. Following this, NP were washed with EtOH or MeCN and rotoevaporated to leave a solid powder with a SPB at around 465 nm (see Figure 3.1). The SPB can be detected using

diffuse reflectance (F(R)). Diffuse reflectance measures the reflectance off of a solid substance from light.[24] A broader absorbance is seen for NP@TiO_2 because of the absorption contribution of the interband transition of TiO_2 absorbing below 390 nm.[25] It is also important to note that for AgNP made in solution, the typical SPB is at 400 nm[19] but diffuse reflectance of the supported AgNP typically show more red-shifted absorbances (see Figure 3.1). Other papers have also noted a red-shift in the typical SPB absorbance when NP are supported on TiO_2 compared to where the same sized particles would absorb in solution.[26] The position of the SPB in supported NP also reflects the size of the NP, the more red-shifted the absorption, the larger the NP sizes.[27]

In the absence of trisodium citrate, the NP form, but oxidize within 24 hours evidenced by the change in colour of the support from orange to white. The band gap of TiO_2 is 3.2 eV corresponding to a band gap below 410 nm depending on its composition of anatase and rutile.[28] The absorption seen in the DR below 390 nm is attributed to the band gap of the TiO_2. TiO_2 has a redox potential of 1.96 V *vs.* NHE (2.2 V *vs.* SCE).[29] Silver has a redox potential of 0.799 V *vs.* NHE and AgNP have a redox potential of 0.371 V.[30] This means the TiO_2 can oxidize the AgNP, however, with the citrate stabilizing the NP (0.79 V (*vs*. NHE))[31], they provide a reducing atmosphere, which can overcome oxidation caused by photooxidation with TiO_2. Under visible irradiation, the transfer of an electron from Ag to TiO_2 is favoured,[25] but may be prevented by the presence of

the citrate. Under UV irradiation (the conditions to make the NP) the opposite is observed (an electron transferred from TiO_2 to the Ag).[25]

This method can also be used with Ag(acac) and support together. Silver acetylacetonate does not need a reducing agent as it releases the Hacac ligand in its protonated form upon irradiation and does not require the use of a stabilizing agent to prevent oxidation.[32] Once Ag(acac) is solubilized in water with the support, irradiation with 9 UVA and 4 UVB lamps in a photoreactor results in a yellow/orange powder after washing and drying and a SPB around 450 nm (see Figure 3.1). The average particle size is 27 nm ± 9 nm, shown in Figure 3.5. It is important to note that in order to image the supported NP, COMPO (composition) mode must be used on the SEM, which is a backscattering technique. Because TiO_2 can also charge with this technique, it makes imaging the NP on TiO_2 very difficult and it is a challenge to get a clear image and good contrast between the NP and the support with the resolution available with this mode. It is difficult to image the NP@TiO_2 with TEM because there is little contrast between the support and the metal NP, so NP cannot be easily imaged.

A solid state synthesis was also attempted unsuccessfully (see Figure 3.1) where all components are added to a round bottom flask and stirred until well mixed (30 minutes) followed by roto-evaporation and irradiation in the solid state while rotating under 4 UVA lamps. A colour change as well as a SPB is noted by UV-Vis spectroscopy, however, in comparison to the slurry method (Figure 3.1), the amount of NP formed is far lower.

The AgNP@TiO_2 (P90) can be seen visually (Figure 3.2) and with SEM in Figure 3.3 and Figure 3.5. The NP size for 4% $AgNO_3$ on TiO_2 is 17 nm ± 17 nm (see Figure 3.4) and for 4% Ag(acac) on TiO_2 (P90) it is 31 nm ± 13 nm (see Figure 3.6).

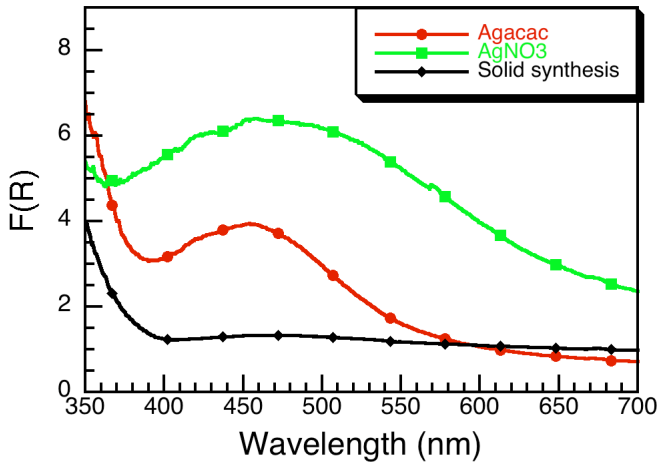

Figure 3.1 Diffuse Reflectance of Ag(acac) and $AgNO_3$ @TiO_2 made using the slurry method at 4% loadings and black trace is solid state synthesis. Peak for $AgNO_3$ at 465 nm and peak for Ag(acac) at 450 nm. The solid state synthesis has a SPB at 470 nm with a lot of scatter.

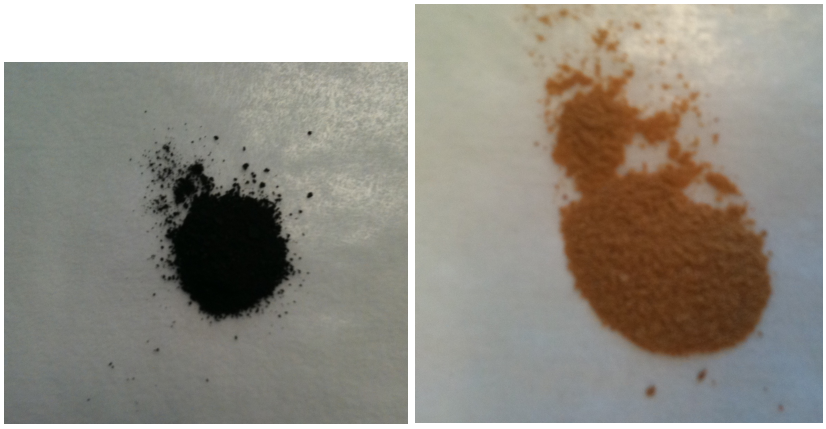

Figure 3.2 Photographs of nanoparticles on support made from 4% $AgNO_3$@TiO_2 (left) and 4% Ag(acac)@TiO_2 (right)

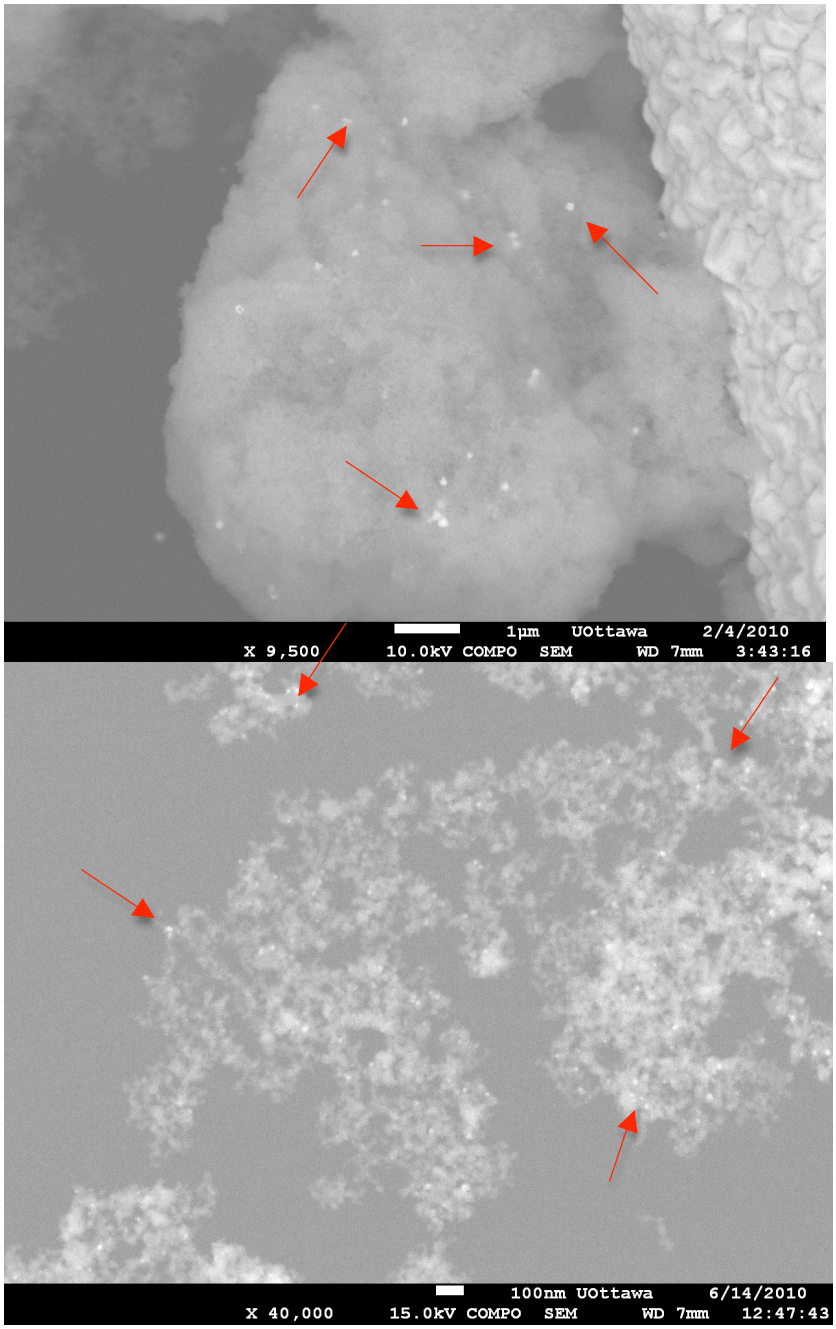

Figure 3.3 SEM images of 4% $AgNO_3$@TiO_2 (P90). The SEM is used in COMPO mode in order to see spots of higher electron density belonging to AgNP. The red arrows point to some of AgNP on the surface, which are the small round brighter spots.

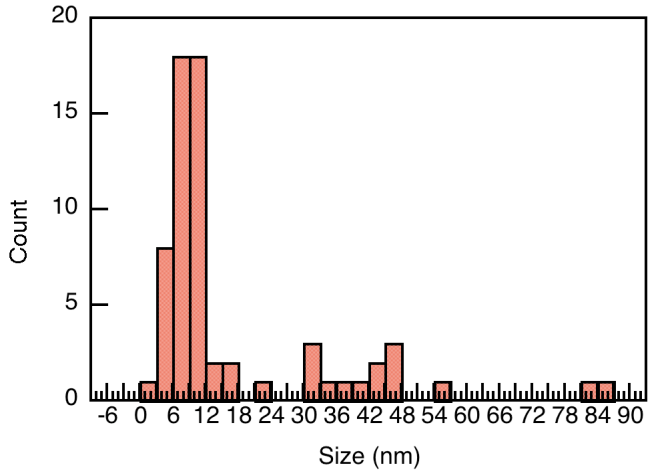

Figure 3.4 Histogram showing size distribution of 4% $AgNO_3$@TiO_2 based on sizing around 60 nanoparticles.

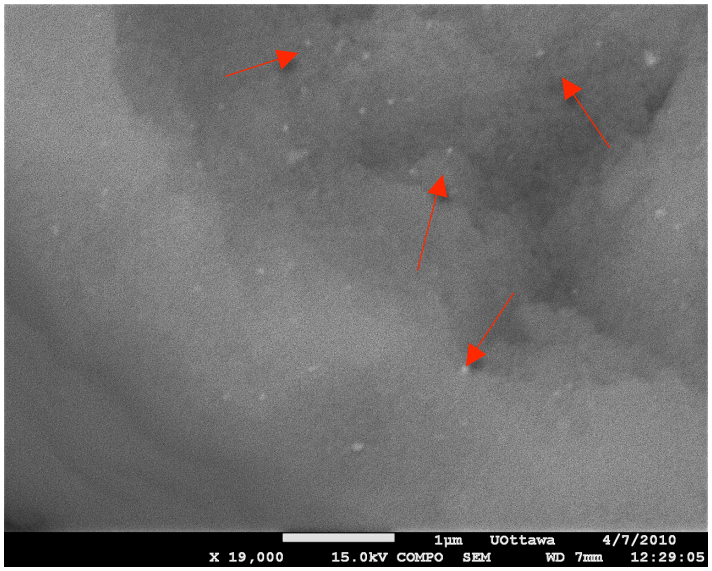

Figure 3.5 SEM of 4% Ag(acac)@TiO_2 (P90). Red arrows point to some AgNP, which are the small bright spots on the surface of the TiO_2.

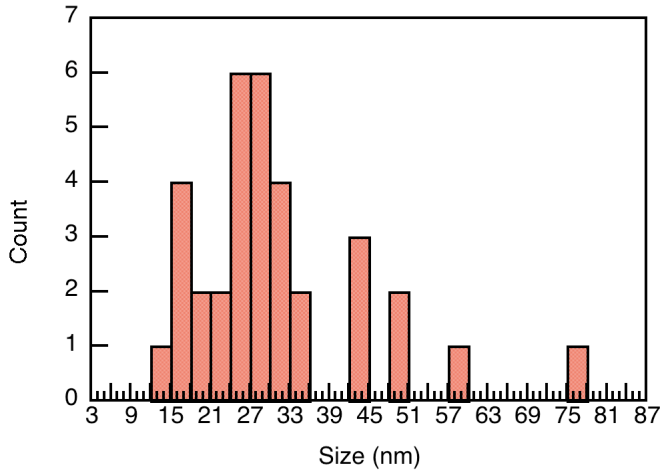

Figure 3.6 Histogram showing 4% Ag(acac)@TiO_2 size distribution based on 33 particles.

3.3.1.2 Supported Copper Nanoparticles

Copper nanoparticles were prepared similarly to the Ag@support with the slurry method. Previous reports have chemically synthesized (*via.* H_2 reduction) CuNP on hydrotalcite, MgO, Al_2O_3, SiO_2, TiO_2, and hydroxyapatite and the NP were shown to be very active toward alcohol oxidations in neat reaction conditions.[33] These composites were confirmed to be comprised of Cu^o by XAFS (X-ray absorption fine-structure spectrum) and exhibited reasonable recyclability (two times).[33] CuNP were also made on zeolites, but showed agglomeration and large particle sizes as well as the formation of copper oxide.[34]

In this work, $Cu(OAc)_2$, I-907, and TOABr were added to an Erlenmeyer flask in MeCN, as seen in Chapter 2. After stirring for 10-15 minutes, HTC was added (enough for a 1% loading of Cu) and stirred for 10 minutes. The slurry was deaerated using Ar gas for 30 minutes following irradiation with 8 UVB lamps in a

photoreactor. Following irradiation, SEM grids were loaded and imaged, showing CuNP were formed on the HTC (see Figure 3.7). The CuNP@HTC are 8 nm ± 3 nm and are fairly monodisperse (see Figure 3.8). All the NP adhered to the support based on SEM and observing the flask when the support settled to the bottom leaving a pink support and a clear supernatant (see Figure 3.9). No further work was able to be done with the Cu@HTC because of the fast oxidation back to Cu(II) after opening the flask to the atmosphere. This was confirmed by the colour change back to the original blue colour of $Cu(OAc)_2$.

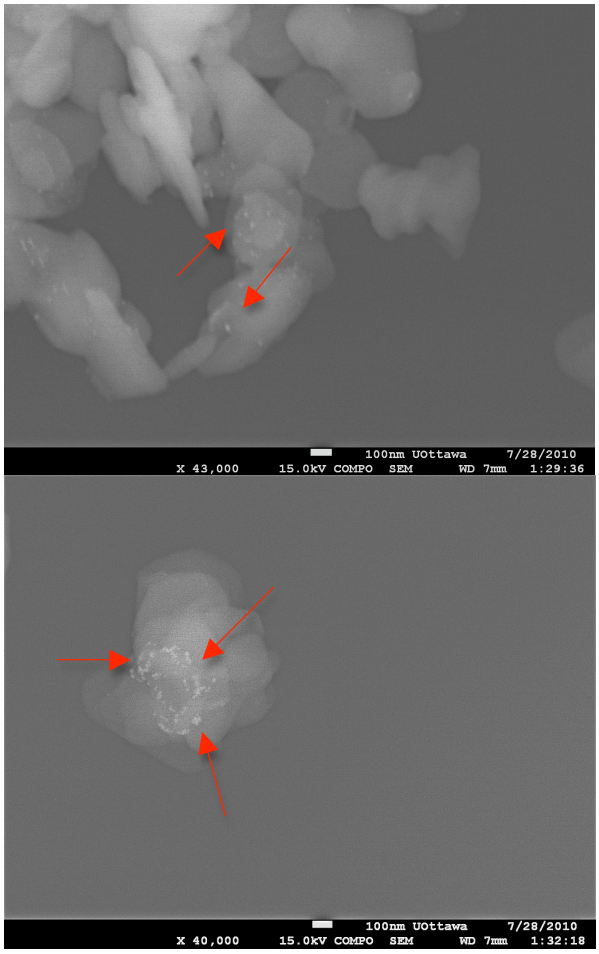

Figure 3.7 SEM images of Cu@HTC. CuNP can be seen as the smaller bright spots on the surface of the larger HTC surface.

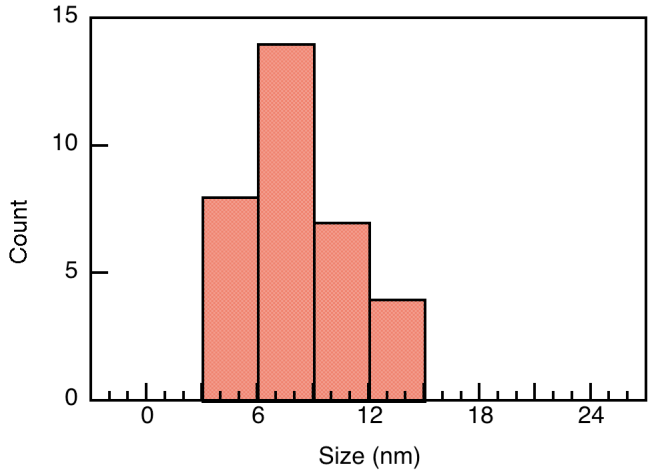

Figure 3.8 Histrogram of CuNP sizes from ImageJ based on the size of 33 CuNP on HTC.

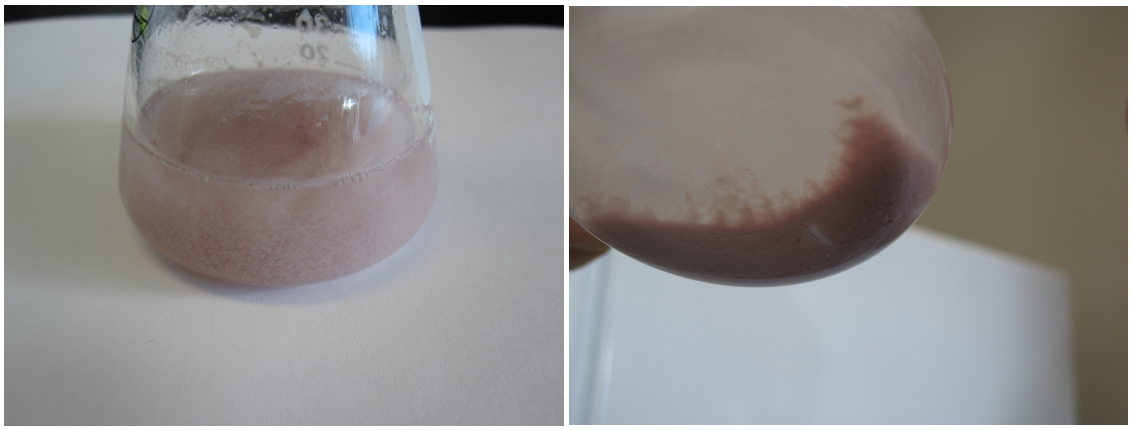

Figure 3.9 Photographs of a suspension of CuNP@HTC. Top: Pink colour indicates the presence of CuNP on the HTC support. Bottom: Support has settled to the bottom of the flask and all the NP have formed on the support since the support is now pink and the supernatant is clear.

3.3.1.3 Shapes@Support

Many efforts were made to either make Ag shapes (including decahedra and plates) on the support (similar to the slurry method) or to make AgNP shapes in solution through LED irradiation[19] and then add them to the support. Attempts were made to synthesize spherical AgNP on TiO_2 followed by LED irradiation (either 590 nm to make plates or 455 nm to make decahedra AgNP) to change

the shape. These attempts were unsuccessful as seen in the SEM (Figure 3.10). The NP size before the LED irradiation is 28 nm ± 4.7 nm and after it is 13.6 nm ± 7.5 nm but remained spherical (see Figure 3.10). The mechanism for the synthesis of the different AgNP shapes involves an aggregation/coalescence of the NP seeds when they are excited by light.[19] The light absorbed is converted to thermal energy, resulting in the NP coalescence and the exciting wavelength causes more particles to form with absorption at that wavelength.[19] Because the NP in this case are already stationary on the support and cannot move, coalescence will not be possible. The diffuse reflectance of the NP before and after irradiation can also be seen in Figure 3.11. The slight blue-shift in the spectrum from 426 nm in the case of spheres to 408 nm after LED irradiation further shows that the NP are likely getting smaller and are not growing to decahedra where an absorbance at 455 nm would be visible.[19]

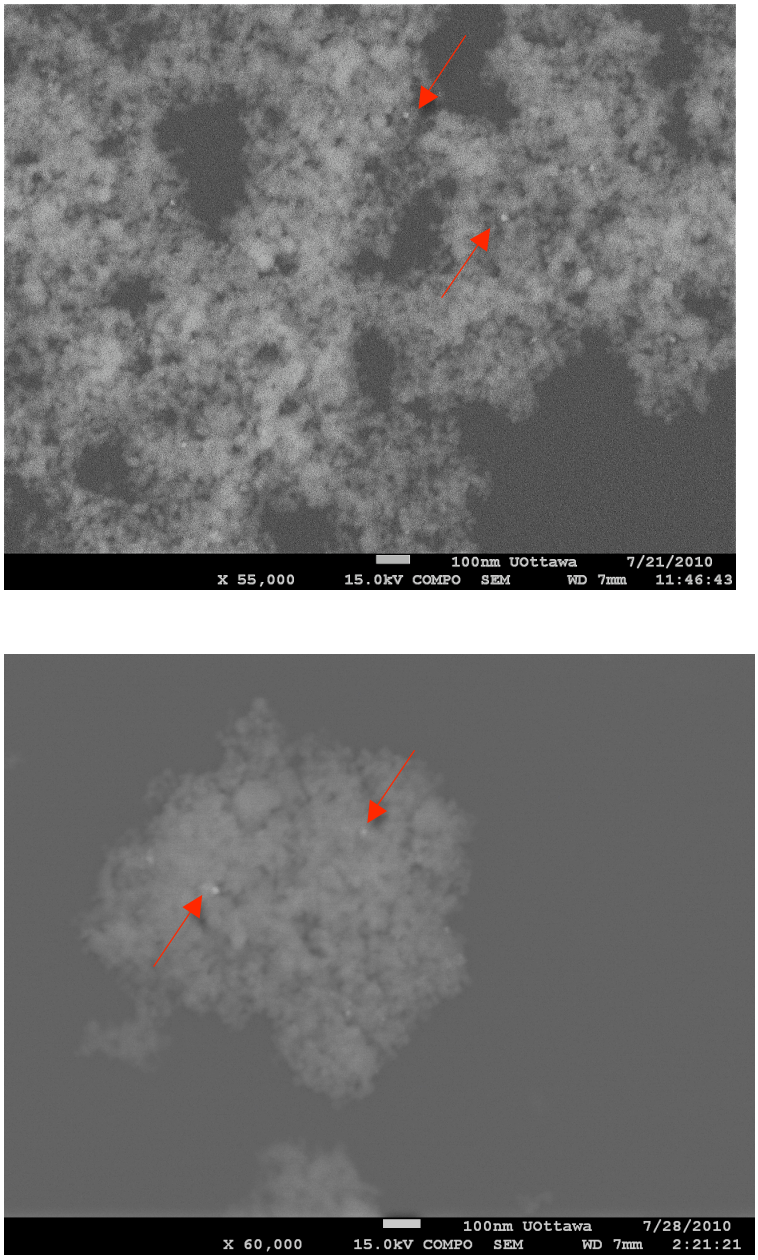

Figure 3.10 TOP: SEM image of Ag@TiO_2 (P90) after slurry synthesis. Small brighter spots indicate AgNP on the TiO_2. Bottom: SEM image of Ag@TiO_2 (P90) after LED irradiation at 455 nm. The small bright spots indicate AgNP, which are now smaller than in the top image. Red arrows indicate some of the AgNP on the TiO_2.

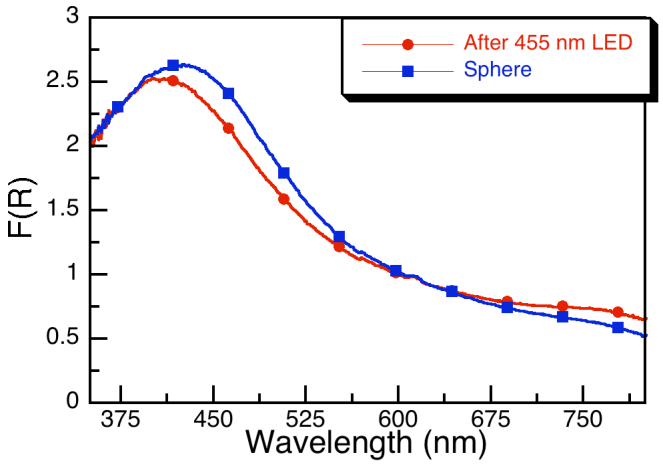

Figure 3.11 UV-Vis diffuse reflectance of sphere@TiO_2 (P90) and the NP@TiO_2 (P90) after LED irradiation with 4 LED lights at 455 nm in a flow cell cuvette.

Another attempt was made at appending the Ag shapes to the supports. The AgNP shapes were synthesized in solution with LED irradiation[19] followed by addition to TiO_2 or HTC; however, these results were not consistent. In some cases the NP would adsorb onto the support surface, while other trials showed little adsorption. This may be explained by the properties of the TiO_2 and the NP. The TiO_2 has an isoelectric potential of 6 and the NPs have a negative surface charge because of the citrate stabilizing them, which may be preventing the association.[35,36] Acid treatment of the TiO_2 was attempted to positively charge the support surface varied to facilitate NP adsorption. This was done by soaking TiO_2 in concentrated HCl for a few hours, then washing many times with water and centrifuging.[37] This process did help the adhesion of the NP, but the quantity of NP adsorbed onto the support surface varied from batch to batch.

Functionalizing SiO_2 with APTES is a common synthesis[20] and AgNP are known to be attracted to amine groups because of interactions between the nitrogen lone pair and the AgNP through π back bonding forming a strong bond.[30,38] All the AgNP shapes adhered to the APTES functionalized SiO_2 with no NP left in solution. Because previous work showed SiO_2 was not an effective support for the catalytic reactions, this functionalization method was used for TiO_2. TiO_2 APTES functionalization was adapted from the procedure for SiO_2 functionalization,[38] and AgNP shapes were found to adsorb well onto these surfaces. TiO_2 (P90) was always used for the APTES functionalization in this work. The loading in the case of APTES functionalized TiO_2 was 0.5%. The NP composites of APTES functionalized TiO_2 are coloured (Figure 3.12, Figure 3.13) depending on the shape added and have DR SPB representative of each shape (Figure 3.14 and Figure 3.15). Seeds, decahedra, and plates in solution have peaks at 398 nm, 463 nm, and 330 nm with scattering >690 nm, respectively (Figure 3.16). On support, seeds, decahedra, and plates have peaks at 430 nm, 445 nm, and scattering >650 nm respectively (Figure 3.14). The SEM images of decahedra@TiO_2 can be found in Figure 3.17, and have an average size of 25 nm ± 8 nm (Figure 3.18). Before addition to support, the decahedra NP have a size of 29 nm ± 4 nm (see Figure 3.17). SEM images of 0.5% AgNP seeds@TiO_2, Figure 3.19, show an average size of 30 nm ± 9 nm (Figure 3.20). Before addition, the seed NP are 5 nm ± 1 nm in size (Figure 3.19 top). The seeds may be agglomerating on the surface of the TiO_2

causing the effective NP size to increase. SEM of the plates@TiO_2 was attempted many times unsuccessfully. The plates in solution can be seen in Figure 3.21. Because of their large size (edge length >100 nm), the smaller sized TiO_2 particles (~7-50 nm)[39] may be sticking to the surfaces of the plates since they are in great excess preventing the visualization by microscopy (COMPO mode depends on the backscattering and is a surface technique).[40] Their presence is confirmed by visual observation of blue colour and diffuse reflectance spectra (Figure 3.12 and Figure 3.16).

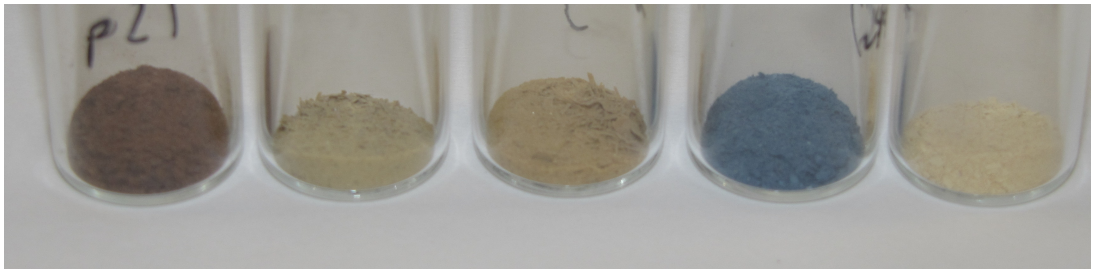

Figure 3.12 Photograph of the supports with different AgNP shapes. TiO_2 type is P90. From left to right: 1%Ag@TiO_2 (slurry method), 0.5% AgNP seeds@TiO_2(APTES), 0.5% decahedra@TiO_2(APTES), 0.5% plates@TiO_2(APTES), 4% $AgNO_3$@HTC

Figure 3.13 Photographs of Left: 1% Ag@TiO_2 (P90) (slurry) and Right: 0.5% Ag@TiO_2 (P90) (slurry)

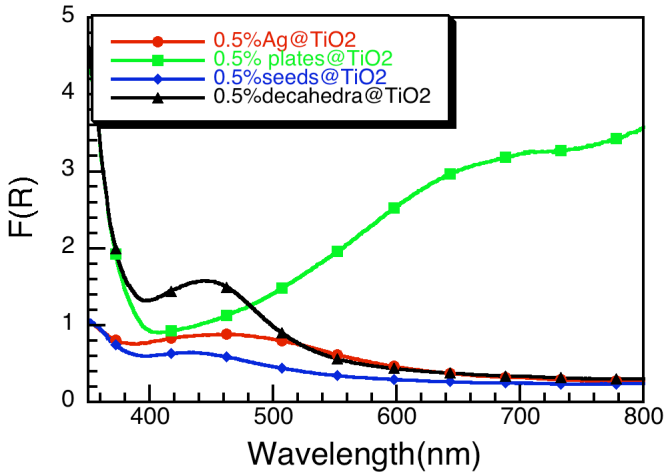

Figure 3.14 Diffuse Reflectance of 0.5% Ag shapes@TiO_2 (P90) (APTES). Scattering at >650 nm for the plates, peaks at 465 nm for 1% Ag@TiO_2 (slurry), 430 nm for seeds, and 445 nm for decahedra.

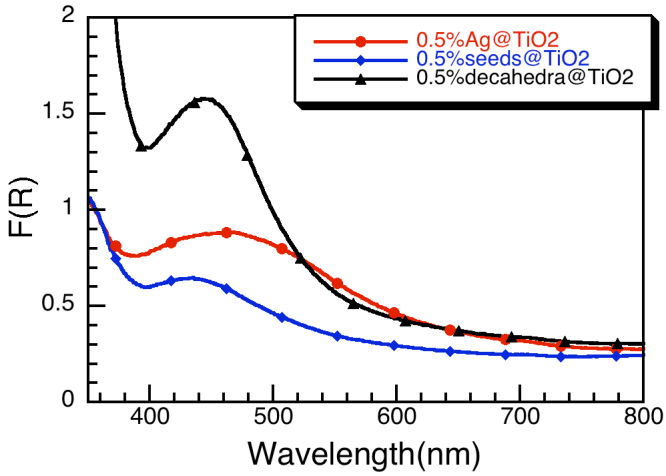

Figure 3.15 Diffuse Reflectance close up of 0.5% Ag@TiO_2 (P90) (slurry method), 0.5% seeds@TiO_2(APTES), and 0.5% decahedra@TiO_2 (APTES).

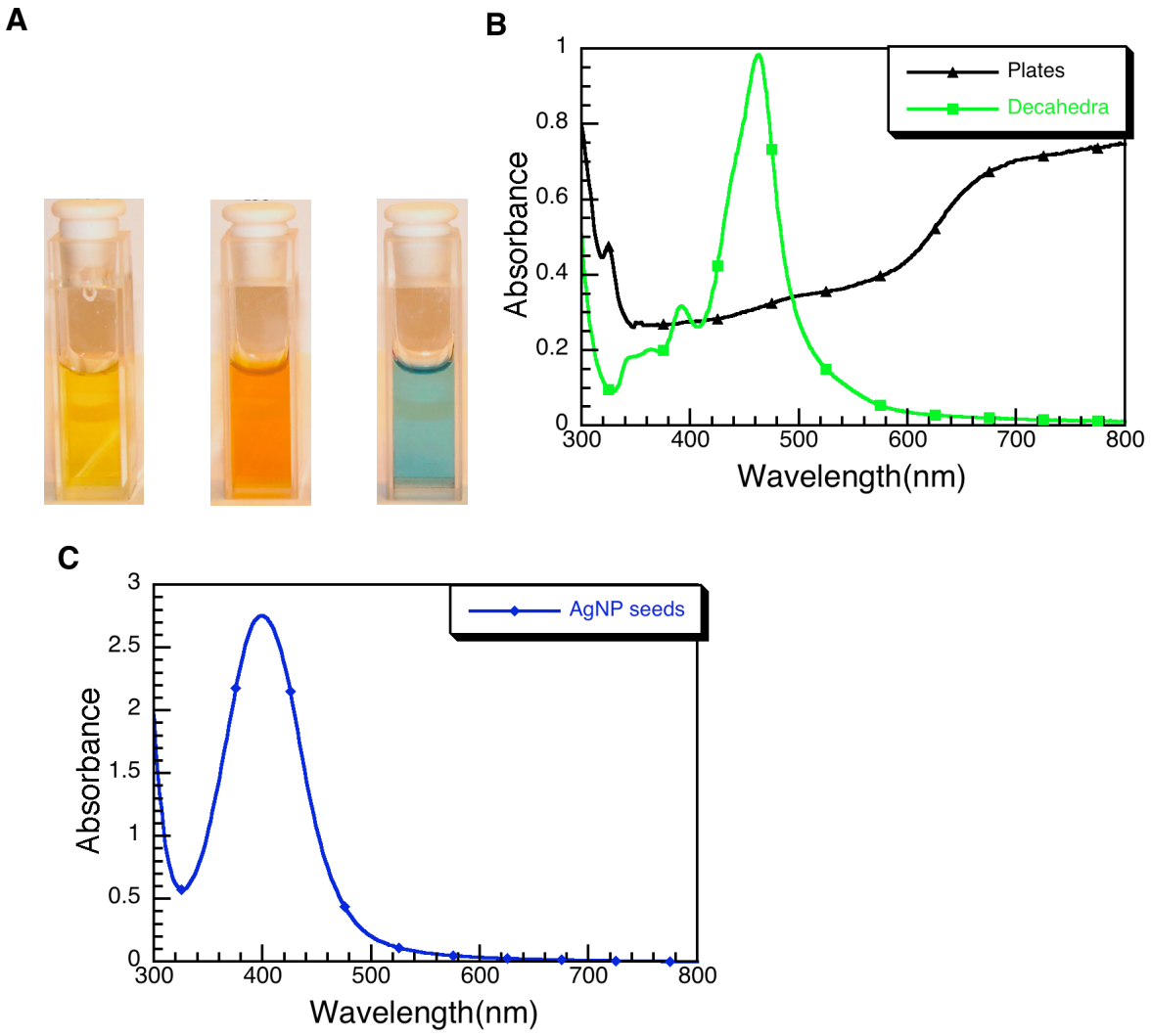

Figure 3.16 A: Photograph of the 0.1 mM colloidal silver seeds, decahedra, and plates respectively.[19] B and C: Absorption spectra of the different colloidal AgNP shapes in solution. Peaks at 398 nm (AgNP seeds (C)), 463 nm (decahedra (B)), and scattering >690 nm and a peak at 330 nm for the transverse mode (plates (B)).

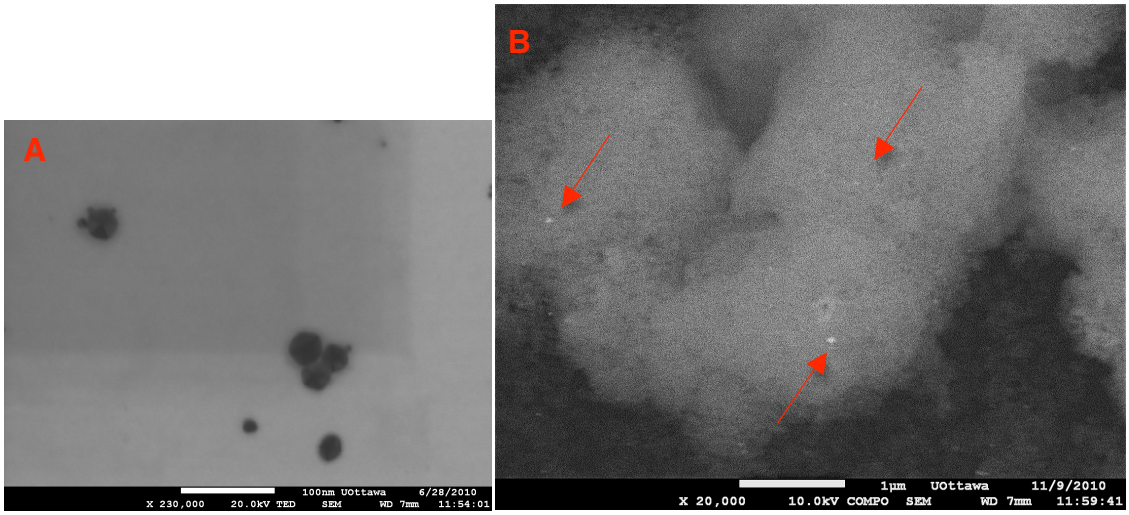

Figure 3.17 SEM images of Ag decahedra in TED mode (A) and Ag decahedra@TiO_2 (P90) (APTES) in COMPO mode (B). Arrows show AgNP on the TiO_2.

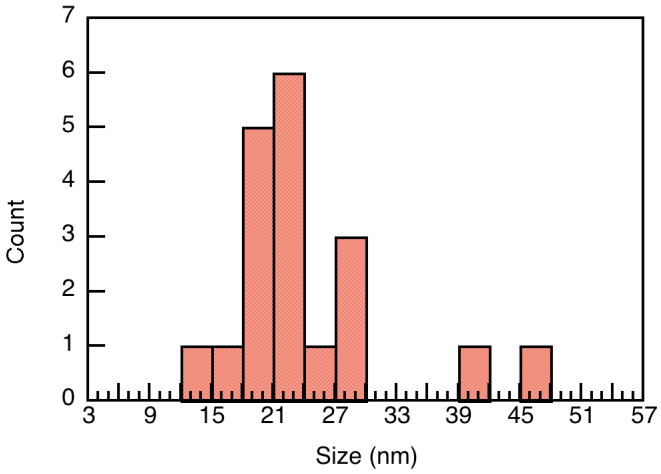

Figure 3.18 Histogram showing particle size distribution of AgNP decahedra@TiO_2(P90) (APTES) based on approximately 20 NP.

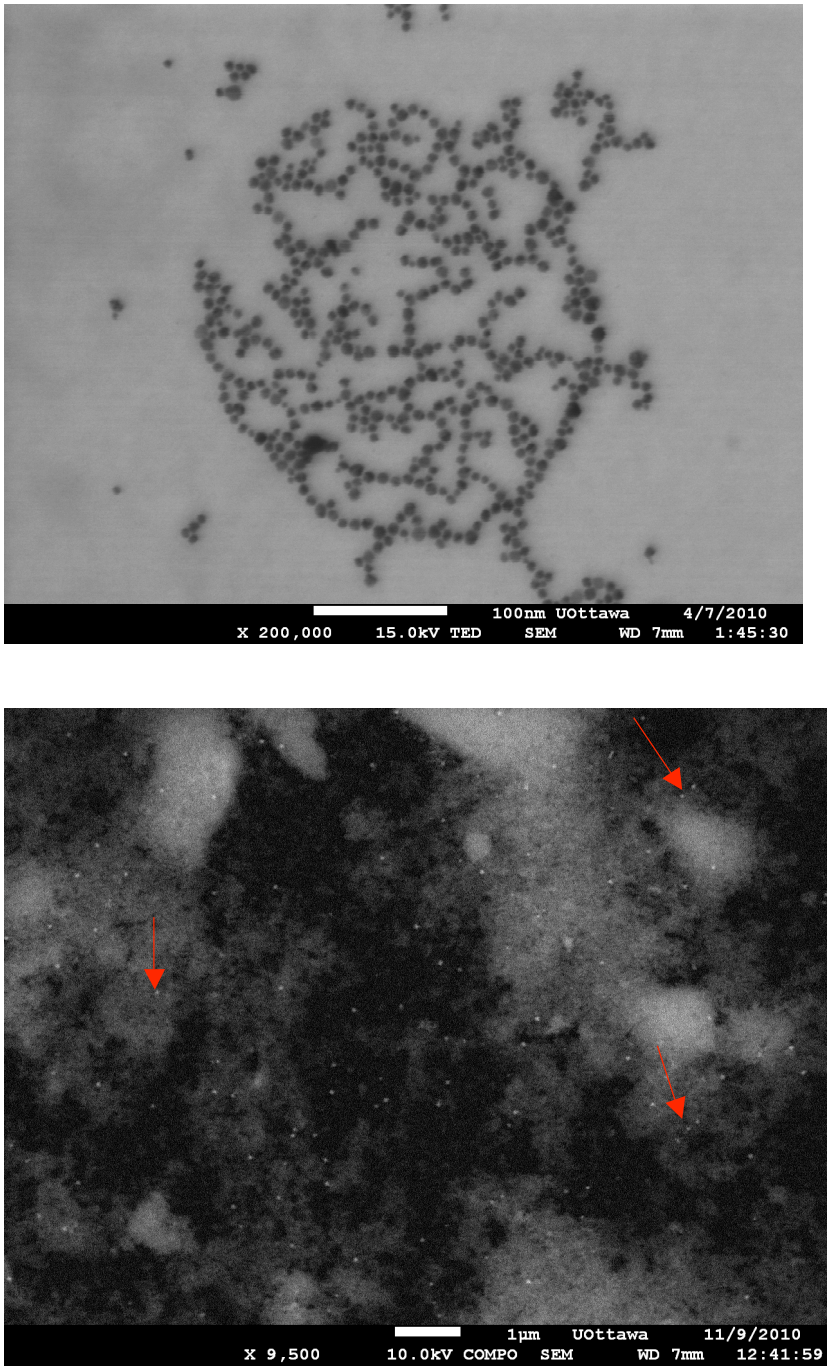

Figure 3.19 SEM images of AgNP seeds in solution (0.2 mM) in TED mode (top) and 0.5% Ag seeds@TiO_2(P90) (APTES) in COMPO mode where red arrows point to some of the AgNP (bottom image)

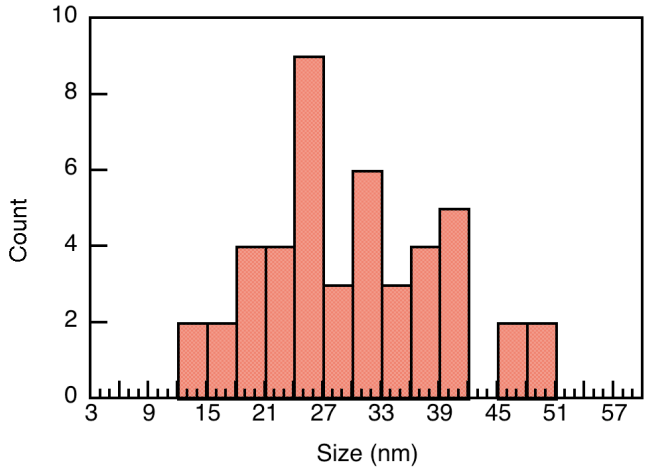

Figure 3.20 Histogram showing size distribution of AgNP seeds@TiO_2(P90) (APTES) based on about 45 nanoparticles.

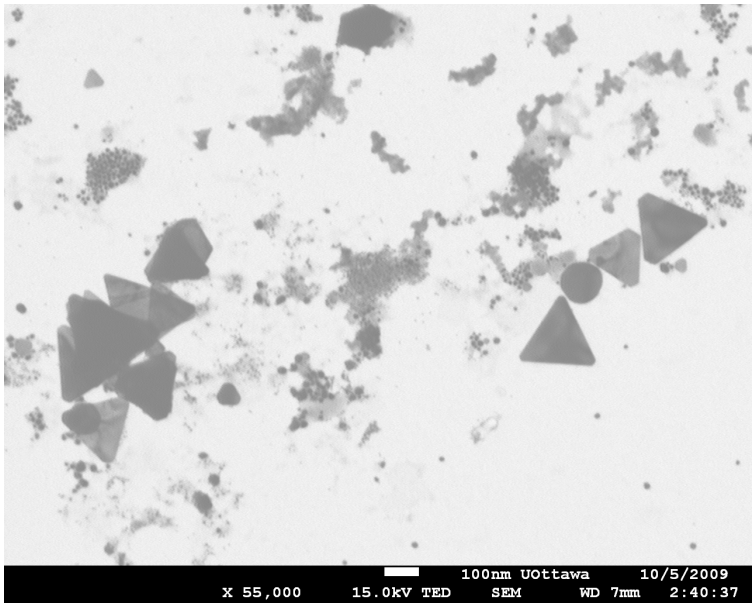

Figure 3.21 SEM image of AgNP plates in TED mode. Some smaller spherical NP are still present, but the majority are plates.

3.3.1.4 Supports

Many supports were used in attempts to get AgNP on the support in situ as well as after synthesis. The supports include TiO_2 (P25, P90, anatase), HTC,

zeolites (NH_4Y, NaY), SiO_2, MgO, hydroxyapatite, and APTES functionalized TiO_2 (P90) and SiO_2. The only supports that worked well were TiO_2 (both P90 and P25) (Figure 3.3) and HTC (Figure 3.23 and Figure 3.22) for the slurry method. Hydrotalcite is a layered double hydroxide containing magnesium and aluminum ($Mg_6Al_2(CO_3)(OH)_{15}{\cdot}4(H_2O)$).[41] The NP made on HTC have a size of 14 nm ± 7 nm based on SEM (Figure 3.24). Previous reports have successfully synthesized NP followed by addition to the support to form the NP composite.[16] In the case of the citrate stabilized NP, this was not possible, with the majority of NP remaining in the supernatant solution. The lack of NP adsorption may be a result of the negative charge of the NP with citrate stabilization[36] and pH of the NP solution, ~ 6.8. The TiO_2 has an isoelectric point of 6,[35] so at pH 6.8 it will carry a slight negative charge, repelling the negatively charged NP, suppressing electrostatic interactions.[18,42] HTC has an isoelectric point of 10,[11] meaning in pH 6.83 the support will carry a more positive charge.[18] This would make it a better support that would promote adhesion of the NP to the support, however, hydrotalcite is hydrophobic and does not suspend in water, which makes addition of the water-soluble particles difficult. Further, the NP are not stable in organic solvents or a mixture of water and acetonitrile. Silica has an isoelectric point of 2,[18] so the NP do not attach to it either because of its negative charge at pH 6.8.[18]

In the slurry method, the AgNP form on the support and stay attached. This may be because the silver ion has a positive charge, attracting it to the

negative TiO_2 surface at slightly basic pH (pH of solution with TiO_2 is around 7.8) through coulombic interactions[18,42] while the citrate acts as a stabilizer to the other exposed AgNP surfaces. Silver nanoparticles synthesized on TiO_2 have been shown to have strong metal-support interactions.[14] The APTES functionalized TiO_2 and SiO_2, however, worked very well for this approach. All the NP were on the support after addition and centrifugation, the supernatant was clear and the support was coloured (Figure 3.12).

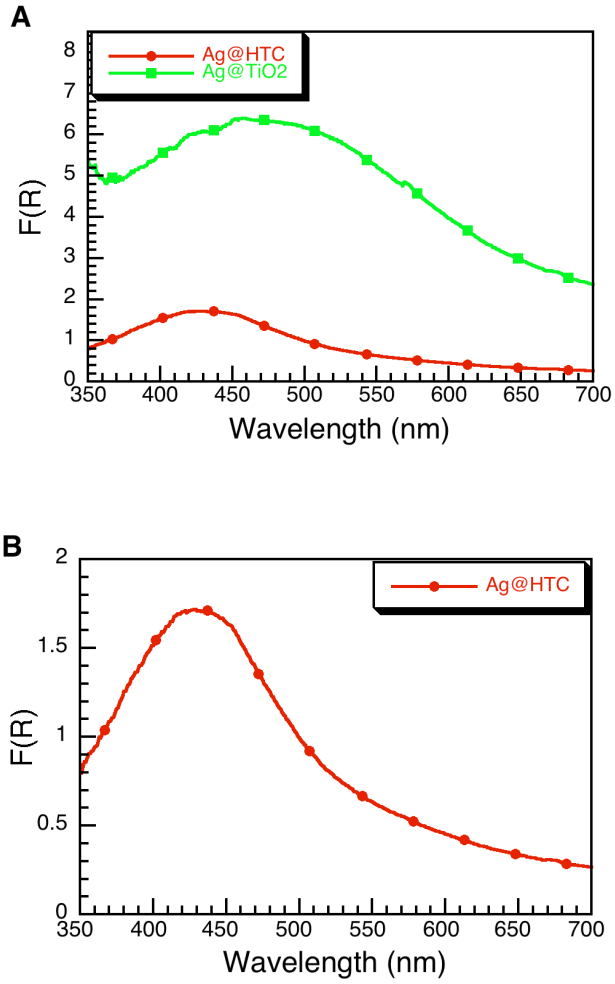

Figure 3.22 A: Diffuse Reflectance of 4% $AgNO_3$@HTC and TiO_2 using the slurry method. B: an expansion of the Ag@HTC showing the SPB at 430 nm.

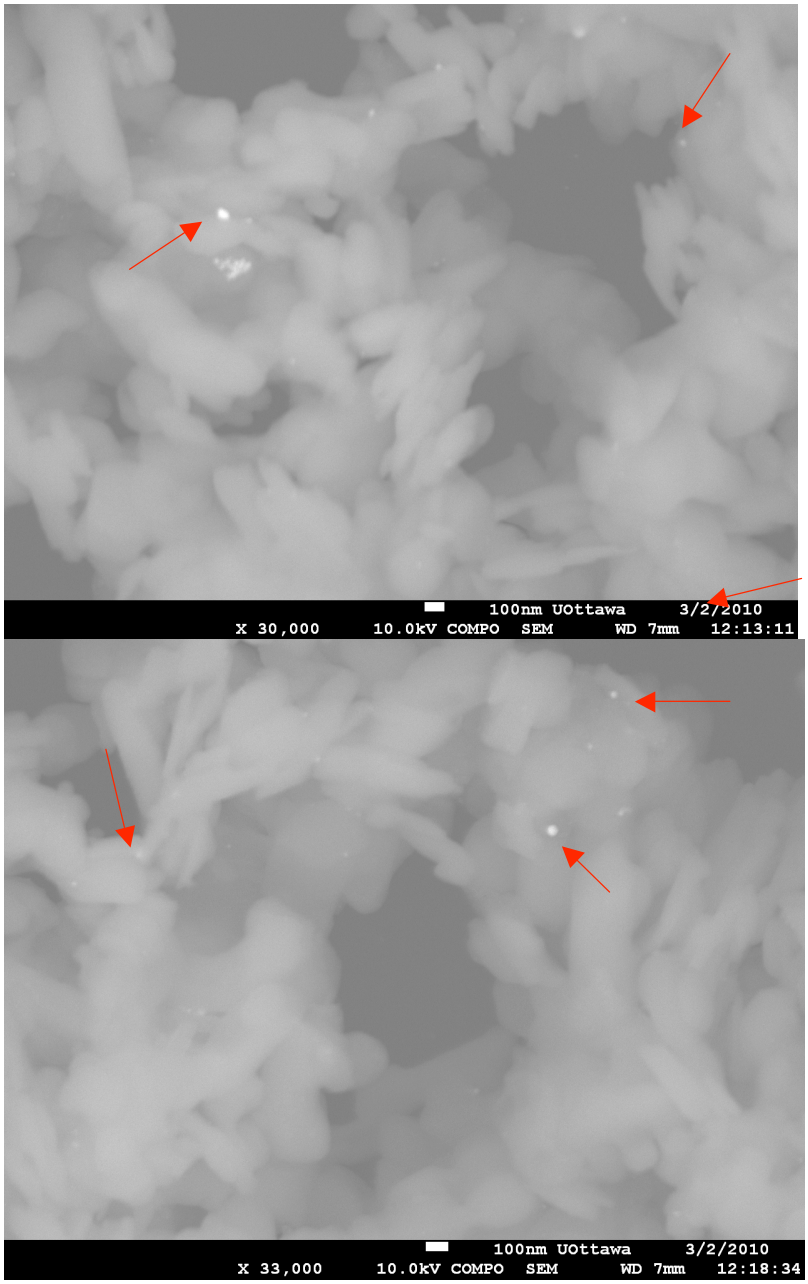

Figure 3.23 SEM images of 4% $AgNO_3$@HTC. Red arrows are pointing out some of the AgNP on the HTC.

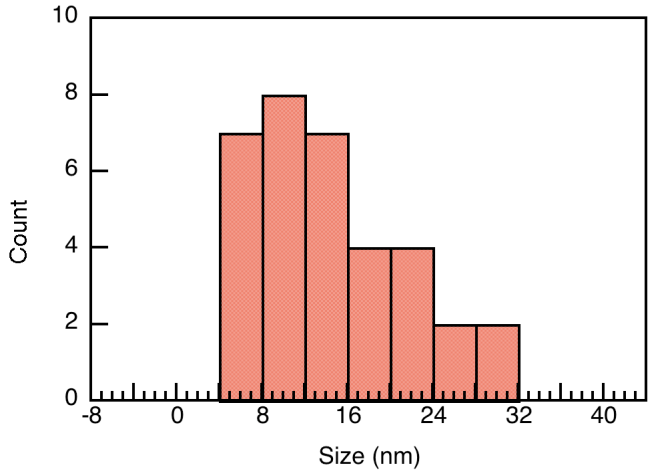

Figure 3.24 Histogram showing distribution of AgNP@HTC based on approximately 35 nanoparticles.

3.3.1.5 Loadings

Samples were made using the slurry method and varying the Ag loading between 0.5 and 4% with respect to the support. With higher loadings, more NP appeared to wash off in the cleaning phase of the synthesis as can be seen by the increased absorption of the supernatant at wavelengths below 400 nm (that of AgNP and around 270 nm of I-2959) in Figure 3.25. After 4 washes and centrifugation, there is a small amount of AgNP washing off as well as Irgacure. The diffuse reflectance of 0.5%, 1% and 4% loadings of Ag@TiO_2 (P90) can be found in Figure 3.26, Figure 3.27, and Figure 3.28 respectively. The 4% loading shows a broader peak, which may indicate more polydisperse NP.[43] The 4% loading of $AgNO_3$ on TiO_2 does have a broader range of NP sizes based on SEM (17 nm ± 17 nm see Figure 3.4) whereas with a 1% loading they are more monodisperse with a size distribution of 9 nm ± 3 nm based on SEM

measurements (see Figure 3.30). Previous work by Grunert *et al.*[14] has shown that the size of the AgNP on the support depends on the metal loading.

When HTC is the support, a 1% loading of Ag in the slurry method results in no NP formation, a 4% loading is necessary to have NP formation. The irradiation time for HTC is also much longer, 1 hr compared to 10 minutes for TiO_2. This could be because there is not enough light getting to the I-2959 to form a ketyl radical to reduce the Ag^{+}.[16] HTC has a larger particle size (>100 nm) than TiO_2 (7-50 nm[44] with a mean size of 21 nm,[39] Figure 3.31), requiring more light to reduce the Ag^{+} with the same amount of solid because of more scattering (Figure 3.23 and Figure 3.31). The larger HTC particle size might prevent light from reaching the I-2959, thus reducing the yield of AgNP formed. As can be seen with the 4% loading, there are less NP forming with HTC compared to 4% Ag@TiO_2 (Figure 3.22) showing that the reduction is less efficient with HTC. The lower yield of NP could also reflect the need for a mixed solvent system of 50:50 MeCN:H_2O to form a suspension of HTC, which is very hydrophobic. This may have reduced the solubility of the other reagents, mainly the citrate, which is not soluble in MeCN.

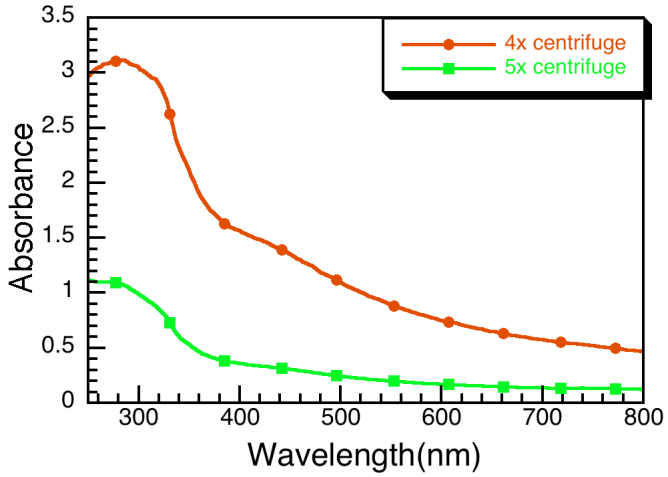

Figure 3.25 UV-Vis of runoff (supernatant) after centrifuging 4 and 5 times ($Ag@TiO_2$ (P90) made in slurry method). After 4 times, can see some AgNP washing off (absorbance ~400 nm) as well as Irgacure that absorbs around 270 nm.

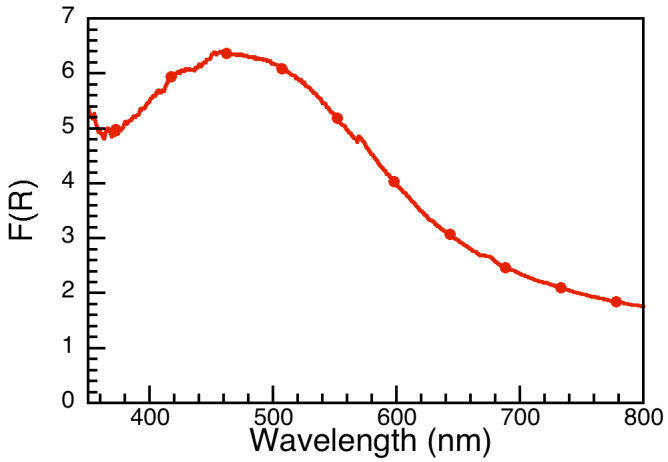

Figure 3.26 Diffuse Reflectance of 4% $Ag@TiO_2$ (P90) (slurry method) with a maximum absorbance at 465 nm.

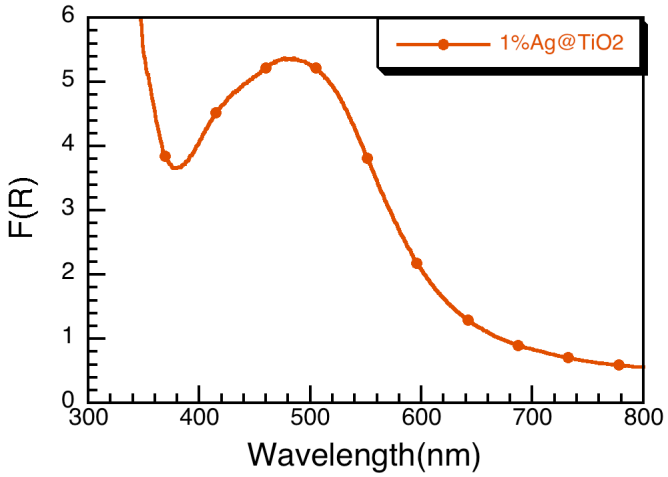

Figure 3.27 Diffuse reflectance of 1% Ag@TiO_2 (P90) (slurry method) with a maximum absorbance at 480 nm.

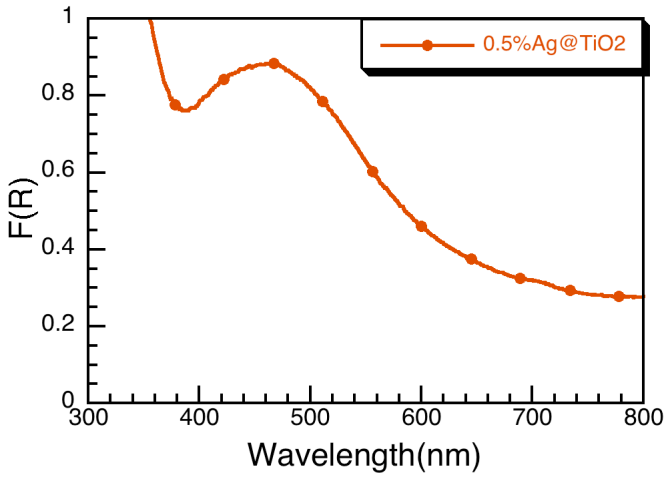

Figure 3.28 Diffuse Reflectance of 0.5% Ag@TiO_2 (P90) (slurry method) with a maximum absorbance at 460 nm.

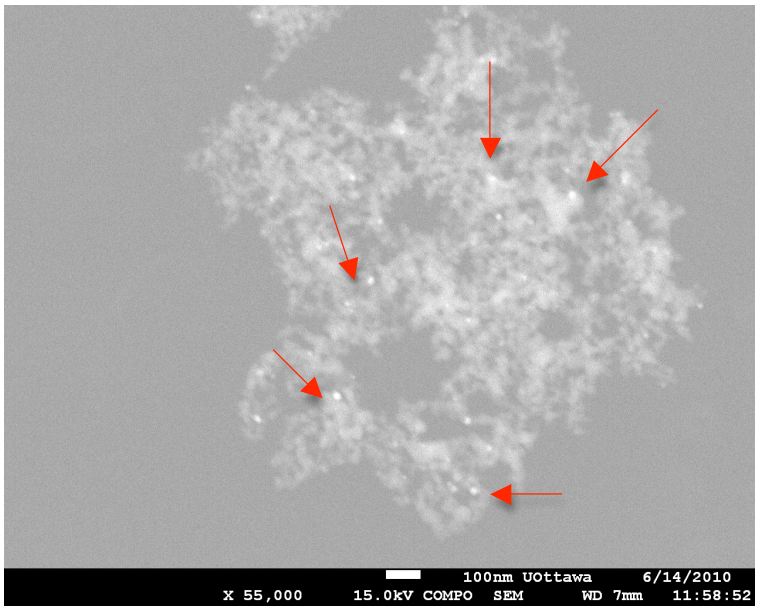

Figure 3.29 SEM image of 1% Ag@TiO_2 (P90) in the slurry method. Red arrows point to some of the AgNP.

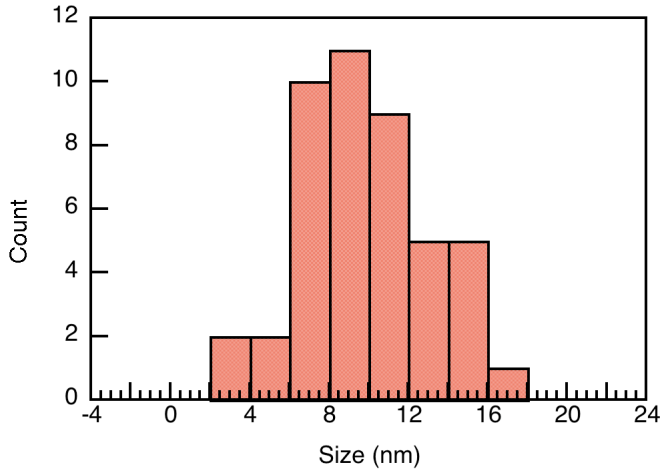

Figure 3.30 Histogram showing particle size distribution of 1% Ag@TiO_2 based on approximately 45 nanoparticles.

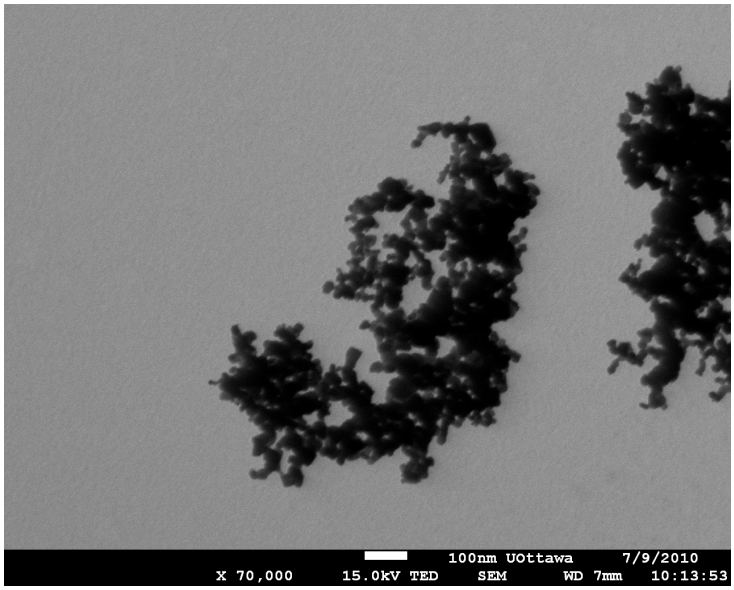

Figure 3.31 SEM image of TiO_2 (P25) alone

3.3.2 Catalysis

Nanoparticle catalysis was tested using alcohol oxidations. Alcohol oxidations have been shown to be catalyzed by AgNP[9] and are a relatively easy reaction not requiring high pressures or temperatures with which to test the catalytic efficiency.

3.3.2.1 Preliminary Reactions and Comparison with Gold Nanoparticles

The oxidation of 4-methoxybenzyl alcohol to 4-methoxybenzaldehyde (4-MBAldehyde) (Scheme 3.3) was tested and the kinetics were monitored every 5 minutes until completion. In 9 mL of toluene, 0.1 mmol of 4-methoxybenzyl alcohol (4-MBA) was used with 138 mg (0.05 mmol Ag) of 4% Ag@TiO_2 (P90) prepared using the slurry method. The kinetics were monitored by GCMS and show that at 40 minutes the reaction has reached 100% completion to the aldehyde (Figure 3.32).

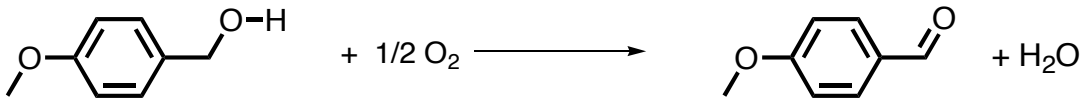

Scheme 3.3 Oxidation of 4-MBA to 4-MBAldehyde using AgNP supported on TiO_2.

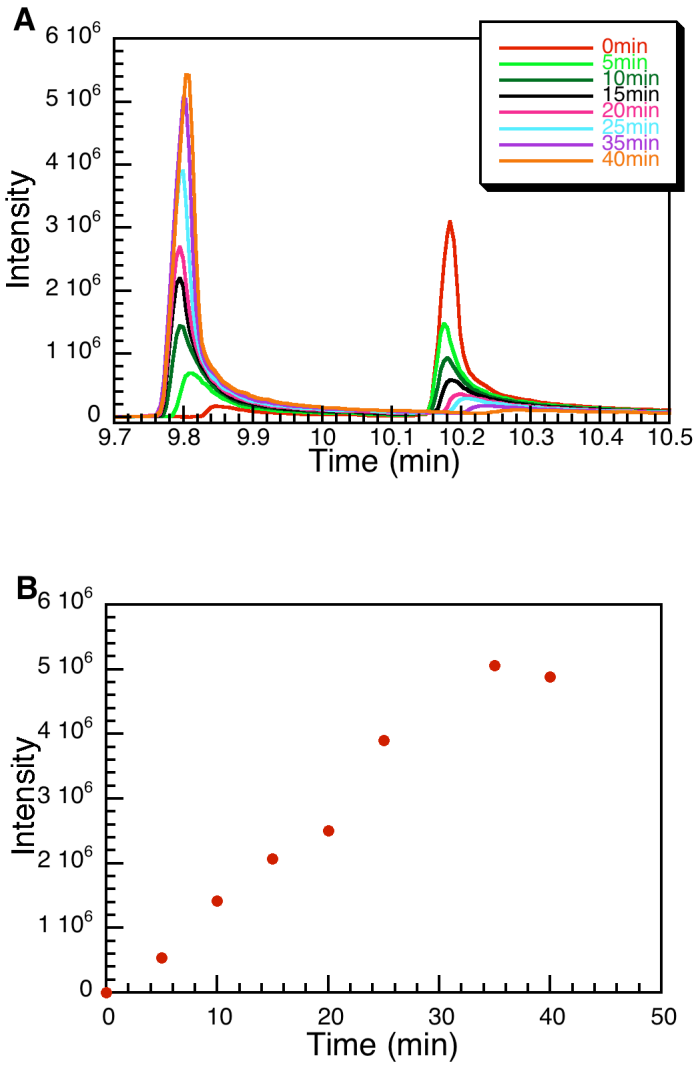

Figure 3.32 A: GCMS of 4-MBA oxidation using 4% Ag@TiO_2 (P90) prepared in the slurry method. Peak at 9.8 minutes is that of the aldehyde and the peak at 10.2 minutes is the alcohol. B: Intensity at the time of each aliquot throughout the reaction monitored at 9.8 minutes retention time (peak in GCMS of the 4-MBAldehyde).

Using the same experimental conditions as above, Ag@HTC was aliquoted after one hour to compare the supports (Figure 3.33). The hydrotalcite is less catalytically active than TiO_2 toward this reaction showing that the support is more than an inert participant in the reaction. Metal oxide supports have been suggested to participate actively in the reaction mechanism of oxidation reactions

where the metal oxide has a surface redox reaction.[18,45] The hydrotalcite cannot participate in this manner since it cannot undergo a surface redox reaction that occurs with the oxygens on the surface of metal oxides. Hydrotalcite is composed of aluminum and magnesium hydroxides, which are considered inactive supports in oxidation reactions.[11,12] Active metal oxides are able to undergo redox reactions providing reactive oxygen species to the reaction.[12]

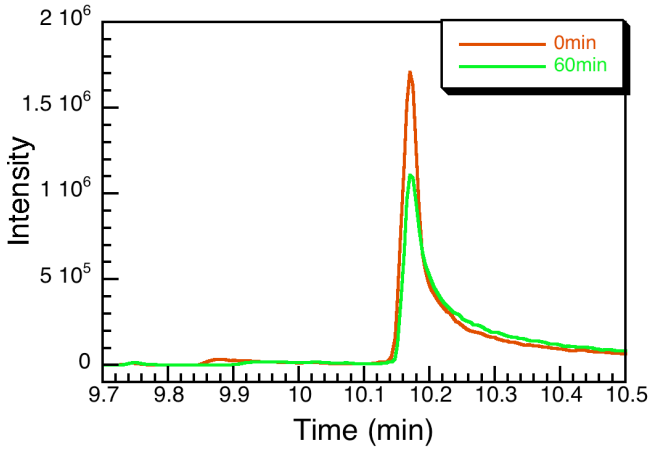

Figure 3.33 GCMS of the products of the oxidation of 4-MBA using Ag@HTC (prepared in slurry method). Peak at 10.2 minutes is the alcohol and the aldehyde will appear at 9.8 minutes.

As a comparison between Ag and Au for this reaction, Ag@HTC was run alongside Au@HTC (prepared using a solid state method) to compare the catalytic effectiveness of the different metal NP for the reaction. The oxidation of *sec*-phenethyl alcohol (Scheme 3.4) was run and aliquots were removed every hour for GCMS analysis. The reaction was carried out under a positive oxygen atmosphere, in toluene at 75°C using 0.1 mmol of alcohol and 150 mg of catalyst (0.056 mmol Ag, 0.0076 mmol Au). The oxidation using the Ag@HTC showed more conversion than that of Au@HTC (see Figure 3.34). There is approximately

a 49.5% conversion to the ketone after 7 hours for Ag@HTC and a 0% conversion for the Au@HTC (see Figure 3.34). This may be a result of the lower amount of Au compared to Ag for the two reactions or may also be a result of silver's higher catalytic activity toward this reaction.

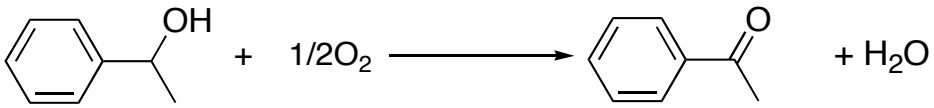

Scheme 3.4 Oxidation of *sec*-phenethyl alcohol to acetophenone.

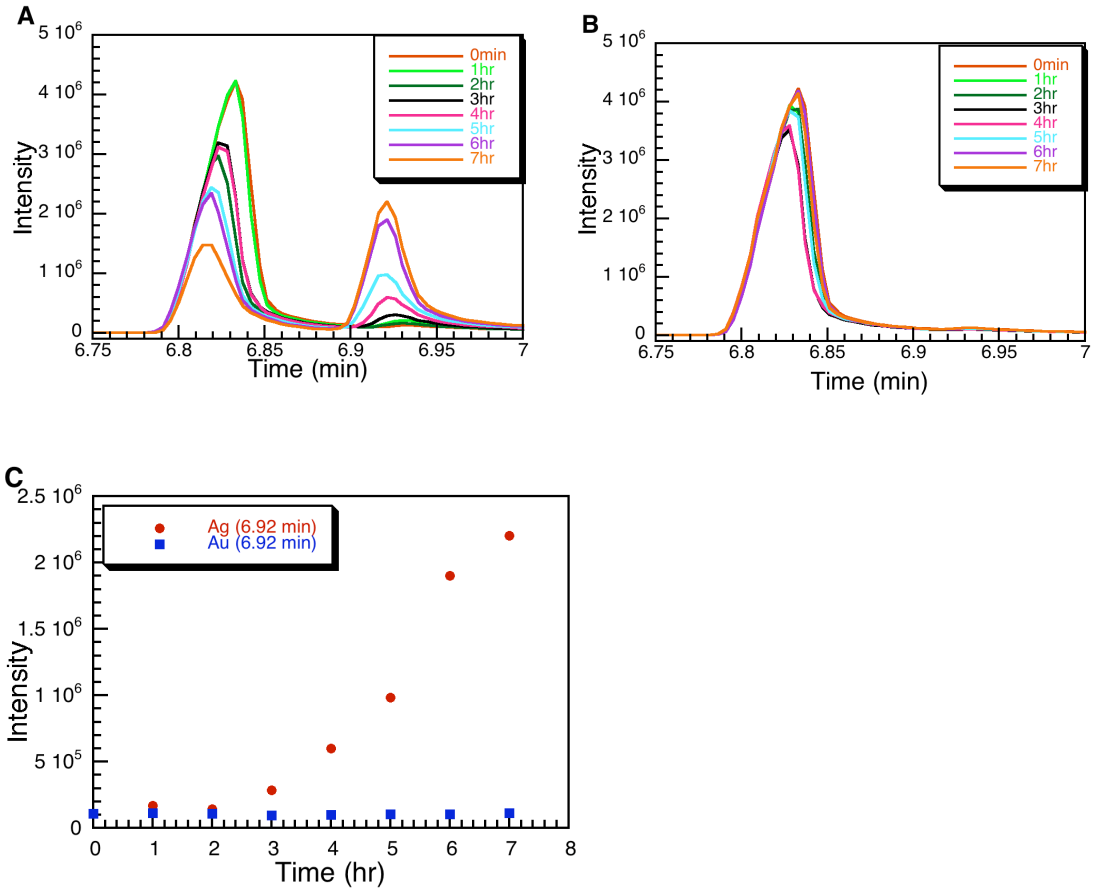

Figure 3.34 GCMS of aliquots of the oxidation of *sec*-phenethyl alcohol to acetophenone using A: Ag@HTC (prepared in slurry method) and B: Au@HTC (prepared in solid state method). Alcohol is seen at 6.83 minutes and the ketone at 6.92 minutes. C: Intensity at a retention time of 6.92 minutes (acetophenone) at each aliquot time throughout the reaction.

3.3.2.2 Screening Process

The amount of catalyst in these experiments is quite high and running each experiment on the bench-top is not time efficient. Experiments were done using the SYMYX high throughput facility at the University of Ottawa to systematically monitor the efficacy of various catalysts and of different catalyst amounts and were analyzed via HPLC-UV spectroscopy.

0.025 mmol of either *sec*-phenethyl alcohol or 4-MBA was heated and stirred at 75°C, under 2 atm of oxygen for 16 hours using either water or toluene as the solvent and a variety of supports (740 nmol of Ag@TiO_2(P90 and P25), SiO_2, HTC) (Figure 3.35). Samples prepared in water had very little conversion, likely because of the minimal solubility of 4-MBA in water. The formation of an emulsion minimized interactions of the 4-MBA with the oxygen and the catalyst. *Sec*-phenethyl alcohol has a solubility of 0.163 mol/L in water[46] but still had little conversion to the ketone attributed to the solvent. Solvents of high polarity have been shown to be poor for oxidation reactions and non-polar solvents have been shown to increase the rate or reaction.[47] For this reason, water was not further examined as a solvent. Silica as a support also had very little conversion, so was also no longer examined as a viable catalyst support. Silica is considered to be an inactive support, and therefore not aiding in catalytic activity.[11] Silica is an irreducible oxide that cannot provide oxygen atoms to the reaction the way that active supports, such as TiO_2 can.[13,48] It has also been reported that for inactive supports, the NP size has a large effect on the catalytic efficiency and only

compare to active supports at particle sizes below 2 nm.[12] With active supports, the size of the NP was shown to be less important, with particles as large as 30 nm on TiO_2 showing good catalytic efficiencies.[12]

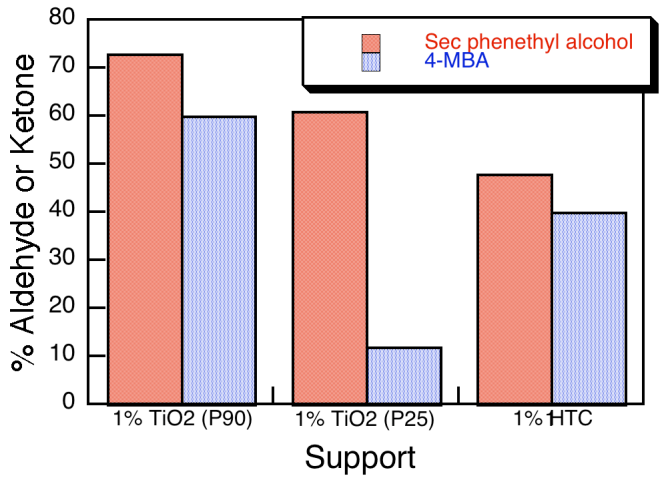

Figure 3.35 Bar graph of percent conversion to the aldehyde or ketone from the oxidation of *sec*-phenethyl alcohol and 4-methoxybenzyl alcohol in toluene using the specified loading of Ag and catalyst support. All were prepared in slurry method.

The reactions gave varying degrees of efficiency. TiO_2 P25 is not as efficient as the P90 for alcohol catalysis. AgNP on hydrotalcite show less catalytic activity compared to those on TiO_2, which was expected based on previous results. This may reflect the likely lower loading of silver on hydrotalcite or the support itself both discussed earlier. The oxidation reaction used as a model from here on was the oxidation of 4-MBA in toluene using TiO_2 (P90).

3.3.2.3 Amount of Catalyst

The amount of catalyst was tested to see what effect this has on the efficiency of the oxidation. The oxidation of 4-MBA in toluene using 0.012 mmol of alcohol and varying the amount of catalyst from 0 mg to 20 mg of 1%

Ag@TiO_2 (P90) made with slurry method. This was done in the SYMYX under 2 atm of oxygen and at 75°C for 16 hours. With just TiO_2 or no catalyst there was 0% conversion to the aldehyde (see Table 3.1), showing that AgNP are necessary for catalysis. The percent conversion to the aldehyde increases as the amount of catalyst increases, Figure 3.36.

Table 3.1 Table showing % aldehyde after oxidation of 4-MBA using different amounts of catalyst (1% Ag@TiO_2 made in the slurry method without APTES).

Amount of 1% Ag@TiO_2(P90)	**% Aldehyde**
0 mg (0 µmol Ag)	0 %
4 mg (0.37 µmol Ag)	55.5 %
8 mg (0.74 µmol Ag)	67 %
12 mg (1.1 µmol Ag)	86.3 %
20 mg (1.85 µmol Ag)	99 %
20 mg just TiO_2 (P90)	0 %
20 mg just HTC	0 %

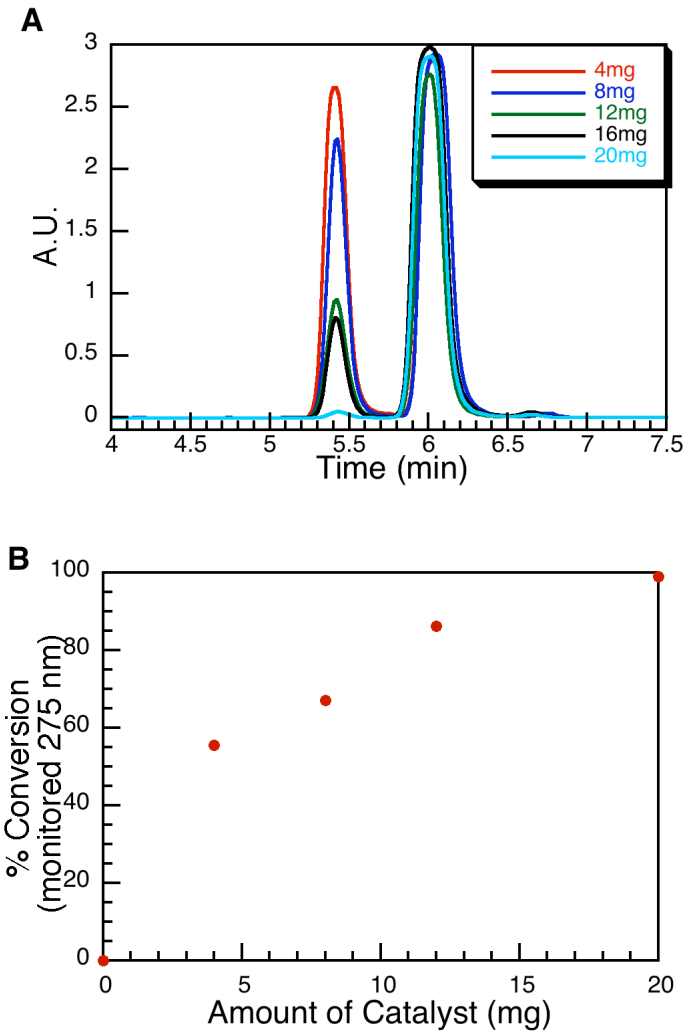

Figure 3.36 A: HPLC spectra of different catalyst amounts monitored at 275 nm. Catalyst is 1% Ag@TiO_2 made in slurry method. Peak just before 5.5 minutes is that of the alcohol and the peak around 6 minutes is that of the aldehyde. B: amount of catalyst versus the % conversion to the aldehyde monitored at 275 nm (absorbance of the aldehyde).

3.3.2.4 Shapes

Using 8 mg of catalyst, reactions were run in the SYMYX using the different catalysts including Ag seeds@TiO_2(APTES), decahedra@TiO_2(APTES), plates@TiO_2(APTES), 1% Ag@TiO_2 (slurry), and 1% Ag@TiO_2(APTES) (slurry). These reactions were done under the same conditions as previously (0.012 mmol 4-MBA, 75°C, 2 atm O_2, 16 hours). There is little difference between the

supported NP made in the slurry method with or without APTES functionalized on the TiO_2, showing that the APTES is not an active player in the catalysis (Table 3.2). The 1% Ag@TiO_2 (slurry) had the highest conversion after 16 hours followed by the plates@TiO_2 and seeds@TiO_2, then the decahedra@TiO_2 (Table 3.2). The near-spherical NP made in the slurry method are the best at catalyzing the oxidation of 4-MBA alcohol. This may be a result of their smaller size compared to the larger shapes or may be because of their edges or facets, which is elaborated on in the next section.

Table 3.2 Table of % conversion to 4-methoxybenzyl aldehyde using the different silver NP and Ag shapes supported on TiO_2. TiO_2 is P90 in all cases.

Support	% Aldehyde
8 mg 1% Ag@TiO_2 (slurry)	94%
8 mg 1% Ag@TiO_2(APTES) (slurry)	97%
8 mg 0.5% seeds@TiO_2(APTES)	64.5%
8 mg 0.5% decahedra@TiO_2(APTES)	57%
8 mg 0.5% plates@TiO_2(APTES)	80%

3.3.2.5 Kinetics

The conditions used for the SYMYX were selected to run the kinetics measurements comparing the different shapes on the bench. The same conditions as outlined previously were used for the oxidation of 0.075 mmol of 4-MBA with 40 mg of catalyst (1% Ag@TiO_2 (slurry), or 0.5% seeds, decahedra,

or plates@TiO_2(APTES)) (see section 3.3.2.4 Shapes). The reactions were done on a 5 mL scale in toluene taking an aliquot every 1-2 hours depending on the rate and monitoring up to 24 hours. The traces can be seen in Figure 3.37 showing that AgNP@TiO_2 made in the slurry method provide the fastest conversion to the aldehyde. The reaction is unimolecular and fits well to first order growth kinetics (Table 3.3). The rate constant for the slurry showed the fastest conversion, 2.04×10^{-4} s^{-1}. The decahedra were the next fastest followed by the plates, and the seeds were the slowest (Figure 3.37). The seeds, plates, and decahedra have rate constants of 4.72×10^{-5} s^{-1}, 8.48×10^{-5} s^{-1}, and 8.85×10^{-5} s^{-1}, respectively.

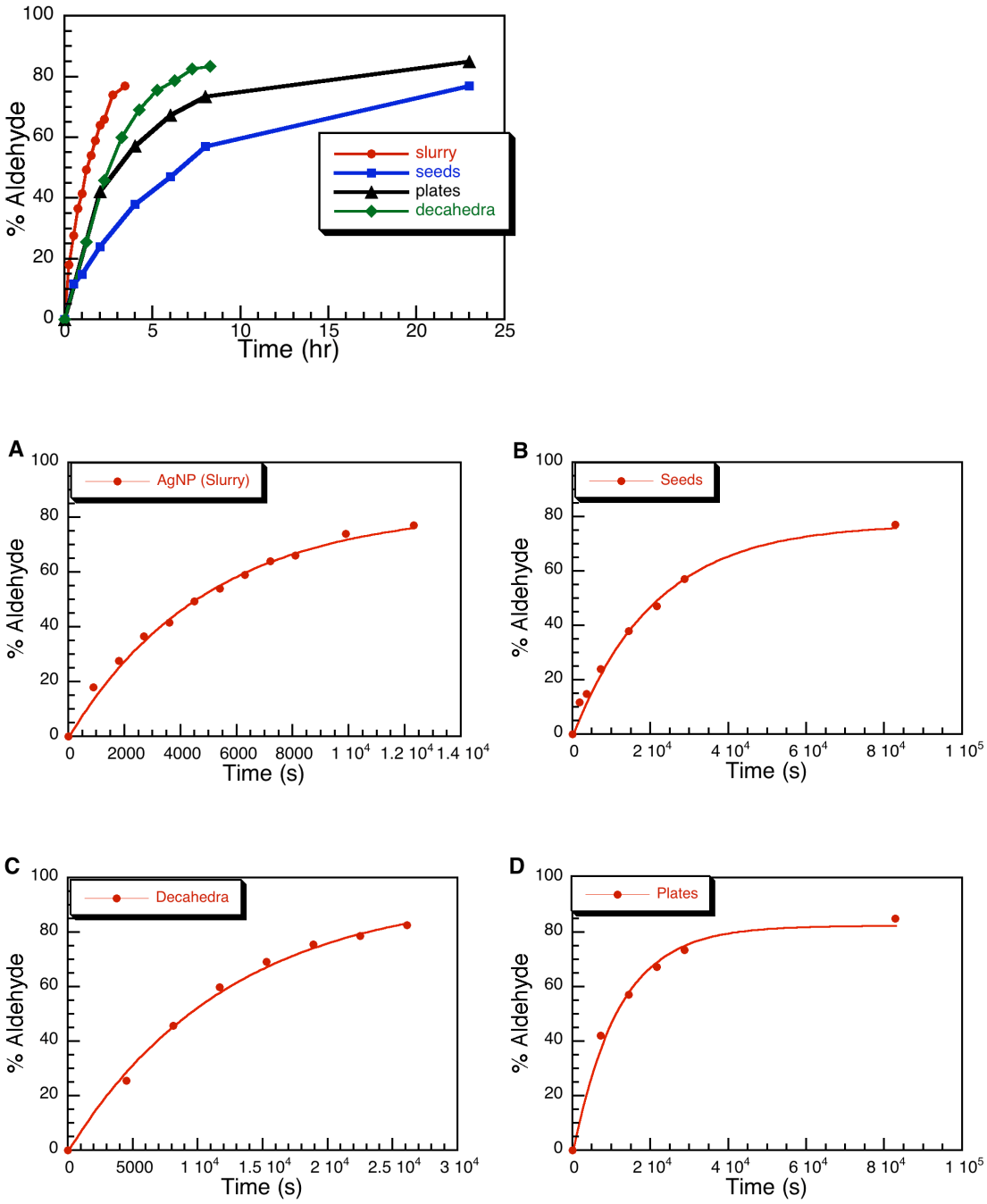

Figure 3.37 Conversion from 4-MBA to 4-MBAldehyde followed using HPLC and monitoring at 275 nm where the aldehyde absorbs. Reaction run on bench, 0.075 mmol alcohol in 5 mL of toluene, with 40 mg of catalyst (0.00185 mmol Ag) using 1% Ag@TiO_2 (slurry), or 0.5% seeds, decahedra, or plates@TiO_2(APTES). A-D show the first order fits for Ag@TiO_2 (slurry) (A), seeds (B), decahedra (C), plates (D). In all cases TiO_2 is P90.

Table 3.3 Table of rate constants and correlation factors for the kinetics of the different shapes in oxidizing 4-MBA.

Shape	Rate Constant (s^{-1})	R
Slurry	2.04×10^{-4}	1.000
Seeds	4.72×10^{-5}	0.995
Decahedra	8.85×10^{-5}	0.999
Plates	8.48×10^{-5}	0.999

Literature has measured the XRD diffraction of the various facets of the shapes. Spherical AgNP have {111} and {200} lattice planes of face centred cubic (fcc) lattice and a small contribution of {220}.[49,50] Plate shaped AgNP have {111} lattice planes and {100} on the transverse mode edges.[50,51] Decahedra shaped AgNP have {111} facets.[51]

Previous work done comparing the catalytic efficiency of cubes, plates, and spheres in colloidal solution for the oxidation of styrene found that the cubic AgNP were the best catalysts followed by spheres, then plates.[50] They attribute the catalytic activity of the shapes solely to their surface crystallographic structure. The higher the surface energy, the more catalytically reactive because it is easier for adsorption and activation on crystal planes with higher surface energy.[50] The {100} facet was stated to be the least catalytically active.[52] Near spherical NP do have some facets and edges and are not a true sphere, usually giving intermediate catalytic activity[52] depending on the size.

This previous work comparing AgNP shapes used a different surface stabilizer for each shape, which makes their comparison more complicated.[50] They also discount the size difference between the different shapes as well as the edges, which can increase the catalytic activity. In the current work, all the different AgNP shapes have the same surface stabilizer, so can be compared more directly. In this case, the decahedra and plates have very stable facets ({111} for decahedra and {111} with a small contribution from {100} for plates),[51] but the spheres have higher energy facets ({200}, and {220})[49,50] making them more reactive for catalysis. The decahedra are the next most catalytically active. The decahedra are a more strained structure and have energetic contributions from the distorted internal lattice.[53] The plates were the slowest catalyst of the three. They have a small contribution of {100}, which is the least catalytically active facet.[52] This low catalytic activity may also have resulted from the larger size of the plates, ~100-200 nm (Figure 3.21), resulting in a decrease in volume to surface area for the reaction to occur.

Another paper looking at different platinum NP shapes investigated the role of the edges in the rate of the catalysis.[52] Atoms located at sharp edges have been shown to be catalytically active sites because they have fewer neighbouring atoms.[52] Moreover, catalysis is known to occur at defect sites on NP surfaces.[52] The decahedra have 15 edges, 7 vertices, and 10 faces. Sharp edges and vertices contain atoms that are chemically very active or atoms that will dissolve leaving behind arrangements of atoms containing catalytically active

sites.[52] This may also explain the increased catalytic activity of the decahedra compared to the plates.

The AgNP seeds are less efficient than the AgNP@TiO_2 (slurry) likely because of the size difference. The AgNP seeds appear to agglomerate on the surface of the APTES covered TiO_2 (see Figure 3.19) and are around 27 nm whereas the AgNP made on the TiO_2 in the slurry method are around 10 nm (see Figure 3.29). The smaller the NP, the higher the surface area-to-volume ratio giving it unique properties.[43] The size of the NP changes its catalytic properties and activity.[17] The smaller the nanoparticle, the higher the surface energy, which makes it more prone to surface reconstruction[17] as well as higher catalytic activity.[8,50] One study looking at the oxidation of *sec*-phenethyl alcohol with AuNP found that as the particle size increased from 2.7 nm to 5.8 nm, the conversion to the ketone decreased from 99% to 22% and they claim that a small NP size is essential for the oxidation of alcohols.[7] Another source notes the same result of higher catalytic activity with smaller NP sizes as well as the increase in catalytic active sites on the NP surface.[25]

Putting size aside, a comparison of the decahedra (~30 nm) and the seeds (~27 nm) show that the decahedra are more catalytically active than the seeds, likely owing to their edges and vertices containing highly catalytically active sites.[52] They both contain the {111} facet and the spheres contain smaller contributions from {200} and {220} facets but the main difference for the catalysis is likely attributed to the edges.

The trisodium citrate is necessary for the stabilization of the NP, but is not aiding in the oxidation; if anything it is hindering the oxidation, since citrate is a common reducing agent used for making metallic NP,[54] having a reduction potential of -1.2 V (*vs.* NHE)[31] and would provide a reducing environment rather than an oxidizing one for the alcohol. However, experiments using Ag(acac) as the silver precursor and photochemically reducing it without any stabilizing or reducing agents, did not show improvement over citrate stabilized NP (Figure 3.38). This may also be a reflection of the reduced catalytic effectiveness of larger NP,[8] since the NP made with Ag(acac) are larger (~33 nm, Figure 3.5) compared to those made with citrate and $AgNO_3$ (~10 nm, Figure 3.29). Other studies have shown the capping layer on a NP can alter its catalytic activity potentially preventing adsorption of reactants and limiting the metal surface available for catalysis.[55]

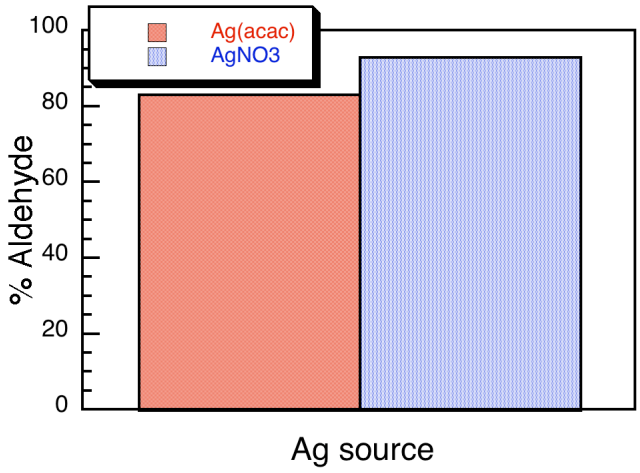

Figure 3.38 % conversion to 4-MBAldehyde using either Ag(acac) or $AgNO_3$ as the silver precursor

The oxidation of 1 mmol of 4-MBA in toluene took 3.3 hours and yielded 77% conversion when carried out on the bench under positive oxygen pressure and heated to 75°C using 0.005 mmol of Ag (for 1% loading). Similarly, after 16 hours in the SYMYX under 2 atm of oxygen, 100% conversion of 4-MBA to 4-MBAldehyde was observed. Because of inherent differences between experimental procedures used in this work, a direct comparison to previous work of NP catalyzed alcohol oxidations could not be made.[7-10,15] However, the catalysts examined in this study show good conversion to product in similar reaction times. The NP size is also larger than that in most studies, making direct comparison impossible.

3.3.2.6 Reusability

The reusability of all the supports was tested in the SYMYX under 2 atm of oxygen at 75°C for 16 hours using 0.012 mmol of 4-MBA and the 0.5% shapes@TiO_2(APTES) or 1% Ag@TiO_2 (slurry). The catalysts were recovered by evaporating the solvent and recovering the solid support. The recycled and new samples were all done in the same plate to assure consistency in the SYMYX trials. All Ag shapes show good reusability (Figure 3.39). After three uses, the AgNP made in the slurry method begin to show fatigue and less conversion. The seeds and decahedra show increased efficiency in their second use. SEM was run on decahedra@TiO_2 after one use to ensure NP were not changed. It showed NP are still on the support with a similar size distribution of 22 nm ± 7 nm

(Figure 3.40 and Figure 3.41). This shows the supports can be used for at least two reactions without showing significant fatigue.

The increase in the catalytic activity of some of the catalysts is likely a result of surface oxygen on the silver that is present after one reaction because of the heating under oxygen atmosphere during the first reaction. Studies have shown that putting silver catalysts under oxygen at elevated temperatures increased the catalytic activity because of a reduced energy barrier.[6] The cleavage of the O-H and C-H bonds in catalytic reactions became exothermic with oxygen-treated Ag catalysts opposed to endothermic without the surface oxygen on the Ag catalyst.[6]

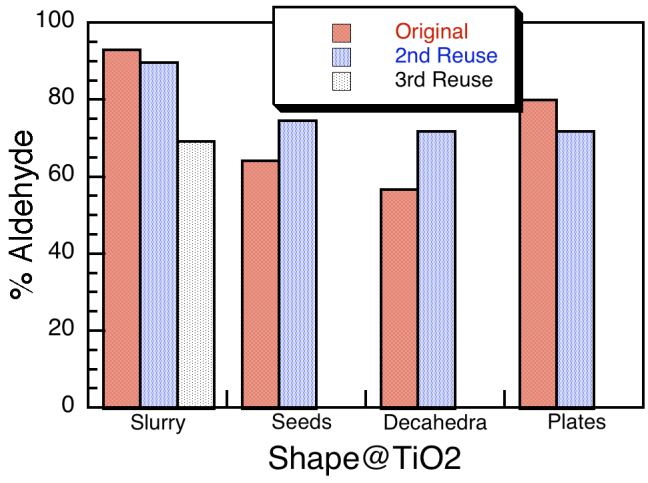

Figure 3.39 Reusability of 1% Ag@TiO_2 (P90) (slurry) for three reactions, 0.5% seeds, decahedra, and plates@TiO_2(P90) (APTES) for two reactions

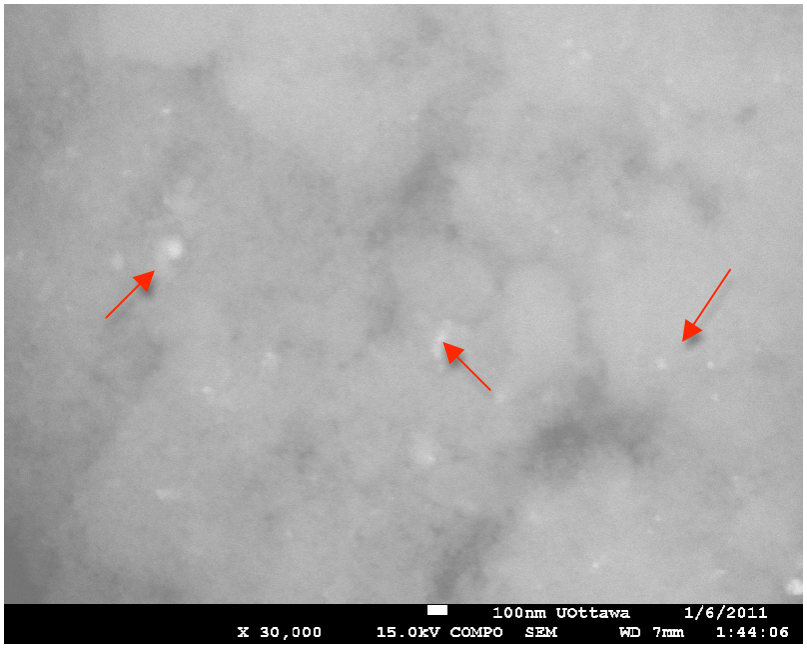

Figure 3.40 SEM of Ag decahedra@TiO_2 (P90) (APTES) after one use, showing NP are still on support. Red arrows point to NP on the TiO_2 surface.

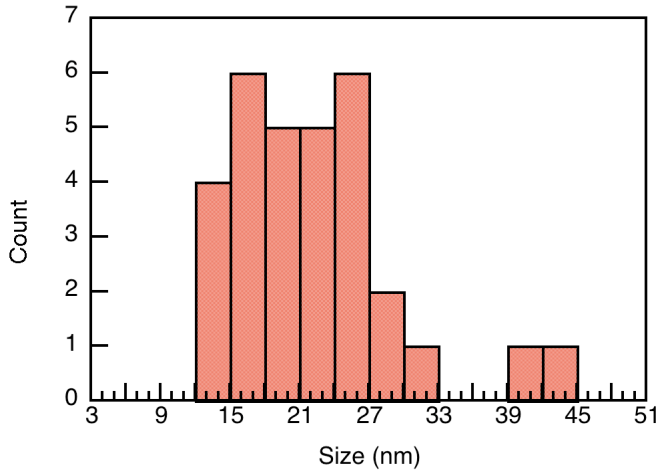

Figure 3.41 Histogram showing particle size distribution of 0.5% Ag decahedra@TiO_2 (P90) (APTES) after one use based on approximately 30 nanoparticles.

3.3.2.7 Role of Oxygen

Oxygen was expected to be necessary for the oxidation, but control experiments done under air and under Ar revealed, surprisingly, that the

oxidation of 4-MBA was equally efficient in all three conditions indicating that oxygen pressure was not necessary for the oxidation (Figure 3.42).

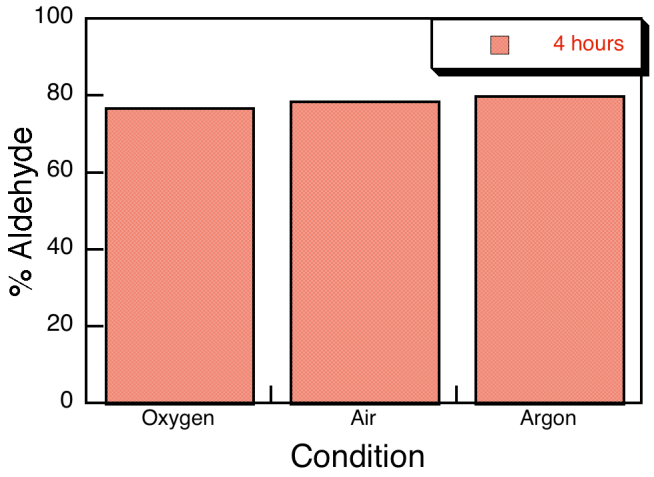

Figure 3.42 Conversion from 4-MBA to 4-MBAldehyde with 0.075 mmol alcohol, 40 mg of support (Ag@TiO_2(P90) (slurry)) in 5 mL toluene under atmosphere of oxygen, air, and argon.

Mitsudome, *et al.* studied the oxidation of *sec*-phenethyl alcohol with Ag@HTC under argon conditions and found that in 16 hours at 130°C 99% conversion to the aldehyde was achieved with 0.045 µmol of Ag.[10] In comparison, in this research, under Ar conditions, in 4 hours at 75°C, with 0.025 mmol Ag supported on TiO_2, 80% conversion is achieved. The amount of catalyst is larger in this case compared to Mistudome, *et al.* and the times for the reaction, solvent, and alcohol are also different, but both are proceeding under argon conditions, and in this case it may be a faster rate since Mitsudome, *et al.* report only after 16 hours.[10] This research also found that Ag@TiO_2 or Ag@SiO_2 showed very little product formation when used under argon.[10] The NP in this study proved to be more efficient under similar conditions. Because air or oxygen

is not necessary, this makes this catalyst unique, interesting, and important because water is no longer formed as a by-product, which would be formed if oxygen was necessary, eliminating the need to dehydrate the reaction mixture. Moreover, this reaction will work in situations where the alcohol has functional groups that are sensitive to oxygen.[10]

A potential mechanism for the oxidation is shown below in Scheme 3.5. The negative surface of the AgNP aids in abstracting a hydrogen from the alcohol, thereby promoting the delocalization of the charge and abstraction of another hydrogen, to produce H_2, and the final aldehyde formation.

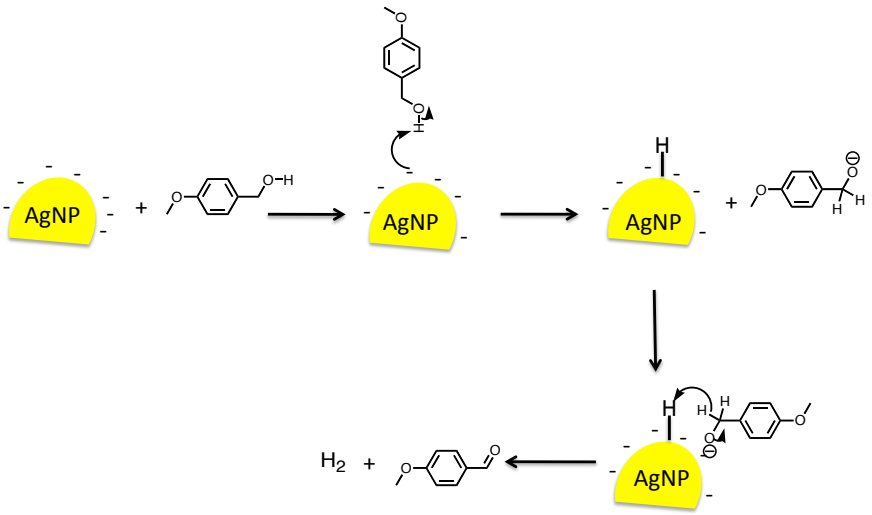

Scheme 3.5 Cartoon mechanism of proposed oxidation of 4-methoxybenzyl alcohol to 4-methoxybenzaldehyde.

It is important to note that in the control experiments with just TiO_2, HTC, or the alcohol alone at the conditions described in all the experiments, there was

0% conversion to the aldehyde, showing the AgNP are necessary for the catalysis.

3.4 Conclusion

This is the first reported one-pot photochemical synthesis of supported AgNP that is able to effectively catalyze reactions. Previous papers report unsuccessful attempts to photochemically generate AgNP@support.[16] In this chapter, AgNP shapes made photochemically have successfully been put onto APTES functionalized TiO_2 allowing their separation from the reaction and reuse. A summary and comparison of the supported NP synthesized can be found in Table 3.4.

Table 3.4 Table summarizing the sizes and SPB maximum of supported NP synthesized and their solution-based counterparts. The solution based NP are indicated along with the solvent. The silver salt precursor is $AgNO_3$ unless otherwise indicated. The copper salt precursor is $Cu(OAc)_2$.

Type of NP	Size (nm)	SPB maximum (nm)
4% Ag@TiO_2 (P90) (slurry)	17±17	465
1% Ag@TiO_2 (P90) (slurry)	9±3	480
4% Ag@HTC (slurry)	14±7	430
4% Ag(acac)@TiO_2 (P90) (slurry)	31±13	455
1% Cu@HTC (slurry)	8±3	----
CuNP (MeCN solution)	16±11	575
0.5% decahedra@TiO_2 (P90/APTES)	25±8	445
Decahedra (H_2O solution)	29±4	463
0.5% seeds@TiO_2 (P90/APTES)	30±9	430
Seeds (H_2O solution)	5±1	398
0.5% plates@TiO_2 (P90/APTES)	----	Scattering >650
Plates (H_2O solution)	Edge length >100	330 and scattering >690

This is the first report of using supported AgNP shapes to compare their effectiveness at catalyzing reactions. AgNP have shown to be able to effectively catalyze the oxidation of 4-MBA and *sec*-phenethyl alcohol in toluene under a positive oxygen atmosphere, in air, as well as under argon atmosphere, showing no difference in catalytic efficiency.

3.4 References

(1) Prucek, R.; Kvitek, L.; Panacek, A.; Vancurova, L.; Soukupova, J.; Jancik, D.; Zboril, R. *J. Mater. Chem.* **2009**, *19*, 8463-8469.

(2) Grouchko, M.; Kamyshny, A.; Ben-Ami, K.; Magdassi, S. *J. Nanopart. Res.* **2009**, *11*, 713-716.

(3) Singh, P.; Kumari, K. *Catal. Lett.* **2009**, *130*, 648-654.

(4) Bracey, C. L.; Ellis, P. R.; Hutchings, G. J. *Chem. Soc. Rev.* **2009**, *38*, 2231-2243.

(5) Sarkar, A.; Mukherjee, T.; Kapoor, S. *J. Phys. Chem. C* **2008**, *112*, 3334-3340.

(6) Shimizu, K.; Miyamoto, Y.; Satsuma, A. *Chem. Cat. Chem.* **2010**, *2*, 84-91.

(7) Mitsudome, T.; Noujima, A.; Mizugaki, T.; Jitsukawa, K.; Kaneda, K. *Adv. Synth. Catal.* **2009**, *351*, 1890-1896.

(8) Ni, J.; Yu, W. J.; He, L.; Sun, H.; Cao, Y.; H.Y., H.; Fan, K. N. *Green Chem.* **2009**, *11*, 756-759.

(9) Mitsudome, T.; Arita, S.; Mori, H.; Mizugaki, T.; Jitsukawa, K.; Kaneda, K. *Angew. Chem. Int. Ed.* **2008**, *47*, 7938-7940.

(10) Mitsudome, T.; Mikami, Y.; Funai, H.; Mizugaki, T.; Jitsukawa, K.; Kaneda, K. *Angew. Chem. Int. Ed.* **2008**, *47*, 138-141.

(11) Chang, C. T.; Liaw, B. J.; Huang, C. T.; Chen, Y. Z. *App. Cat. A: Gen.* **2007**, *332*, 216-224.

(12) Shubert, M. M.; Hackenberg, S.; van Veen, A. C.; Muhler, M.; Plzak, V.; Behm, R. J. *J. Catal.* **2001**, *197*, 113-122.

(13) Weiher, N.; Delannoy, L.; Louis, C.; DRamaker, D. E.; Miller, J. T.; van Bokhoven, J. A. *J. Catal.* **2006**, *240*, 100-107.

(14) Grunert, W.; Bruckner, A.; Hofmeister, H.; Claus, P. *J. Phys. Chem. B* **2004**, *108*, 5709-5717.

(15) Han, J.; Liu, Y.; Guo, R. *Adv. Funct. Mater.* **2009**, *19*, 1112-1117.

(16) Scire, S.; Crisafulli, C.; Giuffrida, S.; Mazza, C.; Riccobene, P. M.; Pistone, A.; Ventimiglia, G.; Bongiorno, C.; Spinella, C. *App. Cat. A: Gen.* **2009**, *367*, 138-145.

(17) Zhou, X.; Xu, W.; Liu, G.; Panda, D.; Chen, P. *J. Am. Chem. Soc.* **2009**, *132*, 138-146.

(18) Corma, A.; Garcia, H. *Chem. Soc. Rev.* **2008**, *37*, 2096-2126.

(19) Stamplecoskie, K. G.; Scaiano, J. C. *J. Am. Chem. Soc.* **2010**, *132*, 1825-7.

(20) Li, H.; Ma, X.; Dong, J.; Qian, W. *Anal. Chem.* **2009**, *81*, 8916-8922.

(21) Scientific, T. *Fluorescamine Protein Assay*, Thermo Scientific - NanoDrop products.

(22) McGilvray, K. L.; Decan, M. R.; Wang, D.; Scaiano, J. C. *J. Am. Chem. Soc.* **2006**, *128*, 15980-15981.

(23) Pacioni, N. L.; Pardoe, A.; McGilvray, K. M.; Chretien, M. N.; Scaiano, J. C. *Photochem. & Photobiol. Sci.* **2009**, *9*, 766-774.

(24) Chalmers, J. M. *Spectroscopy in Process Analysis*; Sheffield Academic Press: Boca Raton, FL, 2000.

(25) Kiyonaga, T.; Jin, Q.; Kobayashi, H.; Tada, H. *Chem. Phys. Chem.* **2009**, *10*, 2935-2938.

(26) Hernandez-Fernandez, J.; Zanella, R.; Aguilar-Elguezabal, A.; Arizabalo, R. D.; Castillo, S.; Moran-Pineda, M. *Mat. Sci. & Eng. B* **2010**, *174*, 13-17.

(27) Lee, B.; Ma, Z.; Zhang, Z.; Park, C.; Dai, S. *Micropor. & Mesopor. Mat.* **2009**, *122*, 160-167.

(28) Hurum, D. C.; Agrios, A. G.; Gray, K. A. *J. Phys. Chem. B* **2003**, *107*, 4545-4549.

(29) Cermenati, L.; Richter, C.; Albini, A. *Chem. Comm.* **1998**, 805-806.

(30) Ivanova, O. S.; Zamborini, F. P. *J. Am. Chem. Soc.* **2009**, *132*, 70-72.

(31) Huerta, F.; Mele, C.; Bozzini, B.; Morallon, E. *J. Electroanal. Chem.* **2004**, *569*, 53-60.

(32) Giuffrida, S.; Ventimiglia, G.; Sortino, S. *Chem. Commun.* **2009**, 4055.

(33) Mitsudome, T.; Mikami, Y.; Ebata, K.; Mizugaki, T.; Jitsukawa, K.; Kaneda, K. *Chem. Comm.* **2008**, 4804-4806.

(34) Pestryakov, A. N.; Petranovskii, V. P.; Kryazhov, A.; Ozhereliev, O.; Pfander, N.; Knop-Gericke, A. *Chem. Phys. Lett.* **2004**, *385*, 173-176.

(35) Pinna, F. *Catal. Today* **1998**, *41*, 129-137.

(36) Dahl, J. A.; Maddux, B. L. S.; Hutchison, J. E. *Chem. Rev.* **2007**, *107*, 2228-2269.

(37) Wang, Z. S.; Li, F. Y.; Huang, C. H. *Chem. Comm.* **2000**, 2063-2064.

(38) Morrill, A. R.; Duong, D. T.; Lee, S. J.; Moskovits, M. *Chem. Phys. Lett.* **2009**, *473*, 116-119.

(39) Zhou, X.; Ni, S.; Zhang, X.; Wang, X.; Hu, X.; Zhou, Y. *Current Nanosci.* **2008**, *4*, 397-401.

(40) Kaczmarek, D. *Scanning* **1997**, *19*, 310-315.

(41) Rozov, K.; Berner, U.; Taviot-Gueho, C.; Leroux, F.; Renaudin, G.; Kulik, D.; Diamond, L. W. *Cem. & Concr. Res.* **2010**, *40*, 1248-1254.

(42) Mori, K.; Kumami, A.; Tomonari, M.; Yamashita, H. *Phys. Chem. C Lett.* **2009**, *113*, 16850-16854.

(43) El-Sayed, M. A. *Acc Chem. Res.* **2001**, *34*, 251-264.

(44) Chen, X.; Mao, S. S. *Chem. Rev.* **2007**, *107*, 2891-2959.

(45) Haruta, M. *Catal. Today* **1997**, *36*, 153-166.

(46) chemBlink 2010; Vol. 2010, p Properties of sec-phenethyl alcohol.

(47) Shapley, P. A.; Zhang, N.; Allen, J. L.; D.H., P.; Liang, H.-C. *J. Am. Chem. Soc.* **2000**, *122*, 1079-1091.

(48) Liu, Z.-P.; Gong, X.-Q.; Kohanoff, J.; Sanchez, C.; Hu, P. *Phys. Rev. Lett.* **2003**, *91*, 266102-1 - 255102-4.

(49) Samanta, S.; Pyne, S.; Sarkar, P.; Sahoo, G. P.; Bar, H.; Bhui, D. K.; Misra, A. *J. Molec. Liq.* **2010**, *153*, 170-173.

(50) Xu, R.; Wang, D.; Zhang, J.; Yadong, L. *Chem. Asian J.* **2006**, *1*, 888-893.

(51) Skrabalak, S. E.; Xia, Y. *ACS Nano* **2009**, *3*, 10-15.

(52) Narayanan, R.; El-Sayed, M. A. *Nano Lett.* **2004**, *4*, 1343-1348.

(53) Tao, A. R.; Habas, S.; Yang, P. *Small* **2008**, *4*, 310-325.

(54) Eustis, S.; El-Sayed, M. A. *Chem. Soc. Rev.* **2006**, *35*, 209-217.

(55) Kuhn, J. N.; Tsung, C. K.; Huang, W.; Somorjai, G. A. *J. or Catal.* **2009**, *265*, 209-215.

CHAPTER 4 –

CONCLUSIONS & FUTURE DIRECTIONS

TABLE OF CONTENTS:

TABLE OF FIGURES:

4.1 Conclusions

Irgacure undergoes a Norrish Type I photocleavage upon exposure to UV light producing two radicals, one that will donate its electron to reduce a copper salt to its zero valent state. This reaction was selected to synthesize copper nanoparticles photochemically using Irgacure 2959 or Irgacure 907 in water and acetonitrile respectively. Using different chloride and bromide containing alkylammonium salts, the CuNP are stabilized in an argon atmosphere. Depending on the alkylammonium salt, the size of the NP as well as the rate of formation differs. Upon exposure to oxygen, the rate of oxidation also differs depending on the stabilizer used, but complete oxidation occurs within 2 hours. Bimetallic copper/silver nanoparticles were also synthesized in attempts to coat the copper with silver to prevent oxidation. The oxidation of these particles also occurred upon exposure to oxygen. Both the copper and silver oxidized returning to their original ionic states. The composition of these NP could not be determined.

Copper nanoparticles were synthesized in an argon atmosphere on hydrotalcite, however oxidized upon exposure to oxygen, so could not be further used in catalytic applications. Silver nanoparticles were synthesized on supports in order to use them for catalytic applications. Silver NP shapes (seeds, decahedra, and plates) were photochemically synthesized[1] and put onto support to use for catalysis to compare the catalytic efficiency of different shapes. The oxidation of 4-methoxybenzyl alcohol to 4-methoxybenzylaldehyde was the

reaction used to monitor and compare the catalytic efficiency and rates of different shapes as well as comparing different supports. The AgNP synthesized on TiO_2 in the slurry method were found to be the best catalyst for this reaction followed by the decahedra, plates, and then seeds. The reaction was found to proceed as effectively under argon atmosphere, showing the mechanism for oxidation does not involve oxygen. The reusability was also tested showing good reusability of all supports after one use, and higher catalytic efficiency in the second use for the decahedra and the seeds.

4.2 Future Directions

4.2.1 Copper and copper-silver nanoparticles

More work needs to be done on characterizing the Cu/Ag bimetallic NP and their composition. Further work should also be done on actually capping the CuNP with a shell of AgNP to prevent their oxidation.

4.2.2 Copper nanoparticle catalysis

CuNP were shown to be synthesized in the slurry method on support (in Chapter 3) but because of their instability to oxygen oxidized readily. Future work includes synthesizing CuNP in ionic liquids, which can slow or prevent oxidation and using them toward catalytic reactions.[2] CuNP have shown to be useful catalysts in a variety of reactions including oxidation, Suzuki cross-coupling, and hydrogenation, among others.[3-5]

4.2.3 Photocatalysis

Some preliminary experiments were done using colloidal NP and excitation with laser at 410 nm of a drop of water containing AgNP and *sec*-phenethyl alcohol. There was no conversion to the ketone seen. This could be because of the low solubility of oxygen in water[6] and the inability to use another oxidizing agent, like H_2O_2 as used in other experiments in our group, because it readily oxidizes the AgNP.

Using 25 mg of 1% supported AgNP on TiO_2 (P25), 200 µL of H_2O_2, 99 µL of sec-phenethyl alcohol in a flat cell cuvette (solvent-less Neat Reaction), and irradiating with a 532 nm laser for 20 minutes showing 74% conversion to the ketone. However, this reaction showed to be sacrificial since after the reaction the Ag@TiO_2 was white and no longer contained any NP as they were oxidized by the H_2O_2.

Experiments could be done using the supported shapes and irradiating the plasmon bands with the respective LEDs of each shape in toluene with the alcohol. The heat generated from the plasmon excitation of the AgNP may be able to replace the heating needed in the alcohol oxidations studied in Chapter 3.

Work on the catalysis is promising, however, more work could be done by attempting to use photochemistry for the catalysis, taking advantage of the heat produced when exciting the SPB of NP.

4.2.4 Platinum nanoparticle synthesis

Platinum nanoparticles have been less studied than gold and silver NP toward catalysis, but have shown to be effective at catalyzing hydrogenation and alcohol oxidations, among others.[7-9] Photochemical synthesis of Platinum NP was successful using K_2PtCl_6 (0.3 mM), with I-2959 (1.2 mM), and TMABr (0.2-1.1 mM) in water and irradiation with 14 UVA lamps for 30 minutes, yielding a brown solution showing increased scattering (Figure 4.1). Other stabilizers

including CTAC and SDS show some NP formation, but not as effectively as TMABr. The NP are mainly less than 5 nm in size as seen by TEM (Figure 4 2).

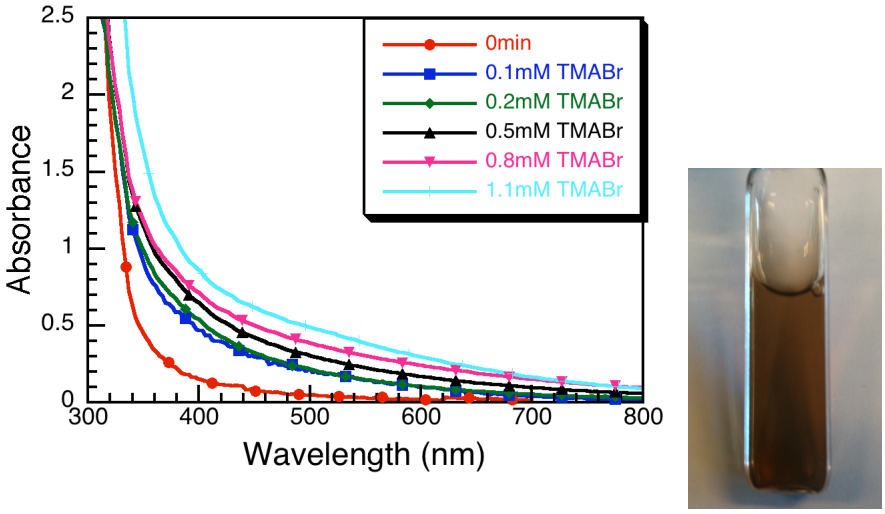

Figure 4.1 Absorption spectrum before and after irradiation of K_2PtCl_6 with I-2959 and different amounts of TMABr. Picture on the right is the PtNP synthesized with TMABr in solution in the cuvette.

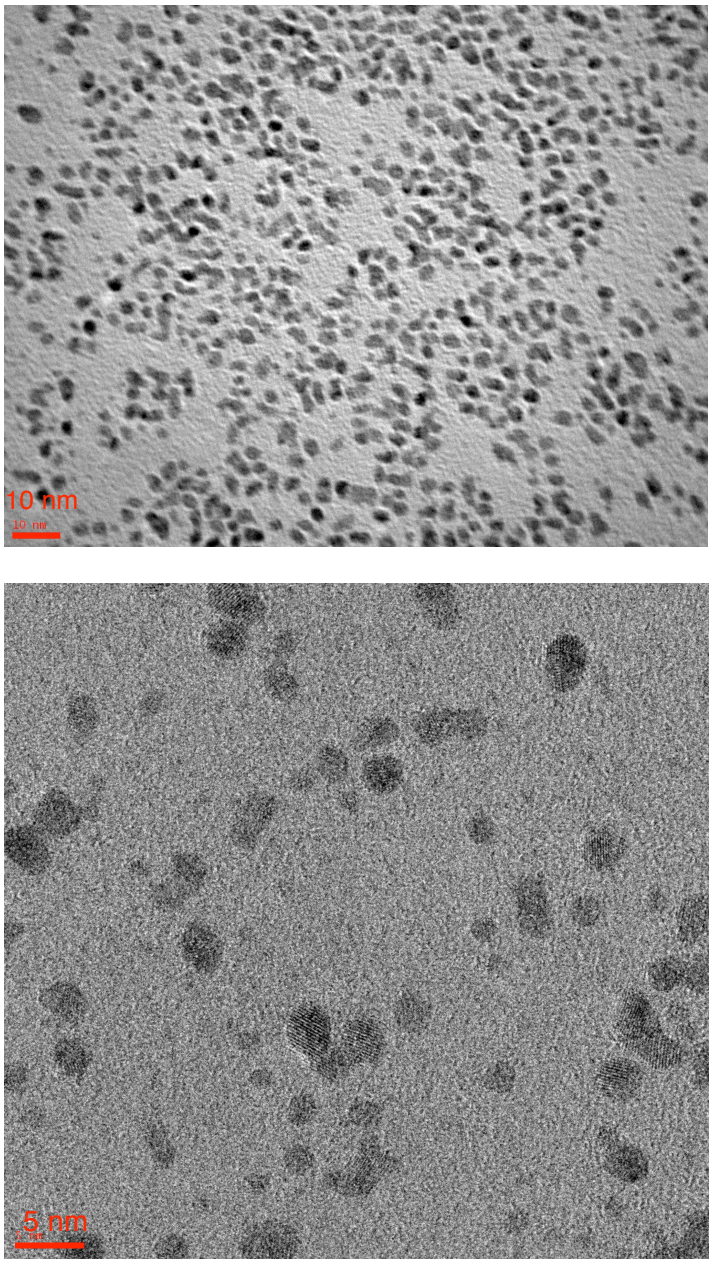

Figure 4 2 TEM images of PtNP made with 0.8 mM TMABr. Scale bars are 10 nm and 5 nm respectively.

4.2.5 Supported platinum nanoparticles

These NP may be very useful for catalytic applications. Attempts were made to synthesize PtNP on support as in the case of the slurry method with silver in Chapter 2. A yellow powder was made, using TMABr and the same

conditions as above with TiO_2 (P25) and some NP were present on the TiO_2 (Figure 4.3), but the pale colour indicated a low yield of NP. More work needs to be done to improve this synthesis and then use these PtNP@support for catalytic reactions. Limited literature[10] is found using supported PtNP for catalytic applications, so this could be explored further using a photochemical approach to synthesizing the catalysts.

Figure 4.3 SEM image of PtNP made on TiO_2 in the slurry method. Red arrows point to the brighter spots, which are PtNP on the TiO_2. Scale bar is 100 nm.

4.3 Final Remarks

Nanoparticles of different metals (Cu, Cu/Ag, Ag, Pt) have been shown to be synthesized with a photochemical approach using Irgacure, which undergoes Norrish type I photocleavage producing a radical capable of reducing metal salts. The growth rate and stabilities of CuNP to oxygen have shown to differ depending on the stabilizer, but are still easily oxidized in atmospheric conditions. Silver nanoparticles were made on support in a slurry method photochemically,

and were shown to be an effective catalyst for oxidation reactions. Silver nanoparticles of different shapes have been made photochemically and attached to a support and show high catalytic activity toward alcohol oxidations in toluene under inert atmosphere and heating. The different shapes show different catalytic efficiencies and have shown to be reusable.

This thesis explored using photochemistry to synthesize different bimetallic and monometallic NP and their use in catalytic applications. This avoids harsh conditions and difficult procedures needed without the use of a catalyst for organic reactions.

4.4 References:

(1) Stamplecoskie, K. G.; Scaiano, J. C. *J. Am. Chem. Soc.* **2010**, *132*, 1825-7.

(2) Zhu, L.; Sun, C. Y.; Cui, Y.; Liang, M.; Zhao, J.; Li, N. *Cryst. Res. Technol.* **2010**, *45*, 398-404.

(3) Singh, P.; Kumari, K. *Catal. Lett.* **2009**, *130*, 648-654.

(4) Grouchko, M.; Kamyshny, A.; Ben-Ami, K.; Magdassi, S. *J. Nanopart. Res.* **2009**, *11*, 713-716.

(5) Bracey, C. L.; Ellis, P. R.; Hutchings, G. J. *Chem. Soc. Rev.* **2009**, *38*, 2231-2243.

(6) Battino, R. *Solubility Data Series*; Pergamon Press: Oxford, 1981; Vol. 7.

(7) Kuhn, J. N.; Tsung, C. K.; Huang, W.; Somorjai, G. A. *J. Catal.* **2009**, *265*, 209-215.

(8) Maity, P.; Gopinath, C. S.; Bhaduri, S.; Lahiri, G. K. *Green Chem.* **2009**, *11*, 554-561.

(9) Song, H.; Rioux, R. M.; Hoefelmeyer, J. D.; Komor, R.; Niesz, K.; Grass, M.; Yang, P.; Somorjai, G. A. *J. Am. Chem. Soc.* **2006**, *128*, 3027.

(10) An, H.; Zhou, J.; Li, J.; Zhu, B.; Wang, S.; Zhang, S.; Wu, S.; Huang, W. *Catal. Comm.* **2009**, *11*, 175-179.

APPENDIX

SEM from Chapter 2

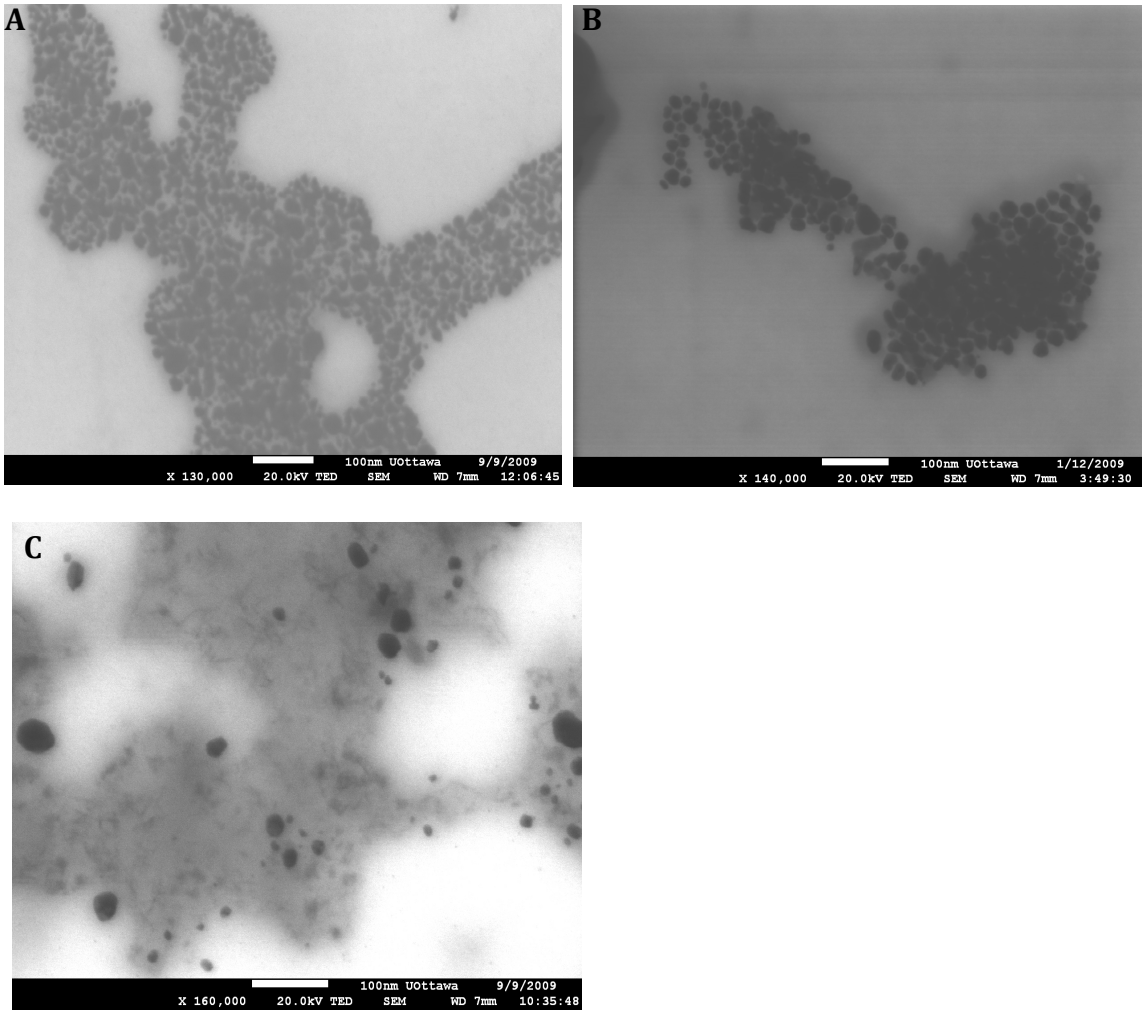

Figure 5.1 SEM images of Cu/Ag NP A: (M1) Cu/Ag NP made together in solution B: (M2) CuNP + AgTFA C: (M3) CuNP + AgNP made separately. Scale bars are all 100 nm. No significant difference can be seen between these images, making determination of the composition not possible.

HPLC from Chapter 3

The following are HPLC spectra of 4-MBA run at 75°C for 16 hours in toluene at a concentration of 30 mM with 8 mg of catalyst unless otherwise stated. The retention time of peaks shift in some cases because of previous column conditions and were identified using UV-Vis. The alcohol absorbs most strongly at 225 nm and the aldehyde absorbs at 275 nm. Chromatographs were all extracted at the wavelength of the aldehyde, 275 nm.

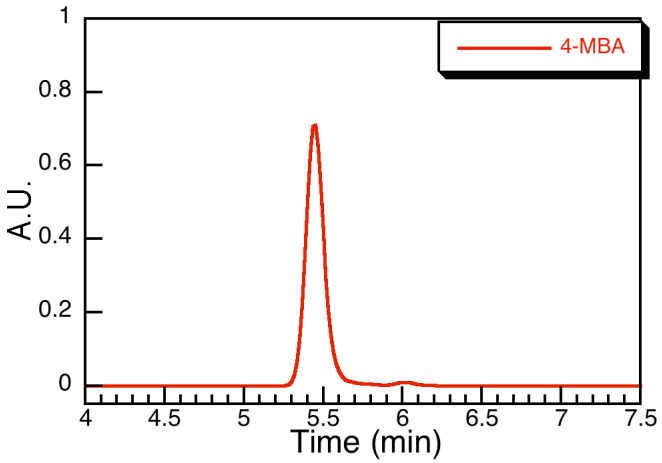

Figure 5.2 HPLC spectrum of 4-Methoxybenzyl alcohol. Peak at 5.5 minutes has a strong absorption at 225 nm.

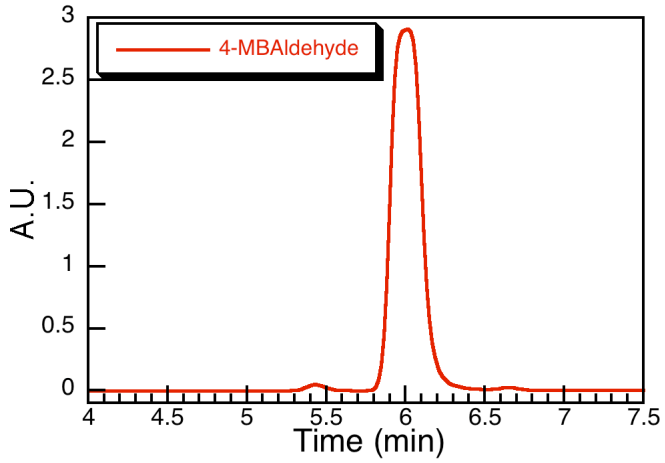

Figure 5.3 HPLC spectrum of 4-Methoxybenzaldehyde. Peak at 6 minutes has a strong absorption at 275 nm.

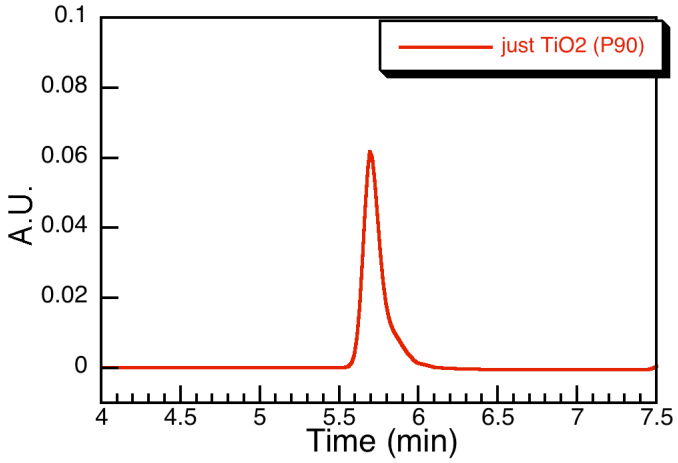

Figure 5.4 HPLC spectrum of 4-MBA oxidation run with 8 mg of TiO_2 and no AgNP. Peak is that of 4-MBA with absorption at 225 nm.

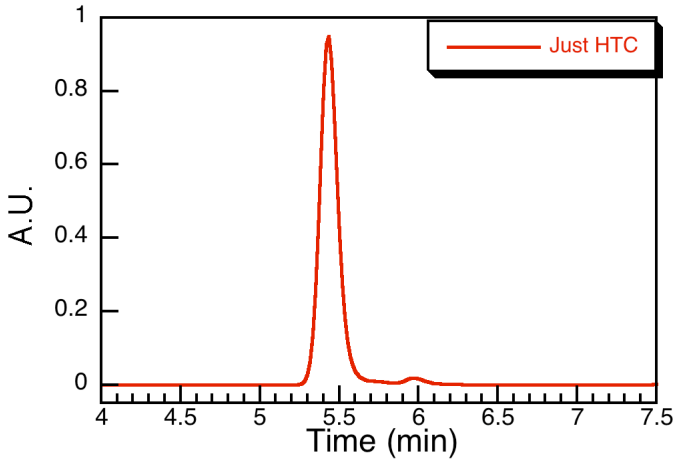

Figure 5.5 HPLC spectrum of 4-MBA oxidation run with 8 mg of HTC and no AgNP. Peak is that of 4-MBA with absorption at 225 nm.

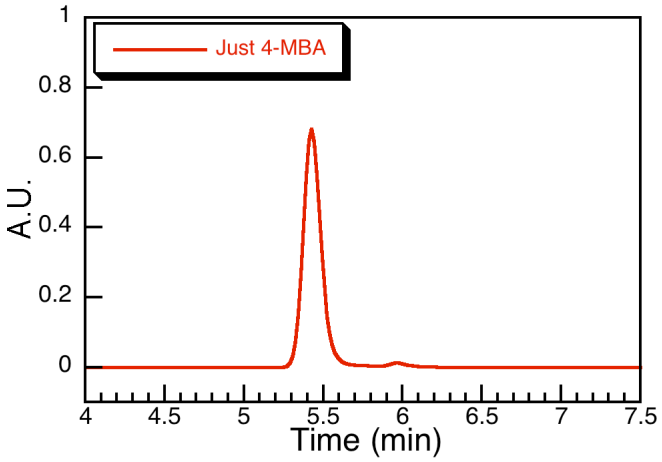

Figure 5.6 HPLC spectrum of 4-MBA oxidation run without any catalyst. Peak is that of 4-MBA with absorption at 225 nm.

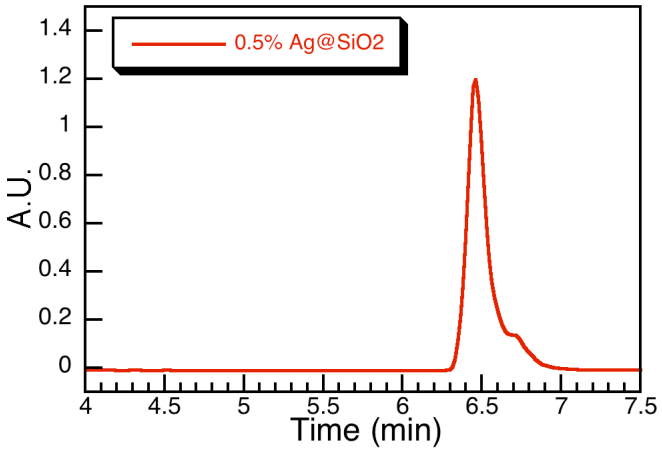

Figure 5.7 HPLC spectrum of 4-MBA oxidation run with 8 mg of 0.5% Ag@SiO_2. Peak is that of 4-MBA with absorption at 225 nm.

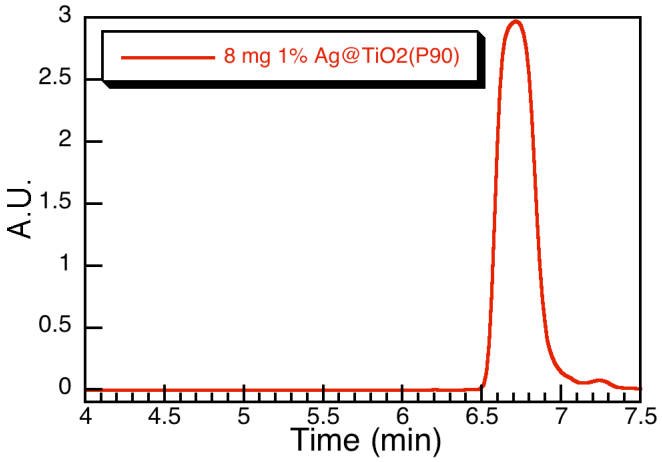

Figure 5.8 HPLC spectrum of 4-MBA oxidation run with 8 mg of 1% Ag@TiO_2 (P90). Peak is that of 4-MBAldehyde with absorption at 275 nm.

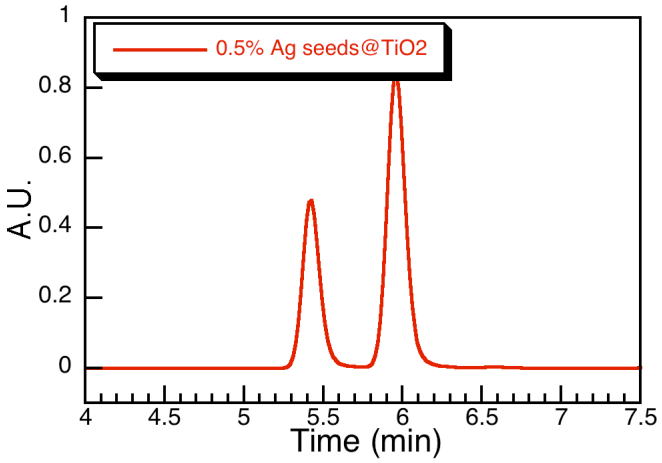

Figure 5.9 HPLC spectrum of 4-MBA oxidation run with 8 mg of 0.5% Ag seeds@TiO_2. Peak around 5.4 minutes is that of 4-MBA with absorption at 225 nm and peak around 6 minutes is that of 4-MBAldehyde with absorption at 275 nm.

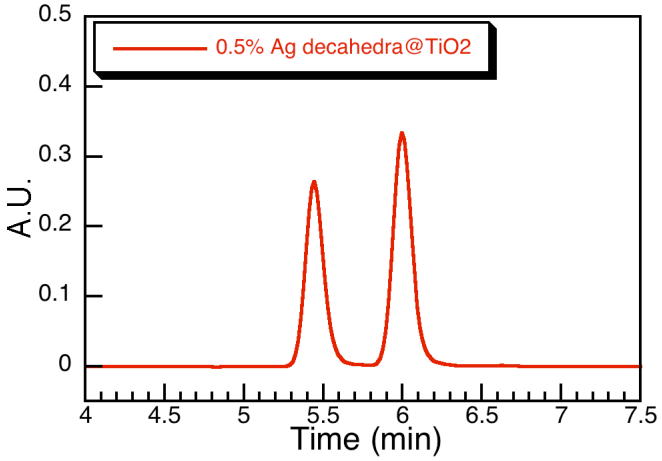

Figure 5.10 HPLC spectrum of 4-MBA oxidation run with 8 mg of 0.5% Ag decahedra@TiO_2. Peak around 5.4 minutes is that of 4-MBA with absorption at 225 nm and peak around 6 minutes is that of 4-MBAldehyde with absorption at 275 nm.

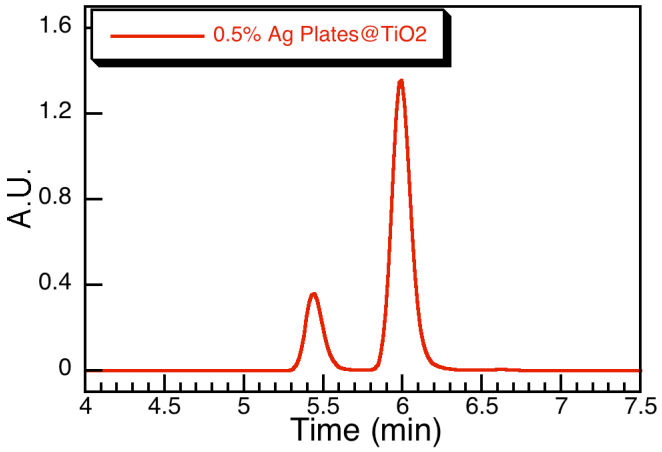

Figure 5.11 HPLC spectrum of 4-MBA oxidation run with 8 mg of 0.5% Ag plates@TiO_2. Peak around 5.4 minutes is that of 4-MBA with absorption at 225 nm and peak around 6 minutes is that of 4-MBAldehyde with absorption at 275 nm.

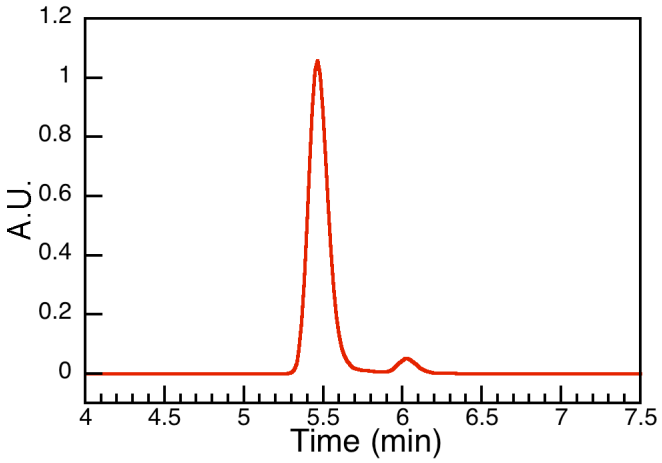

Figure 5.12 HPLC spectrum of 4-MBA oxidation run in water extracted at 275 nm with 8 mg of 1% Ag@TiO_2. Peak around 5.5 minutes is that of 4-MBA with absorption at 225 nm and the small peak at 6 minutes, is the 4-MBAldehyde with absorption at 275 nm.

The following are HPLC spectra of *sec*-phenethyl alcohol run at 75°C for 16 hours in toluene at a concentration of 30 mM unless otherwise stated The *sec*-phenethyl alcohol absorbs most strongly at 215 nm and the aldehyde (acetophenone) absorbs at 240 nm.

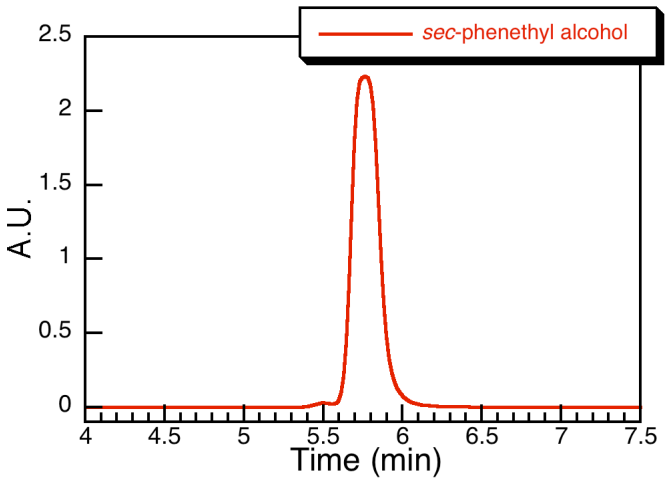

Figure 5.13 HPLC spectrum of *sec*-phenethyl alcohol extracted at 215 nm where the alcohol absorbs. Peak at 5.75 minutes is that of the alcohol, absorbing most strongly at 215 nm.

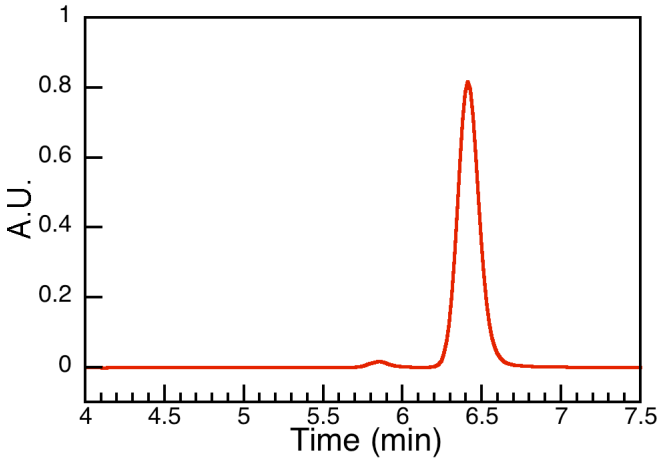

Figure 5.14 HPLC spectrum of *sec*-phenethyl alcohol oxidation run in toluene with 20 mg of 1% Ag@TiO_2. Spectrum extracted at 240 nm. Peak around 6.4 minutes is that of acetophenone with absorption at 240 nm.